Contribution à la caractérisation physique et isotopique des micrométéorites

Clément Suavet

Université de Droit, d'Économie et des Sciences
Paul Cézanne (Aix-Marseille III)

École Doctorale des Sciences de l'Environnement

N° attribué par la bibliothèque

Thèse

Présentée par

Clément Suavet

Pour obtenir le grade de Docteur en Sciences
de l'Université de Droit, d'Économie et des Sciences Paul Cézanne
(Aix-Marseille III)

Discipline : Géosciences de l'Environnement

Contribution à la Caractérisation Physique et Isotopique des Micrométéorites

---

Soutenue publiquement 30/06/2009 devant le jury composé de :

Philippe Claeys	Rapporteur
Luigi Folco	Examinateur
Jérôme Gattacceca	Co-directeur de Thèse
Matthieu Gounelle	Rapporteur
Bruno Hamelin	Examinateur
Pierre Rochette	Directeur de Thèse
Benjamin Weiss	Examinateur

Remerciements

Merci à Pierre Rochette et Jérôme Gattacceca pour m'avoir fait confiance, et pour m'avoir permis de travailler librement tout en étant attentifs à mes besoins.

Merci aux rapporteurs Philippe Claeys et Matthieu Gounelle, ainsi qu'aux examinateurs Luigi Folco, Bruno Hamelin et Benjamin Weiss d'avoir accepté d'évaluer mes travaux.

Merci à Annie-Claude Agnese, Anne Alexandre, Didier Bourlès, Régis Braucher, Daniel Borschneck, Perrine Chaurand, Michèle Denise, Jean Duprat, Cécile Engrand, Yves Gally, Thibault de Garidel-Thoron, Isabelle Hammad, Jean-Jacques Motte, Marie-Magdeleine Nehlil, Christine Paillès, Jérôme Rose, Corinne Sonzogni, Martine Tiercelin, Fabienne Vadeboin.

Merci à Natalia Bezaeva, Cécile Blanchet, Julien Crespin, Edouard Delemotte, Pierre-Yves Descote, Anne-Lise Develle, Aurélien Dhomont, Cécile Fabre, Simon Gascoin, Mickaël Grelaud, Fatim Hankard, Thomas Jacob, Adrien Lambert, Thomas Lauvaux, Guillaume Leduc, Lucie Menabreaz, Aurélie Méreu, Fréderic Neff, Sylvain Petitgirard, Antoine Pommerol, Pierre Rampal, Florence Recorbet, Irène Schimmelpfennig, Magali Troin, Minoru Uehara, Millarca Valenzuela, Boris Weisz.

Merci à ma famille.

Merci à Xue.

Sommaire

Introduction

Chapitre 1

Introduction générale

Les micrométéorites sont les particules extraterrestres de moins de deux millimètres qui tombent sur Terre. Elles constituent la majeure partie du flux de matière extraterrestre vers la Terre [*Love et Brownlee*, 1993 ; *Taylor et al.*, 1998]. Les plus grosses d'entre elles fondent généralement en entrant dans l'atmosphère [*Love et Brownlee*, 1991] : on les appelle sphérules cosmiques en raison de leur forme. Les différences texturales entre les catégories de micrométéorites reflètent des différences compositionnelles originelles (particules chondritiques, métalliques [*Badjukov et al., 2009a*], ou basaltiques [*Gounelle et al.*, 2009 ; *Badjukov et al., 2009b*]), ainsi que des différences de chauffage lors de l'entrée atmosphérique [*Taylor et al.*, 2000 ; *Genge et al.*, 2008]. Des expérimentations tentant de reproduire les textures des micrométéorites par chauffage à partir d'analogues de météoroïdes ont été menées avec succès [*Toppani et al.*, 2001 ; *Toppani et Libourel*, 2003]. Les mesures de nucléides cosmogéniques effectuées sur des micrométéorites semblent montrer que la plupart d'entre elles ont subi dans l'espace une exposition aux rayonnements cosmiques dans des corps du même ordre de taille que leur diamètre actuel [*Nishiizumi et al.*, 1995].

La découverte des micrométéorites remonte à l'expédition du Challenger de 1872 à 1876 [*Murray et Renard*, 1891]. Des sphérules magnétiques contenant du fer natif retrouvées dans les sédiments abyssaux du Pacifique central ont été interprétées comme étant d'origine extraterrestre. Les premières collectes systématiques furent donc obtenues par extraction

magnétique à partir de sédiments marins profonds à très faibles taux de sédimentation [*Brownlee*, 1985]. Cependant, ces collections sont fortement biaisées en faveur des sphérules cosmiques les plus magnétiques, et la diagénèse induit de nombreuses transformations.

Dans le but de prélever des poussières extraterrestres ayant subi un minimum de transformation, la NASA lance dans les années 1980 des récoltes dans la haute atmosphère avec des avions munis de collecteurs. Les particules prélevées sont appelées "interplanetary dust particles" (IDPs) [*Warren et Zolensky*, 1994]. Ces objets diffèrent cependant des micrométéorites en terme de taille (en moyenne 10 μm), minéralogie, composition chimique et isotopique.

L'extraction de micrométéorites à partir de boues constituées de sidérobactéries filamentaires dans les lacs saisonniers groenlandais [*Maurette et al.*, 1990] permet de collecter des échantillons qui n'étaient pas présents dans les sédiments marins, notamment des micrométéorites non-fondues ou partiellement fondues, ainsi que des sphérules cosmiques vitreuses. Cependant, la méthode d'extraction par désagrégation mécanique du sédiment ne permet pas de conserver les types les plus fragiles.

Les collectes dans les champs de glace bleue en Antarctique [*Maurette et al.*, 1991] par fusion de la glace permettent de collecter des échantillons mieux préservés. Un phénomène de surconcentration piège les micrométéorites et poussières terrestres dans les couches de surface. Il suffit alors de faire fondre la glace pour récupérer les micrométéorites par pompage. Bien que beaucoup plus douce que pour les collectes groenlandaises, la méthode est tout de même destructrice pour les types les plus fragiles.

Les puits d'eau potable des stations Antarctiques américaine et japonaise permettent de récupérer des micrométéorites par fusion de neige en profondeur. Les collections de South Pole Water Well [*Taylor et al.*, 1998, 2000] et de Dôme Fuji [*Nakamura et al.*, 1999] se révèlent peu biaisées en ce qui concerne les sphérules cosmiques, mais des problèmes de pollution par des particules anthropogènes se posent en ce qui concerne les micrométéorites non-fondues.

La régression de la calotte glaciaire en Nouvelle Zemble (Russie) laisse des dépôts dans lesquels on peut récupérer des micrométéorites de tous types [*Badjukov et al.*, 2003, 2009a, 2009b].

Les collectes par fusion douce de neige de surface à proximité de la station franco-italienne Concordia [*Duprat et al.*, 2007] se révèlent très fructueuses avec un ratio grains terrestres/poussières extraterrestres supérieur à 1, et des particules ayant subi très peu d'altération, comme en témoigne leur teneur en élements volatiles. Un nouveau type de micrométéorites poreuses ultracarbonacées est observé pour la première fois, et des collectes sur niveaux de neige bien datés permettent d'envisager une étude de la variabilité du flux de microméteorites à l'échelle de la décennie.

Des analyses chimiques et minéralogiques de micrométéorites non-fondues [*Engrand et Maurette*, 1998] permettent de les rattacher aux chondrites carbonées hydratées de type CM et CR : les météorites les plus primitives du système solaire, peut-être d'origine cométaire. Cependant, des différences importantes entre ces objets font que l'on attribue aux micrométéorites un corps parent de type nouveau.

Des analyses isotopiques de l'oxygène de sphérules cosmiques [*Clayton et al.*, 1986 ; *Engrand et al.*, 2005 ; *Yada et al.*, 2005] et de micrométéorites non-fondues [*Matrajt et al.*, 2006] semblent confirmer la parenté avec les chondrites carbonées, bien que les incertitudes analytiques soient élevées. Pour expliquer que les micrométéorites échantillonnent des corps parents différents des météorites, on invoque un corps parent trop friable pour se fragmenter en roches macroscopiques lors des collisions, ou dont les fragments se réduirait en poussière lors de l'entrée atmosphérique.

Des études pétrogéochimiques [*Genge*, 2008] permettent de mettre en évidence une parenté entre certaines micrométéorites non-fondues et les chondrites ordinaires.

De nombreuses questions restent aujourd'hui sans réponse. Quelle est la variabilité du flux de micrométéorites vers la Terre, et ce à toutes les échelles de temps, de l'année au million d'années ? Quelle est la nature des corps parent des micrométéorites, et quelles

sont leurs contributions relatives au flux de matière extraterrestre vers la Terre ?

La majorité des études en cours porte sur les micrométéorites non-fondues : celles-ci ayant subi des changements mineurs lors de l'entrée atmosphérique, elles sont mieux à même de renseigner sur les propriétés initiales de la matière extraterrestre. Cependant, peu d'études ont été menées sur la caractérisation physico-chimique des sphérules cosmiques, qui présentent pourtant un interêt non-négligeable en tant que composant mineur de toutes les surfaces terrestres. De plus, les limitations instrumentales interdisent l'utilisation de nombreuses techniques sur les micrométéorites non-fondues, alors que les plus grosses sphérules cosmiques peuvent présenter une masse ou une taille suffisante.

Il manquait essentiellement d'échantillons suffisamment importants pour permettre des études innovantes sur ces objets connus de longue date. Cette condition fut remplie avec la découverte fortuite de quantités exceptionnelles de micrométéorites de toutes tailles au sommet de Frontier Mountain (Terre Victoria, Antarctique) par P. Rochette, L. Folco et N. Perchiazzi, dans le cadre d'une expedition de recherche de météorites du PNRA en 2003 [*Rochette et al.*, 2008].

Bibliographie

Badjukov, D., Raitala, J. (2003) Micrometeorites from the northern ice cap of the Zovaya Zemlya archipelago, Russia : The first occurence. *Meteorit. Planet. Sci.*, **38** :329–340.

Badjukov, D., Brandstaetter, F., Raitala, J., Kurat, G. (2009a) Unmelted FeNi micrometeorites from the Zovaya Zemlya glacier. *Lunar Planet. Sci.*, **LX**, 1499.

Badjukov, D., Brandstaetter, F., Raitala, J., Kurat, G. (2009b) Unmelted achondritic micrometeorites from the Novaya Zemlya glacier. *Met. Soc.* **72**, 5224.

Brownlee, D. E. (1985). Cosmic Dust : Collection and Research. *Ann. Rev. Earth Planet. Sci.*, **13** :147–173.

Clayton R. N., Mayeda T. K., Brownlee D. E. (1986). Oxygen isotopes in deep-sea spherules. *Earth Planet. Sci. Lett.*, **79** :235–240.

Duprat, J., Engrand, C., Maurette, M., Kurat, G., Gounelle, M., Hammer, C., (2007). Micrometeorites from Central Antarctic snow : The CONCORDIA collection. *Adv. Space Res.*, **392** :605–611, doi :10.1016/j.asr.2006.05.029.

Engrand, C., Maurette, M. (1998). Carbonaceous micrometeorites from Antarctica. *Meteorit. Planet. Sci.*, **33** :565–580.

Engrand C., McKeegan K. D., Leshin L. A., Herzog G. F., Schnabel C., Nyquist L. E., Brownlee D. E.(2005). Isotopic compositions of oxygen, iron, chromium, and nickel in cosmic spherules : Toward a better comprehension of atmospheric entry heating effects. *Geochim. Cosmochim. Acta*, **69** :5365–5385.

Genge, M. J. (2008) Koronis asteroid dust within Antarctic ice. *Geology*, **36** :687–690, doi : 10.1130/G24493A.1.

Genge, M. J., Engrand, C., Gounelle, M., Taylor, S. (2008). The classification of micrometeorites. *Meteorit. Planet. Sci.*, **43** :497–515.

Gounelle, M., Chaussidon, M., Morbidelli, A., Barrat, J.-A., Engrand, C., Zolensky, M. E., McKeegan, K. D. (2009). A unique basaltic micrometeorite expands the inventory

of solar system planetary crusts. *Proc. Natl. Acad. Sci. USA*, **106** :6904–6909.

Love, S. G., Brownlee, D. E. (1991), Heating and thermal transformation of micrometeoroids entering the Earth's atmosphere, *Icarus*, *89*, 26–43.

Love, S. G., Brownlee, D. E. (1993). A direct measurement of the terrestrial mass accretion rate of cosmic dust. *Science*, **262** :550–553.

Matrajt G., Guan Y., Leshin L., Taylor S., Genge M., Joswiak D., Brownlee D. (2006). Oxygen isotope measurements of individual unmelted Antarctic micrometeorites. *Geochim. Cosmochim. Acta*, **70** :4007–4018.

Maurette, M., Hammer, C., Brownlee, D. E., Reeh, N., Thomsen, H. H. (1986). Placers of cosmic dust in the blue lakes of Greenland. *Science*, **233** :869–872.

Maurette, M., Olinger, C., Christophe Michel-Lévy, M., Kurat, G., Pourchet, M., Brandstätter, F., Bourot-Denise, M. (1991). A collection of diverse micrometeorites recovered from 100 tons of Antarctic blue ice. *Nature*, **351** :44–47.

Maurette, M., Immel, G., Engrand, C., Kurat, G., Pillinger, C. T. (1994). The 1994 EUROMET collection of micrometeorites at Cap-Prudhomme, Antarctica. *Meteoritics*, **29** :499.

Murray, J., Renard, A. F. (1891). *Report on the Scientific Results of the H. M. S. Challenger during the years 1873–76*. Neill & Co.

Nakamura, T., Imae, T., Nakai, I., Noguchi, T., Yano, H., Terada, K., Murakami, T., Fukuoka, T., Nogami, K., Ohashi, H., Nozaki, W., Hashimoto, M., Kondo, N., Matsuzaki, H., Ichikawa, O., Ohmori, R. (1999). Antarctic micrometeorites collected at the Dome Fuji station. *Antarctic Meteorite Research*, **12** :183–198.

Nishiizumi, K., Arnold, J. R., Brownlee, D. E., Caffee, M. W., Finkel, R. C., Harvey, R. P. (1995). Beryllium-10 and aluminum-26 in individual cosmic spherules form Antarctica. *Meteoritics*, **30** :728–732.

Rochette, P., Folco, L., Suavet, C., van Ginneken, M., Gattacceca, J., Perchiazzi, N., Braucher, R., Harvey, R.P. (2008). Micrometeorites from the Transantarctic Mountains.

Proc. Natl. Acad. Sci. USA, **105** :18206–18211, doi :10.1073/pnas.0806049105.

Taylor, S., Lever, J. H., Harvey, R. P. (1998). Accretion rate of cosmic spherules measured at the South Pole. *Nature*, **392** :899–903.

Taylor, S., Lever, J. H., Harvey, R. P. (2000). Numbers, types, and compositions of an unbiased collection of cosmic spherules. *Meteorit. Planet. Sci.*, **35** :651–666.

Toppani, A., G. Libourel, C. Engrand, Maurette, M. (2001). Experimental simulation of atmospheric entry of micrometeorites. *Meteorit. Planet. Sci.*, *36* :1377–1396.

Toppani, A., G. Libourel (2003), Factors controlling compositions of cosmic spinels : application to atmospheric entry conditions of meteoritic materials, *Geoch. Cosm. Acta*, *67* :4621–4638.

Warren, J. L., Zolensky, M. E. (1994). Collection and curation of interplanetary dust particles recovered from the stratosphere by NASA. In Zolensky, M. E., Wilson, T. L., Rietmeijer, F. J. M., et Flynn, G. J., editors, *Analysis of Interplanetary Dust, AIP Conf. Proc.*, volume 310, pages 245–253. American Institute of Physics : Houston.

Yada, T., Nakamura, T., Noguchi, T., Matsumoto, N., Kusakabe, M., Hiyagon, H., Ushikubo, T., Sugiura, N., Kojima, H., Takaoka, N. (2005). Oxygen isotopic and chemical compositions of cosmic spherules collected from the Antarctic ice sheet : Implications for their precursor materials. *Geochim. Cosmochim. Acta*, **69** :5789–5804.

Chapitre 2

Structure de cette thèse

La première partie de ce travail de thèse a consisté en la caractérisation d'une nouvelle collection de micrométéorites provenant de la Chaîne Transantarctique : la collection TAM (pour « Transantarctic Mountains »). L'étude de ses propriétés statistiques (distribution en tailles et en types de micrométéorites) a permis de montrer cette collection est peu biaisée, ainsi que d'étudier la distribution en taille des micrométéorites de diamètre supérieur au millimètre, ce qui n'avait jamais été effectué auparavant. La concentration des micrométéorites se fait principalement par chute directe dans les pièges, et les concentrations secondaires par transport sont négligeables. La principale caractéristique de la collection TAM est la très longue durée de collecte (plusieurs centaines de milliers d'années) [*Folco et al.*, 2008, 2009] comparativement à la plupart des autres collections, qui explique la présence de micrométéorites géantes (>400 μm) en nombre jamais atteints dans les autres collections. La collection TAM offre ainsi un objet inédit pour l'étude de la nature du flux de matière extraterrestre à l'échelle de la centaine de milliers d'années, voire du million d'années.

La disponibilité au sein de la collection TAM d'un grand nombre de micrométéorites de diamètre suffisant pour effectuer des mesures magnétiques de particules individuelles rendait possible une caractérisation magnétique statistiquement significative, jamais effectuée auparavant, de cette population d'objets extraterrestres. La deuxième partie de ce docu-

ment présente les résultats de ces mesures, ainsi que leurs conséquences sur les propriétés magnétiques des sédiments dans lesquels les micrométéorites se déposent.

Les analyses isotopiques de micrométéorites effectuées jusqu'à présent se limitaient à des mesures sur échantillons composites, ou à des analyses à la microsonde ionique ayant une grande incertitude analytique. Le grand nombre d'échantillons de sphérules cosmiques ayant des masses de plusieurs centaines de microgrammes dans la collection TAM rendait envisageable d'en sacrifier pour effectuer des analyses destructrices de particules individuelles. Ainsi, nous avons développé un protocole de mesure des trois isotopes de l'oxygène par fluorination laser et spectrométrie de masse sur les matériaux extraterrestres, et l'avons adapté à la mesure d'échantillons microscopiques. Ces mesures ont permis d'obtenir des résultats d'une précision dix fois supérieure aux analyses par microsonde ionique, et de remettre en question la théorie d'un corps parent de type chondrite carbonée pour 99% des micrométéorites. La troisième partie de ce document présente ces résultats et leurs conséquences sur les transferts de matière au sein du système solaire.

Bibliographie

Folco, L., D'Orazio, M., Tiepolo, Tonarini S., Ottolini L., M. Rochette, P., Perchiazzi, N., Laurenzi, M., (2008) Microtektites from Victoria Land, Transantarctic Mountains. *Geology*, **36** :291–294, doi : 10.1130/G24528A.1.

Folco, L., D'Orazio M., Tiepolo M., Tonarini S., Ottolini L., Perchiazzi N., Rochette P., Glass B. P. (2009) Transantarctic Mountain microtektites : geochemical affinity with Australasian microtektites. *Geochim. Cosmichim. Acta*, **73** :3694–3722.

Première partie

Micrométéorites de la Chaîne Transantarctique

Chapitre 3

La collection TAM

3.1 Article *Rochette et al., Proceedings of the National Academy of Science USA*, 2008

Contribution de C. Suavet : Tamisage et tri d'échantillons de sable. Sélection et pesée de micrométéorites. Photographies au microscope électronique à balayage et mesure des micrométéorites. Analyses chimiques XRF. Etude des distributions en taille.

Micrometeorites from the Transantarctic Mountains

P. Rochette[a], L. Folco[b,1], C. Suavet[a], M. van Ginneken[b], J. Gattacceca[a], N. Perchiazzi[c], R. Braucher[a], and R. P. Harvey[d]

[a]Centre Européen de Recherche et d'Enseignement des Géosciences de l'Environnement, Aix-Marseille Université-Centre National de la Recherche, PB80 13545, Aix en Provence, Cedex 4, France; [b]Museo Nazionale dell'Antartide, Università di Siena, Via Laterina 8, 53100 Siena, Italy; [c]Dipartimento di Scienze della Terra, Università di Pisa, Via S. Maria 53, 56126 Pisa, Italy; and [d]Department of Geological Sciences, Case Western Reserve University, 0900 Euclid Avenue, Cleveland, OH 44106

Edited by Norman H. Sleep, Stanford University, Stanford, CA, and approved October 7, 2008 (received for review June 25, 2008)

We report the discovery of large accumulations of micrometeorites on the Myr-old, glacially eroded granitic summits of several isolated nunataks in the Victoria Land Transantarctic Mountains. The number (>3,500) of large (>400 μm and up to 2 mm in size) melted and unmelted particles is orders of magnitudes greater than other Antarctic collections. Flux estimates, bedrock exposure ages and the presence of ≈0.8-Myr-old microtektites suggest that extraterrestrial dust collection occurred over the last 1 Myr, taking up to 500 kyr to accumulate based on 2 investigated find sites. The size distribution and frequency by type of cosmic spherules in the >200-μm size fraction collected at Frontier Mountain (investigated in detail in this report) are similar to those of the most representative known micrometeorite populations (e.g., South Pole Water Well). This and the identification of unusual types in terms of composition (i.e., chondritic micrometeorites and spherulitic aggregates similar to the ≈480-kyr-old ones recently found in Antarctic ice cores) and size suggest that the Transantarctic Mountain micrometeorites constitute a unique and essentially unbiased collection that greatly extends the micrometeorite inventory and provides material for studies on micrometeorite fluxes over the recent (≈1 Myr) geological past.

Antartica | cosmic spherules | solar system composition | unmelted micrometeorites | scoriaceous micrometeorites

Micrometeorites (particles normally less than ≈1 mm in size) constitute the main part of the flux of extraterrestrial matter accreting on Earth (1–3). Quantitative estimates of this flux in terms of amount and composition are thus important for understanding the cycles of extraterrestrial input to the global geochemical budget of planet Earth. Moreover, because micrometeorites may sample a different kind of extraterrestrial matter than meteorites (2), they are very important to understanding the composition of the solar system. A number of micrometeorite collections have been studied previously, including those from deep-sea sediments (1, 4, 5), from secondary concentrations due to the natural melting of glacier ice in Greenland (6), Antarctica (7, 8) and Novaya Zemlya (9), and from artificially melted glacier ice and snow in Antarctica (3, 10–12). Micrometeorites have also been recovered from a variety of terrestrial surfaces (desert soils, beach sands, etc.) (13), showing that their ubiquitous deposition can be evidenced on any surface, provided that the accumulation time is sufficient, weathering is low, and discrimination from terrestrial particles is feasible. One major pending question that justifies the comparative study of the various collections is how the collection setting biases the characteristics of extraterrestrial matter, in terms of type, grain size, hardness, and resistance to weathering. Moreover, the age and duration of the sampled flux is often quite short (in the 100- to 1,000-yr range) or unknown, hindering the detection of possible flux variability over time.

During the Italian 2003 and 2006 *Programma Nazionale delle Ricerche in Antartide* (PNRA) expeditions, we discovered a micrometeorite trap on the tops of the Transantarctic Mountains in Victoria Land (Fig. 1) that may provide insight into these 2 issues. Thousands of micrometeorites up to 2 mm in size were found within the fine-grained bedrock detritus accumulated in the joints and decimeter-sized weathering pits of flat, glacially eroded granitoid summits. These structures trap micrometeorites over the Myr time scale, as testified by the ≈0.8-Myr-old Australasian microtektites found therein (14).

Through size-distribution and frequency-by-type studies of micrometeorite samples collected at Frontier Mountain and the identification of unusual types, we provide evidence that the Transantarctic Mountain micrometeorite collection is a unique and essentially unbiased collection representing a long record of micrometeorite flux over the recent geological past.

Geological Setting

Frontier Mountain (Fig. 1*A*) has been a very productive site for meteorite collection in the 7 EUROMET and PNRA expeditions (15). In the 2001 expedition, a meteorite (FRO 01149) was incidentally found, on the top of the mountain during a geomorphological survey. The meteorite was found at an altitude of ≈2,775 m (i.e., ≈600 m above the present-day ice level), sitting on a glacially eroded surface generated by an ice sheet that overrode Frontier Mountain during a past glaciation (Fig. 1*B*). The ^{26}Al, ^{10}Be, and ^{21}Ne cosmogenic nuclide concentrations of 2 surface granite samples yielded an exposure age of 4.4 Myr. FRO 01149, with a terrestrial age of ≈3 Myr, is the oldest stony meteorite discovered on Earth (fossil meteorites excluded) (16). These findings suggest that the only source of allochthonous material deposited onto this surface since the last local retreat of the Antarctic ice sheet >4 Myr ago is atmospheric fallout including tephra, micrometeorites, and microtektites.

The unusual finding of the FRO 01149 meteorite prompted a second more-thorough search for meteorites at the top of the mountain during the 2003–2004 PNRA expedition. Searches were conducted with the help of a magnetic gradiometer that proved an efficient tool to locate 3- to 20-g meteorites buried in snow during the same expedition (17). Although no meteorites were found on that occasion, the magnetic gradiometer led us to the discovery a large accumulation of micrometeorites. A granitic glacial surface contained scattered weathering pits 10–30 cm in diameter and 5–15 cm in depth. Most of these depressions were empty, but the largest (extending for ≈0.07 m^2), was two-thirds filled with granitic detritus and produced a local magnetic maximum (Fig. 1*C*). Below the wind-sorted gravel and sand, there was a darker and finer material with higher magnetic susceptibility than the granite, thus explaining the magnetic signal in the absence of any meteorite. At the base of the depression, the material was coherent, and looked like loess,

Author contributions: P.R. and L.F. designed research; P.R., L.F., C.S., M.v.G., J.G., N.P., and R.B. performed research; R.P.H. contributed new reagents/analytic tools; P.R., L.F., C.S., M.v.G., J.G., N.P., and R.B. analyzed data; and P.R. and L.F. wrote the paper.

The authors declare no conflict of interest.

This article is a PNAS Direct Submission.

Freely available online through the PNAS open access option.

[1]To whom correspondence should be addressed. E-mail: folco@unisi.it.

This article contains supporting information online at www.pnas.org/cgi/content/full/0806049105/DCSupplemental.

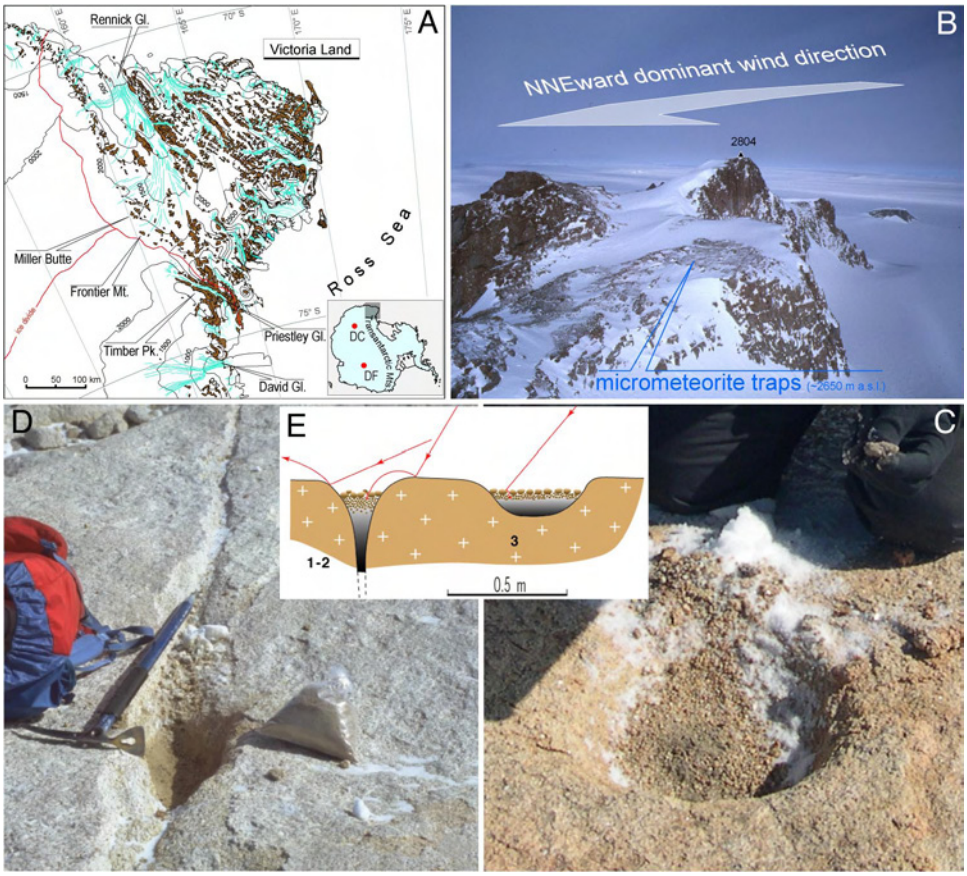

Fig. 1. Transantarctic Mountain micrometeorite traps. (*A*) Sketch map of Victoria Land showing locations at Frontier Mountain, Miller Butte, and Timber Peak where micrometeorites were found. Brown areas represent exposed bedrock, whereas blue and red lines indicate ice flows and ice divides, respectively. (*Inset*) Sketch map of Antarctica showing the location of Victoria Land (shaded area) and EPICA Dome C (DC) and Dome Fuji (DF) ice cores (red dots). (*B*) Aerial view of the top of Frontier Mountain (72°58′ S, 160°30′ E, 2,804 m). (*C*) A type of micrometeorite trap in a weathering pit of a flat granitic surface (sample 3). (*D*) A second type of micrometeorite trap in a granite joint (sample 1). (*E*) Sketch of the proposed accumulation mechanism in the 2 types of micrometeorite traps.

with low density and visible bubble-like cavities. Sample 3 was collected by hand from this lower layer. The other positive magnetic detections (samples 1 and 2, Fig. 1*D*) occurred in a different setting, namely along eroded granitic joints. A total of 1 kg of <2-mm detritus was recovered in 2003 [supporting information (SI) Tables. S1 and S2]. As later revealed by laboratory investigations, the magnetic signals were mainly generated by tephra and thousands of micrometeorites (Tables S1 and S2). In 2006, we thus collected an additional 177 kg of detritus mainly from Frontier Mountain, Miller Butte, and an unnamed nunatak in the Timber Peak area (samples 4–27; Tables S1 and S2).

Fig. 1*E* illustrates the hypothesized mechanism for the accumulation of atmospheric fallout in the 2 types of trap, once a sufficient depression has been generated by weathering and granite disaggregation. During strong winds, no deposition occurs, and size sorting limits the deflation of finer particles, allowing their percolation to the bottom of the depression through an equilibrium layer of coarser granitic detritus. During periods of calm, vertically falling particles will likely be caught inside the gravel layer, ensuring an efficient capture. A snow cover may also lead to no accumulation: Although snow can efficiently trap the falling particles, they will inevitably be wind blown upon snow sublimation unless they are able to make their way to the gravel level.

Sample Preparation and Measurement Techniques

Soil samples 1, 2, and 3 were dried by using vacuum pumping and subsequently dry-sieved through the following meshes: 800, 400, 200, and 100 μm. In this report, we focus on the 4 fractions >100 μm because the extraordinary number and size of large micrometeorites in our collection represent a novelty in micrometeorite research (the smaller fractions remain to be investigated in future works). Micrometeorites were magnetically and visually extracted under the stereo microscope (Tables S1 and S2). Extraterrestrial spherules were easy to identify under the stereo microscope in all magnetic fractions whereas abundant dark, angular, terrestrial grains (mostly tephra) in the <400-μm fraction made the identification of unmelted micrometeorites more difficult. Whole-specimen observations were conducted in a microanalytical scanning electron microscope (SEM-EDS) on particles >200 μm from samples 2 and 3. Lastly, all particles >400 μm and most spherules from the 200- to 400-μm fractions of samples 2 and 3 were embedded in epoxy and sectioned for petrographic investigations under the SEM and bulk chemical analyses by means of electron microprobe (Tables S3 and S4). Extraction from samples 4–27 (the 2006 collection) remains to be completed by following similar procedures, and only preliminary data will be presented in this work.

Micrometeorite Concentration, Size Distribution, and Collection Duration

The number of unmelted micrometeorites identified in the >200-size fractions of samples 2 and 3 are 25; counting for samples 1, 2, and 3 yielded 22 and 3,282 spherules in the >400 and 100- to 400-μm fractions, respectively (Tables S1 and S2). The number of spherules is nearly equal to that obtained by

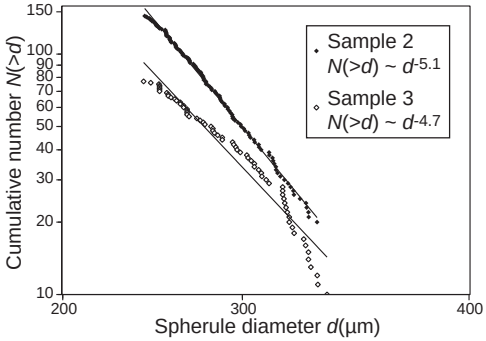

Fig. 2. Cumulative size distribution for Frontier Mountain micrometeorites (cosmic spherules only) in the >200-μm size range for samples 2 (filled diamonds; $n = 158$) and 3 (open diamonds; $n = 65$) collected in the joint and weathering pit, respectively, featured in Fig. 1. Distribution is cut at a spherule diameter of 240 μm to account for bias introduced by sieving, and at $n \leq 10$ for statistical representativeness (see Fig. S1 to view the full distribution).

melting 100 tons of Antarctic blue ice (10), i.e., a concentration of extraterrestrial material 10^5 times higher than in blue ice.

The size of the spherules, measured on whole specimens in the SEM, was used to produce the cumulative size distribution in Fig. 2 (see also Fig. S1). The linear fit in log–log scale for samples 2 and 3 >240 μm yields an exponent of -5.1 ± 0.2 and -4.7 ± 0.4, respectively. Although a minor deficit is observed in the smaller size fraction, these values compare well with the exponents of -5.2 and -5.4 obtained for the South Pole Water Well cosmic spherule collection (18, 19), which is considered to best represent the modern (≈1500–800 AD) flux of micrometeorites. This match excludes significant size sorting in the >200-μm size fraction because of the accumulation mechanism and suggests that our collection is not a secondary concentration by wind transport like the one found at Walcott Névé (8). This conclusion is based on the -2.8 ± 0.3 exponent that we obtained for a Walcott Névé sample of 140 spherules (Fig. S1), which indicates preferential loss of small, wind-blown particles.

During our preliminary work on the >400-μm fraction of the 2006 collection (samples 4–27; Tables S1 and S2), we separated 3,398 cosmic spherules and 135 unmelted micrometeorites up to 2 mm in size (Fig. 3). This population is much greater than that of large micrometeorites in collections worldwide: For instance, "only" 136 particles in the 400- to 1,000-μm size range have been hitherto reported from the richest collection so far, i.e., the South Pole Water Well collection (19).

To estimate the time span during which micrometeorite collection occurred, our analysis is restricted to circular pits, for which the capture surface can be assumed to be the depression surface. From the study of the South Pole Water Well micrometeorite collection (18), we calculate a flux rate of spherules >100 μm of 0.17 yr^{-1} m^{-2} (total number counted: 1,131). Using the surface area of the site 3 pit (0.07 m^2) and the counted spherules (1,497), we derive a deposition time of 130 kyr. The same calculation for another pit from Miller Butte (18c) similar to that of sample 3 yields a 500-kyr duration. ^{10}Be-derived exposure ages (see ref. 20) for experimental procedure) of the quartz grains of the local detritus within the traps are 0.32 ± 0.15 and 0.98 ± 0.10 Myr for samples 1 and 3, respectively (Table S5), i.e., in the same range as the estimated accumulation duration, the FRO 01149 meteorite terrestrial age and the bedrock exposure age.

Number and Types of Micrometeorites and Remarkable Findings

The mineral and bulk chemical composition of 264 sectioned particles studied by electron microscopy further documents their extraterrestrial origin (Tables S3 and S4). The studied set

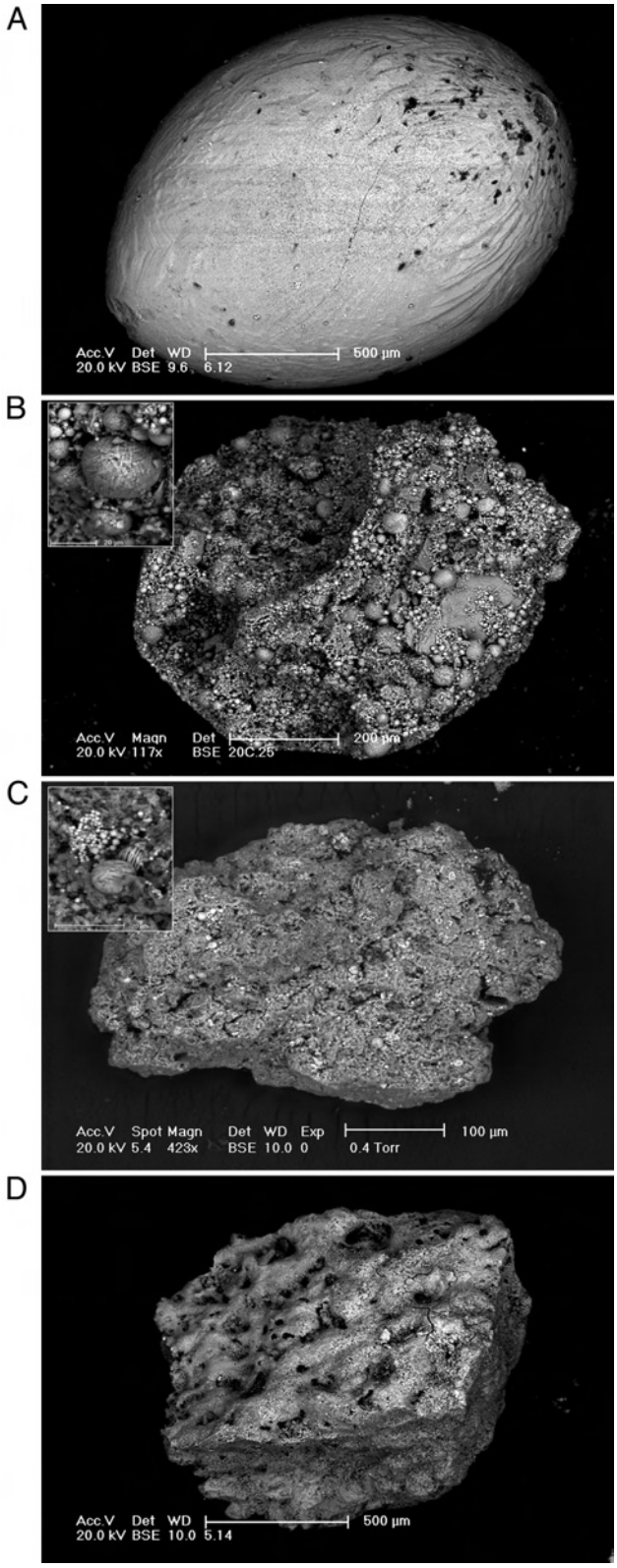

Fig. 3. Transantarctic Mountain micrometeorites (back-scattered electron images): a selection of large specimens. (*A*) A microcrystalline cosmic spherule (6.12) with a maximum elongation of ≈2 mm. (*B*) An ungrouped spherulitic aggregate (20c.25). (*Inset*) Detailed view of the constituting spherules mainly consisting of Fe-oxide dendrites. (*C*) An unmelted fine-grained, C-type micrometeorite (2.1c) ≈400 μm across. (*Inset*) Magnetite framboids. (*D*) An unmelted micrometeorite ≈1 mm in size showing a scoriaceous fusion crust (5.14).

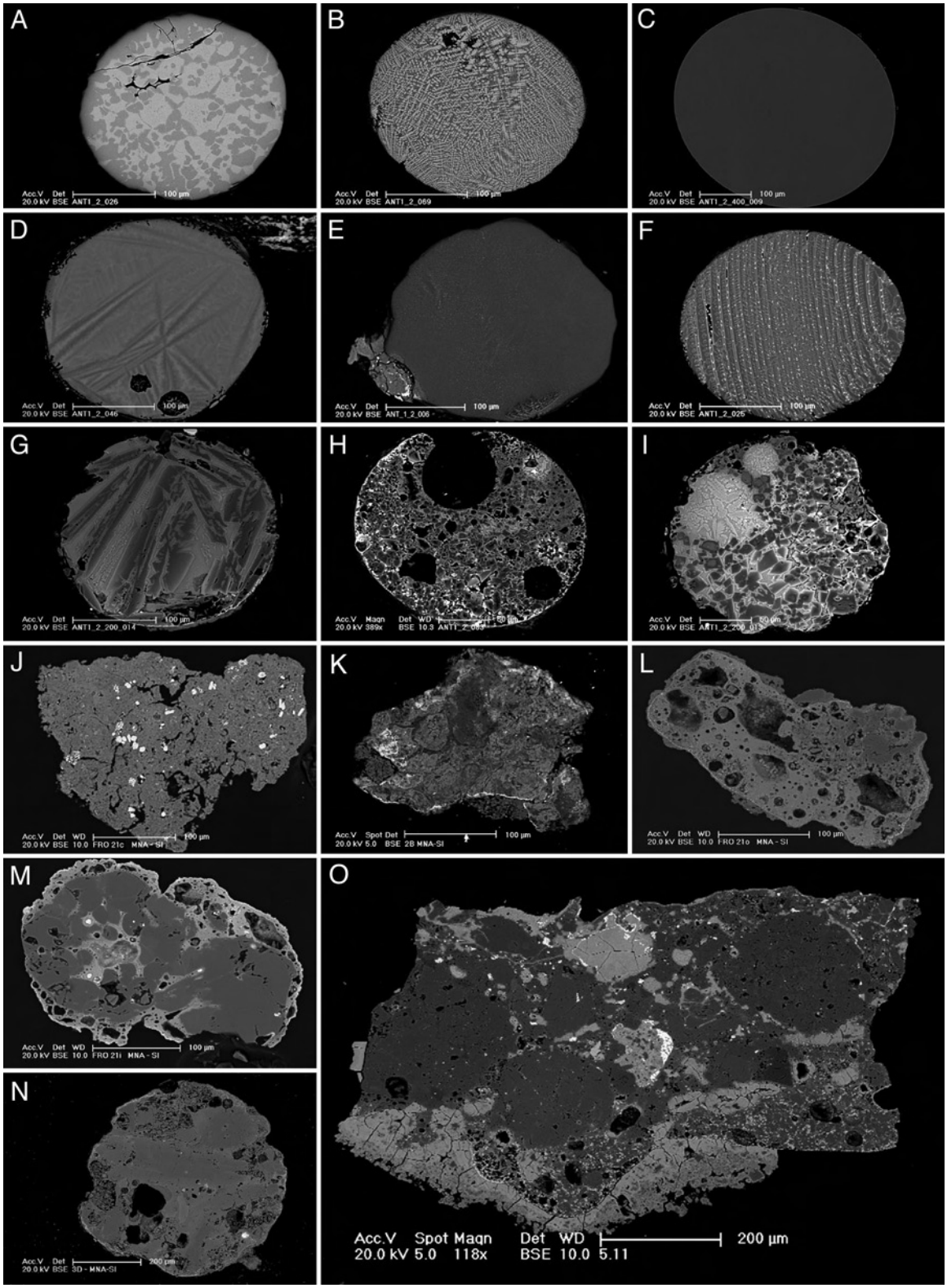

Fig. 4. An inventory of micrometeorite types in the Transantarctic Mountain collection (back-scattered electron images of sectioned and polished micrometeorites). (*A*) An I-type cosmic spherule dominated by magnetite and wüstite intergrowths. (*B*) A G-type cosmic spherule dominated by dendritic magnetite. (*C*) A V-type (vitreous) cosmic spherule (namely a CAT subtype) (2.9). (*D*) An S-type (stony) vesicular cryptocrystalline cosmic spherule (2.46). (*E*) An S-type microcrystalline cosmic spherule (2.6). (*F*) An S-type barred olivine cosmic spherule (2.25). (*G*) An S-type porphyritic cosmic spherule with relatively coarse-grained olivine microphenocrysts (2.14). (*H*) An S-type vesicular porphyritic cosmic spherule with relatively fine-grained olivine microphenocrysts (2.33). (*I*) An S-type, relict bearing, porphyritic olivine cosmic spherule (2.13). (*J*) A C1-type unmelted micrometeorite (see also Fig. 2*C*) (2.1c) (*K*) A C2-type fine-grained unmelted micrometeorite (2B). (*L*) A partially melted scoriaceous micrometeorite (2.1o). (*M*) An unmelted coarse-grained micrometeorite (2.1i) consisting of 2 porphyritic chondrules (see also Fig. S2). (*N*) An unmelted coarse-grained micrometeorite (3D) consisting of a single porphyritic chondrule. (*O*) An unmelted coarse-grained micrometeorite (5.11) with a chondritic structure (see also Fig. 2*D* and Fig. S2). Note that micrometeorites featured in *G–I* and *K–O* are partly or entirely mantled by magnetite rims.

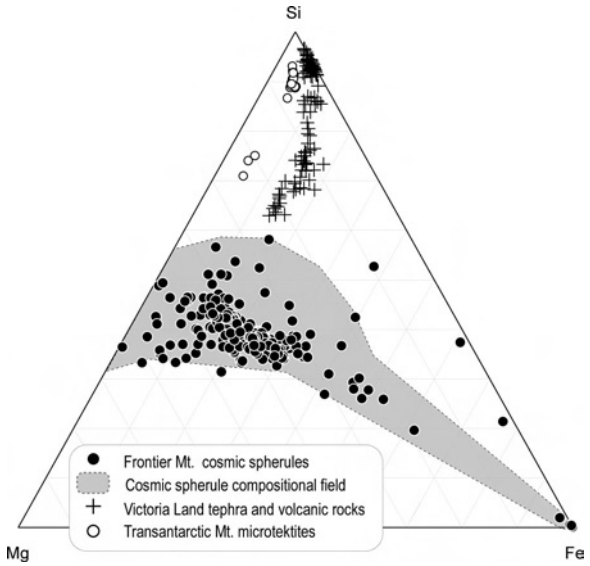

Fig. 5. Mg-Si-Fe (atoms) ternary diagram showing where Transantarctic Mountain micrometeorites (cosmic spherule from Frontier Mountain only) plot relative to other Antarctic, Greenland, and deep-sea cosmic spherules (18), Victoria Land tephra embedded in ice (24), and volcanic rocks (25), and Transantarctic Mountain microtektites (14).

includes cosmic spherules, and unmelted and scoriaceous micrometeorites.

A set of 233 spherules from the 200- to 400-μm size fractions of samples 2 and 3 includes 3% iron type (I-type) spherules consisting mainly of magnetite–wustite intergrowths (Fig. 4*A*), 1% G-type spherules consisting mainly of magnetite dendrites in a silicate glass mesostasis (Fig. 4*B*), 20% V-type spherules consisting of glass (Fig. 4*C*), and 76% S-type spherules consisting of glass, olivine (Fa_{1-47}), and magnetite assemblages with cryptocrystalline (including one Ca-Al-Ti-rich, CAT, spherule; Mg/Si = 1.73), barred and porphyritic olivine textures (Fig. 4 *D–I*). The statistics by type is therefore similar to the South Pole Water Well and Greenland collections (18), which are considered the least-biased collections so far known. The lack of enrichment in denser types (i.e., I- and G-types) and of depletion in lighter and more fragile types (V-types, including hollow spherules) is a further strong indication of minor wind sorting and weathering bias. The bulk composition of Frontier Mountain spherules is similar to that from other Antarctic and non-Antarctic collections and obviously distinct from both the volcanic fallout in the Frontier Mountain region and Transantarctic Mountain microtektites (Fig. 5).

Of the 13 and 12 angular-to-subrounded particles from the 200- to 800-μm fraction of samples 2 and 3, respectively, 7 consists of compact fine-grained mineral assemblages similar to the matrix of C1 (Fig. 4*J*) and C2 (Fig. 4*K*) carbonaceous chondrites, 12 are scoriaceous micrometeorites consisting of highly vesicular melt hosting sparse relic grains mainly of forsteritic olivine and enstatitic pyroxene up to $\approx$100 μm in size (Fig. 4*L*), and 6 are coarse-grained micrometeorites consisting mainly of forsterite and/or enstatite igneous crystals up to $\approx$300 μm in size. Remarkably, 1 of the latter contains 2 type-I porphyritic chondrules (Fig. 4*M* and Fig. S2) and another one (Fig. 4*N*) is a type-II chondrule consisting mainly of olivine ($Fa_{25.6}$), enstatite ($Fs_{20.8}$ $Wo_{2.0}$), chromite, and Fe-Ni metal (Ni = 5.4 wt%). Although possible chondrule-like objects have been described by other researchers in relatively small (< 200 μm) micrometeorites (e.g., ref. 21 and recent abstracts by S. Taylor and M. J. Genge), the relatively large size of Transantarctic Mountain micrometeorites allowed the unequivocal identification of chondritic structures for the first time (Fig. 4 *M* and *O*). This finding conclusively ties part of the micrometerite flux to chondritic material, likely carbonaceous and/or (in agreement with ref. 22) ordinary chondrites.

Six subrounded-to-subangular particles in the 800- to 2,000-μm size range from an additional sample from Frontier Mountain (sample 5) have ordinary chondritic structure and mineralogy. Four particles show readily-to-poorly delineated chondrules (Fig. 4*O*) typical of low- and intermediate-metamorphic grades (petrographic types 4 and 5), whereas 2 others exhibit coarse-grained granoblastic textures typical of high-grade metamorphism (petrographic type 6). The average olivine and low-Ca pyroxene compositions in the various particles varies from Fa_{18} Fs_{17} to Fa_{26} Fs_{22}, respectively, indicating H and L ordinary chondritic chemical classes. Other minerals include high-Ca pyroxene, chromite, Fe-sulfide, Ni-rich iron oxides (as likely weathering products on metal grains), and oligoclase (in granoblastic particles only). One H- and one L-chondritic particle are mantled by a quench-textured igneous layer similar to the fusion crust observed in stony meteorites; this layer is then mantled by a magnetite shell typically observed in unmelted or scoriaceous micrometeorites (Fig. 4*O* and Fig. S2). This is another outstanding finding that relates some of the extraterrestrial flux of micrometeorites to ordinary chondritic material also in the large 800- to 2,000-μm size fraction. The other 4 particles did not show a continuous magnetite shells and may possibly be fragments of even larger particles or meteorite ablation debris.

Remarkably, 2 identical, highly unusual particles (Fig. 3*B*) $\approx$700 μm in size were found on the top of Miller Butte. They mainly consist of a porous aggregate of spherules <50 μm in diameter. The spherules are dominated by magnetite dendrites in an olivine-rich silicate matrix (Fig. S3). The full characterization of these particles remains to be completed. Similar aggregates $\approx$20 μm in size (and/or disaggregated spherules) have been described previously in only 1 of the 2 extraterrestrial dust-rich layers in the Dome Fujii and EPICA Dome C (77°19′ S − 39°42′ E and 75°06′ S −123°21′ E, respectively; see Fig. 1*A Inset*) east Antarctic ice sheet cores, namely the 2,833- and 2,788-m-deep layers with a model age of 481 ± 6 kya (23). The unique characteristics of the above aggregates suggest that they are from the same event recorded in the ice cores, thereby documenting a continental scale distribution of the extraterrestrial debris associated with a major meteoritic event over the whole Antarctic continent.

The interior of the sectioned particles show no-to-moderate terrestrial weathering (Fig. S4) allowing the definition of micrometeorite types and compositions in all cases. For instance, complete barred and porphyritic olivine cosmic spherules occur together with others showing some loss of olivine at their margins, similarly to Novaya Zemlya cosmic spherules (9), whereas 1 G-type spherule showed some loss of glass. Scoriaceous and porous unmelted micrometeorites may contain secondary sulfate minerals (typically jarosite) encrustations on their external surfaces or in their voids. The metal grains in the micrometeorites of ordinary chondrite composition are variably substituted by iron oxides due to terrestrial weathering. The range of weathering levels attests to the varied terrestrial residence times of the different particles. The presence of a number of glassy cosmic spherules in our set is per se evidence in support of minor terrestrial weathering of the deposit (18).

Conclusions

We describe a unique collection of micrometeorites thought to originate through direct in fall on a continental surface, with minimal deposition of terrestrial material, apart from the local bedrock detritus, which can easily be distinguished from the

extraterrestrial material. Thanks to the very old exposure age of the collection surface (≥1 Myr), the studied trap has collected the long-term input of extraterrestrial material over a 0.1- to 1-Myr time interval, depending on the efficiency of the capture according to meteorological conditions and rock surface morphology. Despite their old terrestrial age, micrometeorites appear to have suffered little alteration, thanks to the dry and cold Antarctic plateau conditions, and the population shows no detectable size and compositional bias with respect to the most pristine micrometeorite collections at least in the size fractions (>200 μm) investigated in detail in this study. Future more detailed analyses of this collection are expected to provide a better definition of the composition of the long-term average extraterrestrial flux, compared with short-term (<1,000 yr) collections (in glacier ice) or weathering-biased collections (in deep sea sediments). Indeed, there are no long-term data on unmelted micrometeorites, whereas short-term collections may not sample the compositional flux variability induced by chaotic movements in source bodies (comets and asteroids). The finding of chondrules, ordinary chondritic material, and unique particles likely associated with a continental scale episodic meteoritic event ≈480 kyr ago within the thousands of "giant" micrometeorites (0.4–2 mm) so far found provides a hint of the great potential of the Transantarctic Mountain collection for remarkable advancements in micrometeorite study. We predict that our sampling of the micro-to-macrometeorite transition will bridge the gap between these 2 types of extraterrestrial materials, providing further insight into the paradox of their claimed distinct cometary versus asteroidal provenance.

ACKNOWLEDGMENTS. This work was supported by the Italian Programma Nazionale delle Ricerche in Antartide, the French Institut Polaire Paul Emile Victor, the French Institut National des Sciences de l'Univers–Centre National d'Études Spatiales Planetology program, and by the European Union through the Marie Curie Actions–RTNs ORIGINS (Project ID: 35519).

1. Brownlee DE (1981) in *The Sea* 7, ed Emiliani C (Wiley, New York), pp 733–762.
2. Engrand C, Maurette M (1998) Carbonaceous micrometeorites from Antarctica. *Meteoritics Planet Sci* 33:565–580.
3. Yada T, *et al.* (2004) The global accretion rate of extraterrestrial materials in the last glacial period estimated from the abundance of micrometeorites in Antarctic glacier ice. *Earth Planets Space* 56:67–79.
4. Murray J, Reynard AF (1891) in *Report on the Scientific Results of the H.M.S. Challenger During the Years 1873–76 (Deep-Sea Deposits)* (Neil and Company, Edinburgh), Vol 4, pp 327–336.
5. Blanchard MB, Brownlee DE, Bunch TE, Hodge PW, Kyte FT (1980) Meteoroid ablation spheres from deep see sediments. *Earth Planet Sci Lett* 46:178–190.
6. Maurette M, Jehanno C, Robin E, Hammer C (1987) Characteristics and mass-distribution of extraterrestrial dust from the Greenland ice cap. *Nature* 328:699–702.
7. Koeberl C, Hagen EH (1989) Extraterrestrial spherules in glacial sediment from the Transantarctic Mountains, Antarctica—Structure, mineralogy and chemical composition. *Geochim Cosmochim Acta* 53:937–944.
8. Harvey RP, Maurette M (1991) The origin and significance of cosmic dust from Walcott-Neve, Antarctica. *Proc Lunar Planet Sci Congress* 91:569–578.
9. Badjukov DD, Raitala J (2003) Micrometeorites from the northern ice cap of the Novaya Zemlya archipelago, Russia: The first occurrence *Meteoritic Planet Sci* 38:329–340.
10. Maurette M, *et al.* (1991) A collection of diverse micrometeorites recovered from 100 tonnes of Antarctic blue ice. *Nature* 351:44–47.
11. Duprat J, *et al.* (2007) Micrometeorites from Central Antarctic snow: The CONCORDIA collection. *Adv Space Res* 39:605–611.
12. Taylor S, Lever JH, Harvey RP (1998) Accretion rate of cosmic spherules measured at the South Pole. *Nature* 392:899–903.
13. Brownlee DE (1985) Cosmic dust: Collection and research. *Annu Rev Earth Planet Sci* 13:147–173.
14. Folco L, *et al.* (2008) Microtektites from Victoria Land Transantarctic Mountains. *Geology* 36:291–294.
15. Folco L, *et al.* The Frontier Mountain meteorite trap (Antartica) (2002) *Meteoritic Planet Sci* 37:209–228.
16. Welten KW, *et al.* (2008) Meteoritic and bedrock constraints on the glacial history of Frontier Mountain in northern Victoria Land, Antarctica. *Earth Planet Sci Lett* 270:308–315.
17. Folco L, Rochette P, Gattacceca J, Perchiazzi N (2006) In situ identification, pairing, and classification of meteorites from Antarctica through magnetic susceptibility measurements. *Meteoritic Planet Sci* 41:343–353.
18. Taylor S, Lever JH, Harvey RP (2000) Numbers, types, and compositions of an unbiased collection of cosmic spherules. *Meteoritic Planet Sci* 35:651–666.
19. Taylor S, Matrajit G, Lever JH, Joswiak DJ, Brownlee DE (2007) Size distribution of Antarctic micrometeorites, in *Workshop on Dust in Planetary Systems (ESA SP-643)*, eds Krueger H, Graps A (ESA Publications, Ithaca, NY pp145–148.
20. Braucher R, Lima CV, Bourles DL, Gaspar JC, Assad MLL (2004) Stone-line formation processes documented by in situ-produced ^{10}Be distribution, Jardim River basin, DF, Brazil. *Earth Planet Sci Lett* 222:645–651.
21. Genge MJ, Gilesky A, Grady MM (2005) Chondrules in Antarctic micrometeorites. *Meteoritic Planet Sci* 40:225–238.
22. Genge MJ (2008) Koronis asteroid dust within Antarctic ice. *Geology* 36:687–690.
23. Narcisi B, Petit JR, Engrand C (2007) First discovery of meteoritic events in deep Antarctic (EPICA-DOME C) ice cores. *Geophys Res Lett* 34, L15502, 10.1029/2007GL030801.
24. Curzio P, Folco L, Laurenzi MA, Mellini M, Zeoli A (2008) A tephra chronostratigraphic framework for the Frontier Mountain blue-ice field (northern Victoria land). *Quat Sci Rev* 27:602–620.
25. LeMasurier WE, Thomson JW (1990) Volcanoes of the Antarctic Plate and Southern Oceans in *Antarctic Res Ser* 48 (Am Geophys Union, Washington DC), pp 487.

Chapitre 4

Propriétés statistiques de la collection TAM

4.1 Article *Suavet et al., Polar Science*, 2009

Contribution de C. Suavet : Tamisage et tri par densité et magnétisme d'échantillons de sable. Sélection et pesée des micrométéorites. Photographies au microscope électronique à balayage et mesure des micrométéorites. Identification des textures et classification des micrométéorites. Analyses chimiques XRF et microsonde électronique. Etude des distributions en taille et de l'altération. Analyse des données. Ecriture de l'article.

Available online at www.sciencedirect.com
ScienceDirect
Polar Science 3 (2009) 100–109
http://ees.elsevier.com/polar/

Statistical properties of the Transantarctic Mountains (TAM) micrometeorite collection

Clément Suavet [a,*], Pierre Rochette [a], Myriam Kars [a], Jérôme Gattacceca [a], Luigi Folco [b], Ralph P. Harvey [c]

[a] *CEREGE, Aix Marseille Université, CNRS; Europôle Méditerranéen de l'Arbois, PB 80, 13545 Aix en Provence cedex 04, France*
[b] *Museo Nazionale dell'Antartide, Università di Siena, Siena, Italy*
[c] *Department of Geological Sciences, Case Western Reserve University, Cleveland, OH, USA*

Received 21 December 2008; revised 23 June 2009; accepted 25 June 2009
Available online 8 July 2009

Abstract

Micrometeorites have been recovered from traps located at the summit of nunataks in the Transantarctic Mountains (TAM), Antarctica. They constitute the TAM micrometeorite collection. Micrometeorites accumulated by direct infall for hundreds of thousands of years. This long collection duration is confirmed by the wide range of weathering by dissolution of olivine in the stony micrometeorites from the TAM collection. A statistical study of the size distribution and frequency by type of this collection, and comparison with other Antarctic micrometeorite collections (the South Pole Water Well collection and the Walcott Névé collec tion), suggest that the TAM collection is essentially unbiased. Thanks to the very long exposure of the traps, large diameter (>1000 μm) micrometeorites are present in sufficiently large numbers to allow a statistically meaningful estimate of their size distribution in this size range for the first time. We found that the slope of the size distribution remains constant in the 100–1600 μm size range. Therefore, the size distribution of micrometeorites in this size range is controlled by a single process.

Keywords: Antarctica; Micrometeorites; Size distribution; Weathering

1. Introduction

Micrometeorites are terrestrially collected extraterrestrial particles smaller than about 2 mm (Taylor et al., 2007). They constitute the main part of the mass flux of extraterrestrial matter accreted on Earth (Love and Brownlee, 1993; Taylor et al., 1998). Micrometeorites can be recovered from any terrestrial surface provided that the accumulation time is sufficient, weathering is low, and discrimination from terrestrial particles is feasible. Studied collections comprise samples taken from deep-sea sediments, seasonal lakes in Greenland, Antarctic eolian sedimentary traps, ice and snow, and continental sands (see review in Taylor and Lever, 2001; Duprat et al., 2007). Thanks to the very dry climatic conditions and the limited contamination by industrial or volcanic particles, Antarctica is one of the most productive areas for the recovery of micrometeorites. However, concentration processes or sampling methods can introduce biases in the collections. In order to study the influx of extraterrestrial matter to the Earth in terms of mass and composition, it is necessary to avoid these biases, or at least to quantify them. Biases in the particles' size in collections

* Corresponding author.

1873 9652/$ see front matter
doi:10.1016/j.polar.2009.06.003

can be evidenced with the study of the size distribution of micrometeorites. The exponent factor of the cumulative size distribution allows to estimate potential deficits by comparison with the least biased collections. Biases in the composition of the flux can be evidenced by a study of the frequency by type of melted micrometeorites (cosmic spherules), and with the ratio of unmelted to melted micrometeorites.

Rochette et al. (2008) reported the discovery of a new type of trap for micrometeorites at the summit of the Transantarctic Mountains (TAM) nunataks and presented a new collection: the TAM micrometeorite collection. The main characteristic of this collection is the very long exposure of the sedimentary traps, as evidenced by cosmogenic nuclides measurements (e.g., Rochette et al., 2008; Welten et al., 2008) and the presence of ~0.8 Myr old microtektites (Folco et al., 2008, 2009). Thanks to this long exposure, large micrometeorites are present in large numbers: 3500 micrometeorites with diameter > 400 μm, and 128 micrometeorites with diameter > 800 μm were counted as to date (December 2008). Based on the study of the cumulative size distributions of micrometeorites from Frontier Mountain in the >240 μm size range, Rochette et al. (2008) argued that the TAM collection is essentially unbiased. Indeed, the exponent slopes are close to that of the least biased micrometeorite collection known: the South Pole Water Well (SPWW) collection (Taylor et al., 2000, 2007). According to Taylor et al. (2007), the ratio of unmelted to melted micrometeorites is <0.1 for diameters > 150 μm, and it falls to <0.008 for diameters > 425 μm. In this study, we present in greater details the statistical properties size distribution in the 100 1600 μm size range, distribution by type of cosmic spherules, weathering grade and fracturing of the TAM collection. In order to highlight the singularity of the TAM collection, we compared it with the Walcott Névé collection.

2. Samples: origin and preparation

The TAM micrometeorite collection was recovered during the 2003 and 2006 *Programma Nazionale di Ricerche in Antartide* (PNRA) expeditions. The first samples were collected in 2003 at the summit (2700 masl) of Frontier Mountain (72°59.282′S 160°20.166′), from weathering pits (sample 3) or eroded granitic joints (samples 2, 4, 5, and 6). Fig. 1 features examples of such traps. More samples were collected in 2006 from joints at the summit (2600 masl) of Miller Butte (72°42.751′ 160°11.994′, sample 15), and from another location at the summit of Miller Butte (72°42.645′S 160°12.119′E), in weathering pits (samples 18a, 18b, 18c, 18d, and 18e) or eroded granitic joints (samples 19, 19a).

Micrometeorites were also extracted from ~180 g of sediment from a Walcott Névé moraine in order to compare with the TAM collection. The setting of the extraterrestrial particles rich sediments was described by Harvey and Maurette (1991). Concentration of extraterrestrial particles occurs at different locations around the Walcott Névé area of the Transantarctic Mountains, Victoria Land, Antarctica (Fig. 2). After they fall on fresh snow in Antarctica central regions, micrometeorites travel in the ice flow. When they reach the ablation zone of the glacier, they are transported downwind and downslope by strong katabatic winds to the eolian sediment traps: crests of moraines, weathering debris around boulders and exposed areas of snow.

Sediment samples were wet sieved at 100, 200, 400, 800 μm for Frontier Mountain and Walcott Névé samples, and at 400, 800 μm for Miller Butte samples. Fractions were separated using magnetic extraction for some samples (see Table 1). Walcott Névé sample was separated using heavy liquids (methylene iodide MI, $\rho = 3300$ kg/m^3) and the light fraction was further sorted by magnetic extraction. Micrometeorites were hand-picked under a binocular microscope.

3. Analytical methods

Micrographs of the micrometeorites were taken at CEREGE (Aix-en-Provence, France) with a scanning electron microscope (SEM, Hitachi S-3000N) using a 24 kV accelerating voltage, either with secondary electrons (SE) or backscattered electrons (BSE). Bulk chemical analyses were made using a Micro X-Ray Fluorescence (XRF) microscope (Horiba XGT-5000 at CEREGE, accelerating voltage 30 kV). The beam diameter is 100 μm or 10 μm. Beam penetration is of the order of 100 μm, so the analysis is an average of the weathered outer layer and the more pristine inner material. The XRF instrument is calibrated for a semi-infinite medium, therefore these analyses are only semi-quantitative. After these analyses, selected micrometeorites from Frontier Mountain, Miller Butte and Walcott Névé were embedded in epoxy and polished. SEM images of the sections were taken at CEREGE (Hitachi S-3000N, 24 kV acceleration voltage, BSE). Wavelength dispersive spectrometry (WDS) chemical analyses (Cameca SX 50, accelerating voltage 15 kV, beam current 10 nA) were

Fig. 1. The TAM micrometeorite traps. (A and D) eroded granitic joint at the summit of Miller Butte (sample 21 and sample 19 with author L. Folco, respectively). (B) Weathering pit at the summit of Miller Butte (sample 18c with author P. Rochette). (C) Detail image of the bottom of a granitic joint at the summit of Miller Butte (sample 16).

performed at Istituto di Geoscienze e Georisorse, CNR. U. O. Padova (Italy), on polished sections of micrometeorites from Frontier Mountain and Walcott Névé, and at Université Pierre et Marie Curie, Paris (France) on polished sections of Miller Butte micrometeorites.

4. Results

4.1. Types and chemical compositions

Chemical analyses allowed us to discard terrestrial materials and to confirm the extraterrestrial composition of the selected micrometeorites. It was also possible to identify iron cosmic spherules from the chemical analyses results. A major elements ternary plot (Fig. 3) of Frontier Mountain, Miller Butte and Walcott Névé particles with the compositional range of cosmic spherules (Taylor et al., 2000) shows that the particles identified as extraterrestrial have different composition from local volcanic rocks. Fig. 4 shows the distribution of molar Fe/(Mg + Si) for selected Frontier Mountain and Miller Butte micrometeorites, and for Walcott Névé and SPWW micrometeorites. Characteristic surface features of micrometeorites can be identified in whole particle SEM images. SEM images of the polished sections enabled classification of the micrometeorites into different categories (Genge

Fig. 2. Sampling site for the Walcott Névé micrometeorite collection, in a moraine downwind of an icefield. The sampling box is ~15 cm across.

et al., 2008) according to the texture: S-type (stony: barred olivine, porphyritic olivine, and cryptocrystalline textures), I-type (iron), G-type (dendritic magnetite in glass), V-type (glass). Table 1 shows the proportions of different types among cosmic spherules.

4.2. Size frequency distribution

The diameters of the spherules were estimated optically under the binocular microscope or from the SEM pictures. We assumed that the particles are ellipsoids with equal minor and intermediate axes ($a \geq b = c$). The diameter used in the size distribution is therefore $\sqrt[3]{a \cdot b^2}$. The slope exponent of the size distribution is calculated by the least squares method. For sample 3, the size distribution (Fig. 5A) only includes micrometeorites from the magnetic fraction. An aliquot of 7.8% of the 100 200 µm size range and the whole >200 µm magnetic fractions were studied. A composite size distribution was obtained by combining the whole >200 µm data with the 100 200 µm data multiplied by 12.8. The exponent slope of the size distribution is −4.5. In order to estimate the bias induced by the magnetic extraction, we compared the exponent slopes for the magnetic fraction and non-magnetic fraction of sample 18c in the 200 400 size range. As shown in Fig. 5B, the exponent slopes are not significantly different (−4.8 for the non-magnetic fraction, and −5.0 for the magnetic fraction). Fig. 5C presents the size distribution of sample 18c in the 200 800 µm size range. As

Table 1
Distributions by type for Frontier Mountain (FRO), Miller Butte (MIL), Walcott Névé (WAL) and South Pole Water Well (SPWW) cosmic spherules.

Sample	Size	Fraction	S type	G type	V type	I type	Number
FRO 2	>200 µm	*m*	78%	1%	16%	5%	169
3	>200 µm	–	84%	1%	14%	1%	85
4	>400 µm	*m*	*na*	*na*	*na*	1%	82
5	>400 µm	*m*	*na*	2%	*na*	3%	133
6	>400 µm	*m*	*na*	3%	*na*	5%	116
MIL 15	>400 µm	*m*	*na*	*na*	*na*	7%	87
18c	>200 µm	*m*	*na*	*na*	*na*	3%	920
18[a]	>400 µm	*m*	*na*	0.4%	*na*	4%	239
19	>400 µm	*m*	*na*	*na*	*na*	2%	95
19b	>400 µm	*m*	*na*	1%	*na*	2%	308
WAL	>100 µm	*hm*	83%	2%	10%	6%	126
SPWW	>100 µm	–	83%	1%	15%	1%	1130

m: only the magnetic fraction was studied; *hm*: separation was made with heavy liquids, the light fraction was further sorted magnetically; *na*: identification of this type was not attempted.
[a] Samples 18a, 18b, 18c, 18d and 18e considered together.

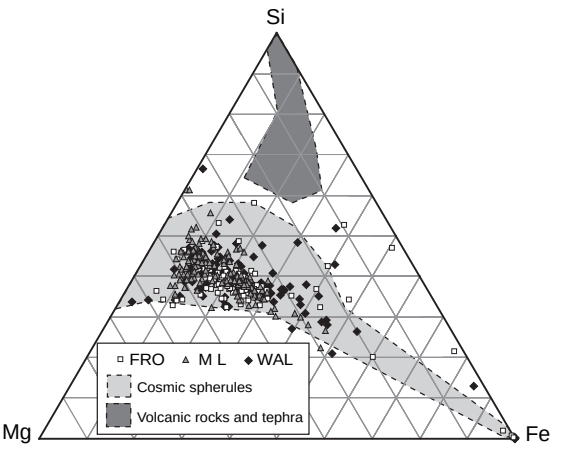

Fig. 3. Mg–Si–Fe (in atoms %, obtained by electron microprobe) ternary diagram showing where Transantarctic Mountain micrometeorites from Frontier Mountain and Miller Butte plot relative to other Antarctic, Greenland and deep sea cosmic spherules (Taylor et al., 2000), Victoria Land tephra embedded in ice (Curzio et al., 2008) and volcanic rocks (LeMasurier and Thomson, 1990).

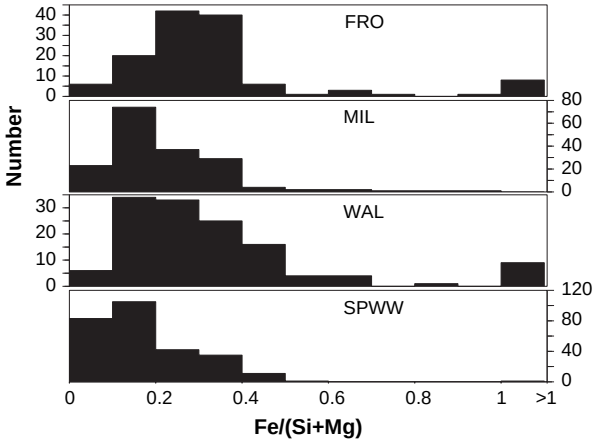

Fig. 4. Molar Fe/(Si + Mg) histograms for of Frontier Mountain (FRO) (magnetic extract), Miller Butte (MIL), Walcott Névé (WAL) (heavy fraction (methylene iodide, ρ 3300 kg/m^3) and magnetic fraction of the light fraction) and South Pole Water Well (SPWW) (Taylor et al., 2000) micrometeorites.

only half of the 200 400 μm size fraction was searched whereas the >400 μm size fraction was fully searched the distribution is a composite obtained by multiplying by 2 the data in the 200 400 μm size range. The exponent slope is −4.8. The size distribution of all TAM micrometeorites in the 400 800 μm size fraction for which diameter was measured (Fig. 5D) gives an exponent slope of −5.2. When only I-type micrometeorites of the TAM collection are considered, the slope is −6.3 (Fig. 5E). Due to the small number of particles available, the size distribution for micrometeorites larger than 1000 μm had never before been estimated reliably. The TAM collection offers a unique opportunity to study large micrometeorites. Fig. 6 shows SEM images of large cosmic spherules and unmelted micrometeorites from the TAM collection. The size distribution of all micrometeorites >800 μm from the TAM collection for which diameter was measured (Fig. 5F) has an exponent slope of −5.2. The Walcott Névé collection shows a −2.9 exponent slope on the 200 400 μm size range (Fig. 7).

4.3. Weathering and fractures

As seen on SEM images of the TAM micrometeorites, surface state indicates only moderate weathering, e.g. partial dissolution of olivine leading to spongy structure near the surface. In order to quantify this weathering, we measured the maximum depth at which olivine is dissolved in stony spherules from Frontier Mountain sample 2 and Walcott Névé sample. The depth was determined optically on SEM images of the polished sections of the particles (Fig. 8A and B). The histograms of maximum dissolution depth are shown in Fig. 8. Fractures are also visible on some spherules, they can be observed externally or on the section of the micrometeorite (Fig. 9). Despite their much younger age, Walcott Névé micrometeorites show more fractures (16% of micrometeorites) than Frontier Mountain sample 2 (6% of micrometeorites).

5. Discussion

From Fig. 4, micrometeorites with a molar Fe/(Mg + Si) > 1 seem to be over-represented in samples collected at Frontier Mountain. This bias is due to the magnetic separation used to collect micrometeorites. This is also the case for Walcott Névé micrometeorite collection, which was sorted by density and magnetism. The molar Fe/(Mg + Si) distribution for a Miller Butte sub-sample that did not experience separation is very close to that of the SPWW collection, except for a relative deficit of micrometeorites with ratios <0.1. This good agreement between SPWW and TAM collections indicates that micrometeorites recovered from the Transantarctic Mountains are representative of the extraterrestrial influx in term of bulk chemistry.

The proportions by types in the TAM collection are very similar to the SPWW collection, except for an enrichment in G- and I-type spherules when only the magnetic fraction was studied (G- and I-type spherules contain larger amounts of magnetite than S- and V-type). From samples for which the non-magnetic fraction was also searched, we can estimate an average proportion of the magnetic extract of 61% of the total number of spherules. Extrapolated G- and I-type proportions for the whole fraction (magnetic + non-magnetic) are closer to the SPWW values. The statistics for sample 3 are given for a representative sub-sample for which the non-magnetic fraction was also searched: the distribution is almost identical to that of the SPWW collection. The Walcott Névé collection shows an enrichment in G- and I-type spherules, and a deficit in V-type spherules. This bias may come from the separation method, but it could also be due to the concentration process, either during transportation in the ice flow, or at a later stage when particles were wind-blown.

The apparent deficit in the smaller and larger size range observed for a number of samples is due to

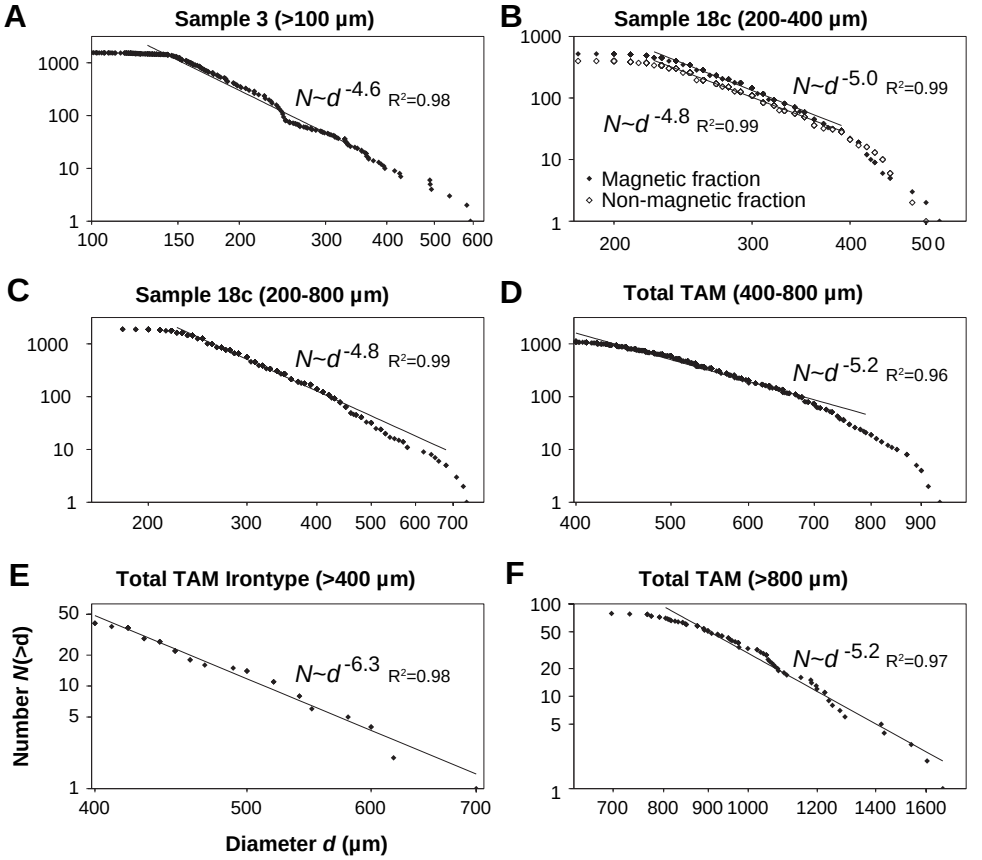

Fig. 5. Cumulative size distributions. A) Magnetic fraction of sample 3 in the >100 µm size range. The slope is calculated on the 130–350 µm size range. B) Sample 18c, 200–400 µm size range. The distributions of the magnetic and non magnetic fractions are plotted. The slopes are calculated on the 225–400 µm size range. C) Sample 18c, 200–800 µm size range. The number of micrometeorites in the 200–400 µm size range is the estimated number in the sample, as only half of that fraction has been studied. The slope is calculated for micrometeorites with diameter > 225 µm and with $N > 10$. D) Transantarctic Mountains samples, 400–800 µm size range. The slope is calculated on the whole 400–800 µm size range. E) Iron type micrometeorites from the Transantarctic Mountains collection with diameter > 400 µm. The slope is calculated on the whole size range. F) Transantarctic Mountains samples, >800 µm in size. The slope is calculated for all samples with diameter > 800 µm.

sieving: particles with a diameter slightly smaller than the mesh size may be retained in the smaller size fraction. Conversely, particles larger than the mesh size can break into the sieve thanks to an elongated shape, or mesh imperfections. This is the reason why the distribution curves are fitted only in the central part of the distribution.

The size distribution of samples 3 and 18c (200 800 µm size range) are slightly less steep than the −5.0 to −5.4 slopes of the SPWW collection (Taylor et al., 2007), which is the least biased collection known for cosmic spherules. The size distributions of sample 18c (200 800 µm size range), and of all TAM micrometeorites (400 800 µm and >800 µm size ranges), match very well that of the SPWW collection. Furthermore, the total numbers of micrometeorites counted (including cosmic spherules for which the diameter was not measured on SEM images): 3500 with diameters > 400 µm, and 128 with diameters > 800 µm, give a slope of −4.8. These results indicate that the TAM collection is essentially unbiased: no significant size bias (due to e.g. wind sorting) is affecting the TAM collection in the investigated sites.

The oscillation observed around 250 µm in the size distribution of the magnetic fraction of sample 3 may come from the method used to obtain a composite sample: as only part of the 100 200 µm fraction was actually searched, we had to multiply the number of spherules in the small fraction to scale it to that of the larger fraction. The effect of sieve mesh size is visible above the nominal threshold (200 µm) because

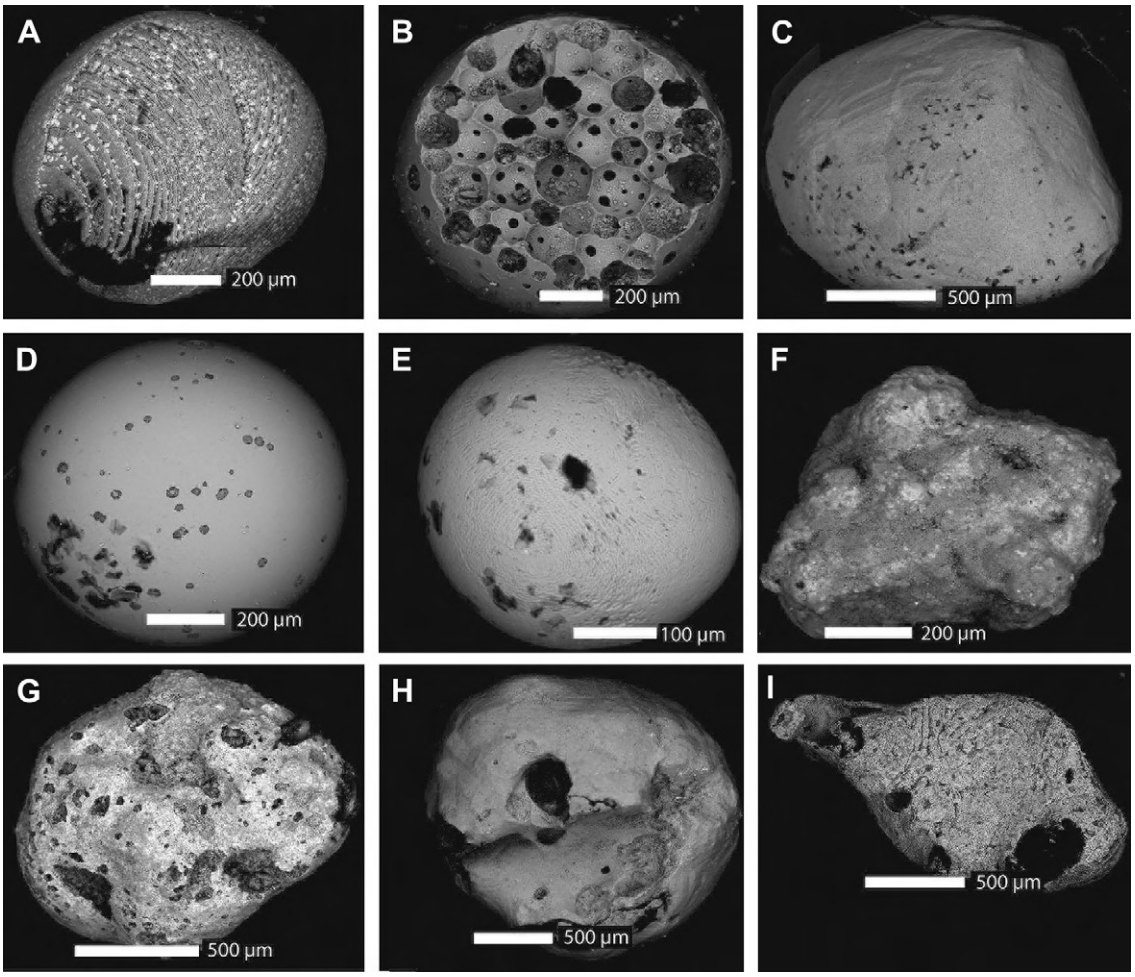

Fig. 6. Backscattered electron images of large micrometeorites. (A) Barred olivine cosmic spherule. (B) Glass cosmic spherule with "bubbles". (C) Barred olivine cosmic spherule with fine grains. (D) Glass cosmic spherule. (E) Iron cosmic spherule. (F and G) Large unmelted micro meteorites. (H) Barred olivine cosmic spherule with a flattened shape. (I) Barred olivine cosmic spherule with a "tail".

elongated spheroids can pass through a mesh size smaller than their long axis and because of imperfections of the mesh (some being significantly larger than 200 µm).

The fact that the exponent slopes for the distribution of the magnetic and non-magnetic fractions are similar indicates that the physical process controlling the size distribution is independent from the chemistry and density of the spherules. Indeed, the non-magnetic fraction is dominated by less dense glassy spherules, while the magnetic fraction is dominated by barred olivine (with porphyritic, G- and I-types) spherules. When only I-type micrometeorites are considered, the slope of the distribution is steeper, which was also noticed by Taylor et al. (2000).

The fact that the slope of the distribution is consistent in the 100 1600 µm size range suggests that a single process controls the size distribution of extraterrestrial particles in this size range. It is also a strong evidence to discard the breakup of larger meteoroids as the origin of the largest micrometeorites of the TAM collection, as the size distribution for meteorites has a very different −1.5 slope (calculated from Jull (2006)), which is the consequence of both preatmospheric size distribution and breakup during atmospheric entry.

Unlike the TAM samples, the Walcott Névé collection shows a strong deficit in smaller particles that cannot be accounted for by a sieving bias. Wind may blow smaller particles away and prevent them

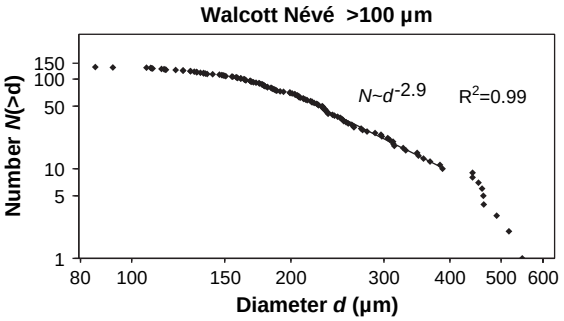

Fig. 7. Cumulative size distribution of Walcott Névé cosmic spher ules. The slope is calculated on the 200–400 µm size range.

from settling down in the moraines. Assuming that micrometeorites with diameter > 400 µm are not affected by this effect, the deficit would be 75% for 200 µm micrometeorites, according to the slope difference. The superficial dissolution observed in all Walcott Névé spherules is consistent with a likely young age. The range of dissolution is much wider for the TAM collection, as expected for micrometeorites with ages ranging from present to $\sim$1 Myr. The exposure ages for the traps (Rochette et al., 2008) were estimated with cosmogenic nuclides measurements, and from the total number of micrometeorites in the weathering pits of samples 3 and 18c normalized to pit surface and known accumulation flux, i.e. the collection duration.

Surface fractures on micrometeorites from the Walcott Névé may result from impact after wind transportation, while the penetrative fractures may be due to swelling or cryoclasty. Lower fracturing of the TAM collection is consistent with our assumption of negligible secondary wind transport, and the fact that the deposits are devoid of ice. The snow precipitation is removed by wind and sublimation without passing through liquid state.

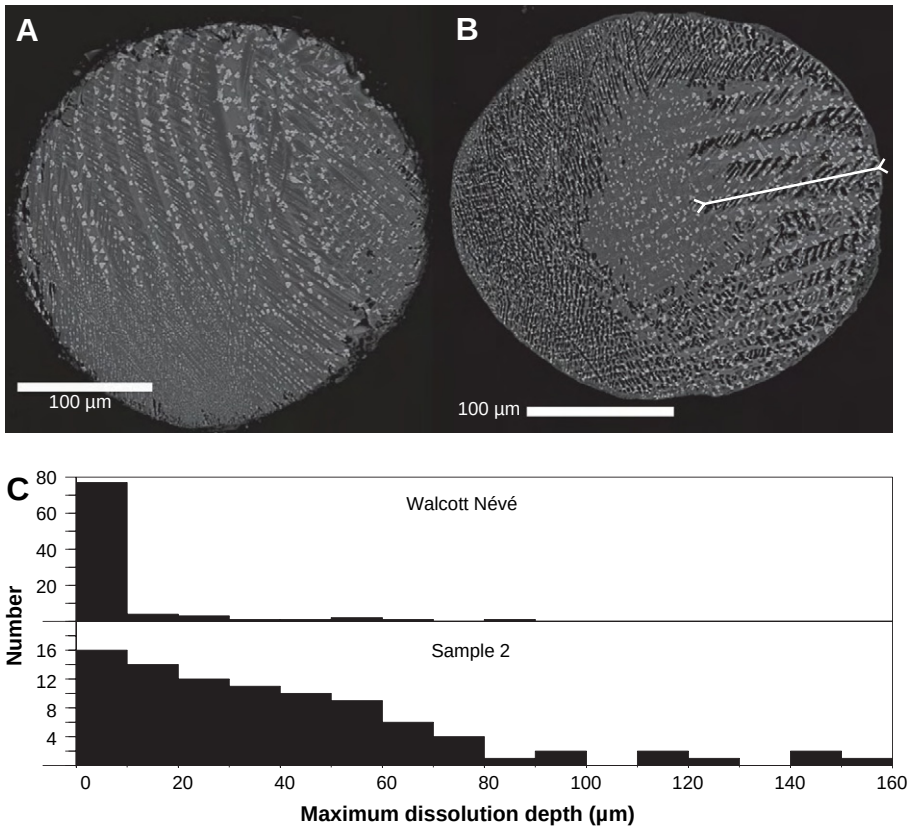

Fig. 8. A) Backscattered electron image of barred olivine cosmic spherule from Frontier Mountain that suffered little weathering. B) Back scattered electron image of barred olivine cosmic spherule from Frontier Mountain for which olivine has been etched by weathering, leaving only glass and magnetite grains. The ‘‘maximum dissolution depth’’ used for the histogram is indicated. C) Maximum dissolution depth distribution for TAM sample 2 (Frontier Mountain) and Walcott Névé collection.

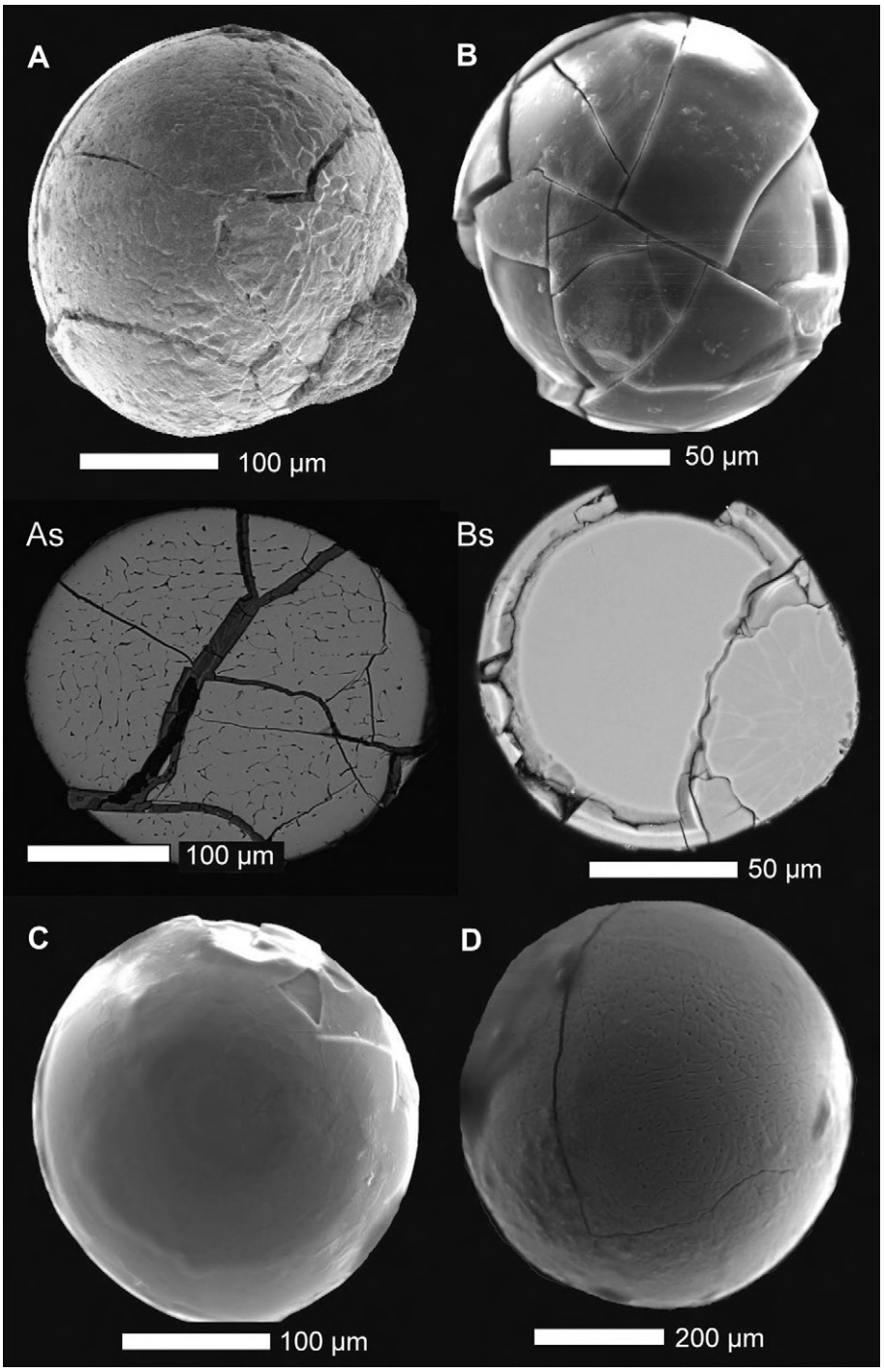

Fig. 9. Backscattered electron images of cosmic spherules from Frontier Mountain (A) and Walcott Névé (B, C and D) showing penetrative fractures (polished sectionc images As and Bs) and surface fractures (C and D).

6. Conclusion

The study of the distribution by type and size distribution of the TAM collection shows that this collection is essentially unbiased. The proportions for each type of cosmic spherules are similar to the least biased collections. Particularly, no deficit in glassy cosmic spherules seems to occur. The ~ -5 exponent

slope of the size distribution is similar to that of the least biased collections, and it is the same for the whole 100 1600 μm size range, which suggests that the size distribution of micrometeorites in this diameter range is controlled by a single process. The contrast with the features exhibited by the Walcott Névé secondary wind-blown concentration demonstrates that secondary concentration is very limited in the TAM collection.

The TAM collection provides researchers with a huge amount of micrometeorites, including a statistically significant number of particles with large diameters (>800 μm). The availability of such samples opens new horizons for destructive analyses such as laser-ablation oxygen isotope measurements on single micrometeorites or magnetic measurements (Suavet et al., 2008, 2009). The TAM collection also offers a great opportunity to study the composition of the flux of micrometeorites on the ~1 Myr time scale.

Acknowledgements

This work was supported by the Italian Programma Nazionale delle Ricerche in Antartide, the French Institut Polaire Paul Emile Victor, the French Institut National des Sciences de l'Univers Centre National d'Etudes Spatiales Planetology program, the European Union through the Marie Curie Actions RTNs ORIGINS (Project ID: 35519), and by the French Agence Nationale de la Recherche (Project ID: ANR-05-JCJC-0133).

References

Curzio, P., Folco, L., Laurenzi, M.A., Mellini, M., Zeoli, A., 2008. A tephra chronostratigraphic framework for the Frontier Mountain blue ice field (northern Victoria land, Antarctica). Quat. Sci. Rev. 27, 602–620.

Duprat, J., Engrand, C., Maurette, M., Kurat, G., Gounelle, M., Hammer, C., 2007. Micrometeorites from Central Antarctic snow: t he CONCORDIA collection. Adv. Space Res. 392, 605–611, doi:10.1016/j.asr.2006.05.029.

Folco, L., Rochette, P., Perchiazzi, N., D'Orazio, M., Laurenzi, M.A., Tiepolo, M., 2008. Microtektites from Victoria Land Trans antarctic Mountains. Geology 36, 291–294, doi:10.1130/G24528A.1.

Folco, L., D'Orazio, M., Tiepolo, M., Tonarini, S., Ottolino, L., Perchiazzi, N., Rochette, P., 2009. Transantarctic Mountain microtektites: geochemical affinity with Australasian micro tektites. Geochim. Cosmochim. Acta 73, 3694 3722, doi:10.1016/j.gca.2009.03.021.

Genge, M.J., Engrand, C., Gounelle, M., Taylor, S., 2008. The classi fication of micrometeorites. Meteorit. Planet. Sci. 43, 497–515.

Harvey, R.P., Maurette, M., 1991. The origin and significance of cosmic dust from the Walcott Névé, Antarctica. Lunar Planet. Sci. 21, 569–578.

Jull, A.J.T., 2006. Terrestrial ages of meteorites. In: Lauretta, D.S., McSween Jr., H.Y. (Eds.), Meteorites and the Early Solar System II. The University of Arizona Press, Tucson, pp. 889–905.

LeMasurier, W.E., Thomson, J.W., 1990. Volcanoes of the Antarctic Plate and Southern Oceans. In: Antarctic Res. Series 48. Amer ican Geophysical Union, Washington, pp. 487.

Love, S.G., Brownlee, D.E., 1993. A direct measurement of the terres trial mass accretion rate of cosmic dust. Science 262, 550–553.

Rochette, P., Folco, L., Suavet, C., van Ginneken, M., Gattacceca, J., Perchiazzi, N., Braucher, R., Harvey, R.P., 2008. Micrometeorites from the Transantarctic Mountains. Proc. Natl. Acad. Sci. USA 105, 18206–18211, doi:10.1073/pnas.0806049105.

Suavet, C., Rochette, P., Gattacceca, J., Folco, L., 2008. Microme teorites: a possible bias on the sedimentary magnetic record. Geochem. Geophys. Geosyst. 9, Q11002, doi:10.1029/2008GC002160.

Suavet, C., Gattacceca, J., Rochette, P., Perchiazzi, N., Folco, L., Duprat, J., Harvey, R.P., 2009. Magnetic properties of micro meteorites. J. Geophys. Res. 114, B04102, doi:10.1029/2008JB005831.

Taylor, S., Lever, J.H., 2001. Seeking unbiased collections of modern and ancient micrometeorites. In: Peucker Ehrenbrink, B., Schmitz, B. (Eds.), Accretion of Extraterrestrial Matter Throughout Earth's History. Kluwer Academic/Plenum Publishers, London, pp. 205–219.

Taylor, S., Lever, J.H., Harvey, R.P., 1998. Accretion rate of cosmic spherules measured at the South Pole. Nature 392, 899–903.

Taylor, S., Lever, J.H., Harvey, R.P., 2000. Numbers, types and compositions of and unbiased collection of cosmic spherules. Meteoritics Planet. Sci. 351, 651–666.

Taylor, S., Matrajt, G., Lever, J.H., Joswiak, D.J., Brownlee, D.E., 2007. Size distribution of Antarctic micrometeorites. Paper pre sented at Workshop on Dust in Planetary Systems, National Aeronautics and Space Administration, Kaua'i Hawai'i, 26–30 September.

Welten, K.C., Folco, L., Nishiizumi, K., Caffee, M.W., Grimberg, A., Meier, M.M.M., Kober, F., 2008. Meteoritic and bedrock constraints on the glacial history of Frontier Mountain in northern Victoria Land, Antarctica. Earth Planet. Sci. Lett. 270, 308–315.

Deuxième partie

Caractérisation Magnétique des Micrométéorites

Chapitre 5

Propriétés magnétiques des micrométéorites

5.1 Article *Suavet et al., Journal of Geophysical Research*, 2009

Contribution de C. Suavet : Photographies au microscope électronique à balayage et pesée des micrométéorites. Analyses chimiques XRF. Mesures des aimantations rémanentes naturelles, désaimantations thermiques et en champ alternatif. Saturation des micrométéorites, mesure des aimantations rémanentes à saturation et désaimantations en champ alternatif. Mesure des propriétés d'hystéresis. Mesure des susceptibilités magnétiques et de l'anisotropie de susceptibilité magnétique. Mesures de susceptibilité magnétique à différentes températures. Analyse des données. Ecriture de l'article.

JOURNAL OF GEOPHYSICAL RESEARCH, VOL. 114, B04102, doi:10.1029/2008JB005831, 2009

Magnetic properties of micrometeorites

C. Suavet,[1] J. Gattacceca,[1] P. Rochette,[1] N. Perchiazzi,[2] L. Folco,[3] J. Duprat,[4] and R. P. Harvey[5]

Received 28 May 2008; revised 14 December 2008; accepted 29 January 2009; published 4 April 2009.

[1] Most micrometeorites are strongly magnetic: the signal of a single micrometeorite may exceed the signal of a weakly magnetized standard sediment sample. Micrometeorites contain abundant magnetite, mostly produced by high-temperature oxidation during atmospheric entry. In this study, we carried out measurements on 520 micrometeorites (505 melted cosmic spherules, 6 partially melted scoriaceous micrometeorites, and 9 unmelted micrometeorites). The natural remanent magnetization and the saturation isothermal remanent magnetization have been measured, followed by alternating field or thermal stepwise demagnetization. The natural remanent magnetization is in the range of 0.4–300 A/m for cosmic spherules; it is a stable thermal remanent magnetization acquired by quenching in the Earth's magnetic field. The range is 3.8–16 A/m for scoriaceous micrometeorites and 78–525 A/m for unmelted micrometeorites, which may have preserved a preatmospheric magnetization. The magnetic susceptibility is in the range of 0.005–2.9 SI for cosmic spherules and is in the range of 0.06–0.12 SI for scoriaceous and unmelted micrometeorites. Temperature-dependent susceptibility analyses and thermal demagnetization indicate that magnetite is cation substituted in cosmic spherules. Different populations of magnetite grains may have different degrees of cation substitution within a single micrometeorite. Anisotropy of magnetic susceptibility measurements indicates that micrometeorites are strongly anisotropic (anisotropy degree >15%) and that most have oblate fabrics consistent with the parallel habit of magnetite in barred olivine cosmic spherules.

Citation: Suavet, C., J. Gattacceca, P. Rochette, N. Perchiazzi, L. Folco, J. Duprat, and R. P. Harvey (2009), Magnetic properties of micrometeorites, *J. Geophys. Res.*, *114*, B04102, doi:10.1029/2008JB005831.

1. Introduction

[2] Micrometeorites (MMs) are terrestrially collected extraterrestrial particles smaller than about two millimeters. They constitute the main part of the mass flux of extraterrestrial matter accreted on Earth [*Love and Brownlee*, 1993; *Taylor et al.*, 1998]. MMs have been found in deep-sea sediments, in seasonal lakes in Greenland, in Antarctic eolian sedimentary traps, ice and snow, and in continental sands (see *Taylor and Lever* [2001] for a review). Extraterrestrial matter is usually rich in iron (on average 20 wt% and up to 95%). In space, the major iron-rich phases are Fe-Ni alloys, iron sulfides and magnetite [e.g., *Rochette et al.*, 2008a]. Petrographic studies of MMs have shown that substituted magnetite is abundantly produced by atmospheric high-temperature oxidation of the primary iron bearing phases (metal, sulfide, olivine, and pyroxene) [*Love and Brownlee*, 1991; *Robin et al.*, 1992; *Toppani et al.*, 2001; *Toppani and Libourel*, 2003; *Genge et al.*, 2008]. Depending on the amount of melting and oxidation, most to all of the primary reduced iron-bearing phases will be transformed into magnetite, although relics of metal and sulfides are sometimes described in MMs. Melting occurs above a critical size of $\sim$100 μm, but unmelted to partially melted larger grains can be observed. Fully melted MMs are called cosmic spherules (CSs) owing to their spherical/ellipsoidal shape. Partially melted MMs have scoriaceous textures (ScMMs). The smallest particles experience little melting during atmospheric entry (unmelted fine-grained MMs (FgMMs) and coarse-grained MMs (CgMMs)). In this study, we measured the magnetic properties of 506 MM from different locations in Antarctica (490 CSs, 6 ScMMs, 7 FgMMs and 2 CgMMs), and 14 CSs from other origins (Greenland lake sediments and Pacific Ocean sediments). This is the first study of this kind, besides the measurement of 14 Iron-type cosmic spherules by *Marfaing et al.* [2008]. Owing to their continuous influx, MMs are a minor constituent of every surface material on Earth. The study of the magnetization and magnetic susceptibility distributions of MMs allowed *Suavet et al.* [2008] to estimate their potential contribution to the magnetic properties of sediments. The study of the magnetization of unmelted micrometeorites is also important to decipher potential preatmospheric magnetizations and to understand and

[1]CEREGE, Aix-Marseille Université, CNRS, Aix-en-Provence, France.
[2]Dipartimento di Scienze della Terra, Università di Pisa, Pisa, Italy.
[3]Museo Nazionale dell'Antartide, Universit di Siena, Siena, Italy.
[4]CSNSM, Orsay, France.
[5]Department of Geological Sciences, Case Western Reserve University, Cleveland, Ohio, USA.

0148-0227/09/2008JB005831$09.00

quantify the processes by which extraterrestrial materials acquired remanence in the Solar System.

2. Samples: Origin and Preparation

[3] In order to assess possible effects of terrestrial weathering, we analyzed samples with different terrestrial residence times (the time elapsed since the MMs fell on Earth) ranging from tens of years to hundreds of thousands of years, and different residence conditions on Earth. The studied collections are as follows:

[4] 1. MMs found in natural traps at the top of Frontier Mountain (204 CSs) and Miller Butte (180 CSs and 4 ScMMs), in the Transantarctic Mountains, Victoria Land, Antarctica [*Rochette et al.*, 2008b]. The samples were collected during the 2003 and 2006 PNRA (Programma Nazionale di Ricerche in Antartide) expeditions. These traps are believed to have sampled direct cosmic infall for several hundreds of thousands of years, as evidenced by the presence of ~0.8 Ma old microtektites [*Folco et al.*, 2008].

[5] 2. We analyzed 82 CSs and 1 ScMM that were extracted from eolian sediment traps on the crests of moraines of the Walcott Névé, Transantarctic Mountains, Antarctica [*Harvey and Maurette*, 1991]. These MMs were incorporated into snow that was compacted into firn and ice. They were transported in a glacial flow before it was ablated. The entrained MMs were then transported by wind and deposited in sedimentary traps on the crests of moraines.

[6] 3. 17 studied MMs (16 CSs and 1 ScMM) were sampled from surface snow of Dome C, Antarctica: these samples are part of the CONCORDIA collection [*Duprat et al.*, 2007]. The studied samples were extracted from the snow layers corresponding to years 1970 to 1980.

[7] 4. We analyzed 8 CSs, 7 FgMMs and 2 CgMMs found in the Cap Prudhomme blue ice fields, on the East Antarctic ice sheet [*Maurette et al.*, 1991]. This collection was obtained by melting hundreds of tons of blue ice. The MM were carried by the ice flow prior to their collection.

[8] 5. 11 CSs from Greenland seasonal lake sediments [*Maurette et al.*, 1986] were analyzed.

[9] 6. 3 CSs were extracted from Pacific deep-sea sediments that are curated at the Lamont-Doherty Earth Observatory Deep-Sea Sample Repository. The sediment samples were chosen from low sedimentation rate environments (0.08–0.2 cm/ka) of cores 5–38 (Eocene zeolitic clay, North East Pacific, 38°42.12′N, 140°21.27′W) [*McManus et al.*, 1970] and 16–160 (Pleistocene zeolitic clay, from the west flank of the East Pacific Rise, 11°42.27′N, 130°55.81′W) [*van Andel et al.*, 1973].

[10] For Frontier Mountain, Miller Butte, Walcott Névé and Pacific Ocean sediments, the MMs were extracted using different techniques depending on the original sample, after wet sieving at 200, 400, 800 μm (400, 800 μm for Miller Butte). The fractions were separated using heavy liquids (methylene iodide, ρ = 3300 kg/m^3) and the light fraction was further sorted by magnetic extraction (which therefore excluded this fraction from natural remanent magnetization (NRM) analyses). The Miller Butte sample was the only one that did not require further separation after sieving owing to its high concentration of cosmic particles. Potential extraterrestrial particles were handpicked under a binocular microscope. Selection was made according to the morphology of the particles.

3. Analytical Methods

[11] Micrographs of the MMs were taken at CEREGE (Aix-en-Provence, France) with a scanning electron microscope (SEM, Hitachi S-3000N) using a 24 kV accelerating voltage, either with secondary electrons (SE) or backscattered electrons (BSE). A number of physicochemical analyses were performed on the samples. The largest MMs were directly weighed using a micro balance (1 μg precision). Bulk chemical analyses were made using a Micro X-Ray Fluorescence (XRF) microscope (Horiba XGT-5000 at CEREGE, accelerating voltage 30 kV). The analyses are performed with a 100 μm or 10 μm diameter beam. Beam penetration is of the order of 100 μm, so the analysis is an average of the weathered outer layer and the pristine inner material. The XRF instrument is calibrated for a semi-infinite medium, therefore these analyses are semiquantitative. All magnetic measurements were performed at CEREGE. The NRM and saturation isothermal remanent magnetization (sIRM), which was imparted in an inducing field of 1 T, were measured on MMs with a 2G Enterprises DC Squid cryogenic magnetometer. The magnetic moment of the sample holder is in the range of 7.9×10^{-12}–1.1×10^{-10} Am^2, with a median value of 3.2×10^{-11} Am^2. After saturation, the IRM of the sample holder is in the range of 4.32×10^{-10}–1.9×10^{-9} Am^2, with a median value of 6.9×10^{-10} Am^2. The reproducibility is within a range of $\pm 2.8 \times 10^{-12}$–1.2×10^{-11} Am^2, with a median value of $\pm 5.7 \times 10^{-12}$ Am^2. Some samples were subjected to stepwise alternating field demagnetization of NRM and sIRM (at 2, 4, 6, 8, 10, 15, 20, 25, 30, 40, 50, 60, 80, and 100 mT), or thermal demagnetization of sIRM (at 200, 250, 300, 380, 400, 415, 480, 500, 530, 560 and 580°C). For thermal demagnetization, samples were wrapped in aluminum foil after saturation, and during the whole process of heating and measurement of moment. The magnetic moment of the aluminum foil is $9 \pm 5 \times 10^{-11}$ Am^2. Hysteresis parameters were measured with a Princeton Measurements Corporation (PMC) Alternating Field Magnetometer (AGM) with a peak field of 0.3 T or 0.5 T for the hysteresis loop (noise level of $\sim 10^{-11}$ Am^2). A systematic correction was made for the sample holder (measured at least once per measurement session). However, the effect of this correction on hysteresis parameters values is small (±0.02 on the ratio of saturation remanent magnetization and saturation magnetization, ±0.3 mT on the value of the coercive field). Some of the largest samples (FRO1, FRO2 146–158, FRO3 7–22, see Data Set S1 in the auxiliary material)[1] were measured with a PMC Vibrating Sample Magnetometer (VSM) with a peak field of 0.5 T (noise level of $\sim 10^{-9}$ Am^2).[1] Magnetic susceptibility was measured with a KLY 2 Kappabridge (noise level of $\sim 5 \times 10^{-13}$ m^3) or MFK1-FA magnetic susceptibility meter for some samples (noise level of $\sim 3 \times 10^{-13}$ m^3). The sample holder was measured frequently (every 2–3 samples) to cancel the effect of the instrumental drift. We measured

[1] Auxiliary material data sets are available at ftp://ftp.agu.org/apend/jb/2008jb005831. Other auxiliary material files are in the HTML.

sample 05-13-01 (total magnetic susceptibility = 5.4×10^{-12} m^3) with the MFK1-FA meter at different times during the measurement session (20 measurements) to evaluate reproducibility. The standard deviation of these measurements is $\sigma = 1.6 \times 10^{-13}$ m^3. The anisotropy of magnetic susceptibility was measured on the largest samples using the MFK1-FA meter. Temperature-dependent magnetic susceptibility analyses were performed in an argon atmosphere on 6 samples using the MFK1-FA meter equipped with a CS3 furnace (a furnace correction was made on the data). After these analyses, MMs from Frontier Mountain, Miller Butte, Walcott Névé and the Pacific Ocean were embedded in epoxy and polished. SEM images of the sections were taken at CEREGE (Hitachi S-3000N, 24 kV acceleration voltage, BSE). Wavelength dispersive spectrometry (WDS) chemical analyses (Cameca SX 50, accelerating voltage 15 kV) were performed at Istituto di Geoscienze e Georisorse Padova, Italy, on polished sections of MM samples from Frontier Mountain and Walcott Névé, and at Université Pierre et Marie Curie, Paris, France, on polished sections of MM samples from Miller Butte. Two CSs, representative of iron and stony spherules, were studied through synchrotron X-Ray diffraction data, collected at BM8-GILDA beamline, ESRF, Grenoble. A monochromatic beam (λ = 0.6904 Å for the stony particle and λ = 0.7761 Å for the iron particle, calibrated against X-Ray absorption of pure metal foils) was used and the diffractions were collected with a Fuji Imaging-Plate (IP) detector. The beam dimension on the sample was 0.2 × 0.2 mm. The sample to detector distance and the image plate tilt were calibrated with X-Ray powder diffraction of standard LaB_6 (NIST-SRM 660a). Data were collected up a *d*-space resolution of ~0.8 Å for both data sets, and reduced with the Fit2D software [*Hammersley*, 1997]. Phase identification was performed through the EVA (Bruker-AXS) software. A Rietveld study was performed through the TOPAS software (A. A. Coelho, TOPAS-ACADEMIC, 2004) to determine the relative abundances of the phases.

4. Characterization of Micrometeorites

[12] Chemical analyses confirm that all spherules in our samples are of extraterrestrial origin. Such origin (with respect to impact, volcanic or anthropogenic spherules) is evidenced by the presence of Ni and Cr, the abundance of Mg (Mg ≫ Al, and Mg ≈ Si), and the very low level of Ti, K, Al with respect to terrestrial matter. For unmelted angular material, morphology is less distinctive and the chemical analysis was necessary to distinguish between terrestrial (e.g., tephra) and extraterrestrial particles. Figure 1 presents a Mg-Si-Fe (atoms) ternary plot of the Antarctic CSs we have studied, with the compositional range of Greenland,

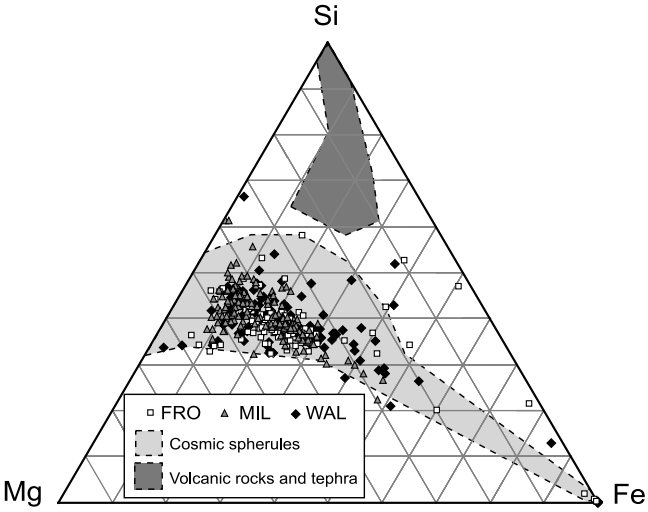

Figure 1. Mg-Si-Fe (atoms) ternary diagram presenting the wavelength dispersive spectrometry chemical analyses results for Frontier Mountain, Miller Butte, and Walcott Névé micrometeorites. Local volcanic rocks [*LeMasurier and Thomson*, 1990] and tephra [*Curzio et al.*, 2008] have a different compositional range, which allows distinction between extraterrestrial and terrestrial particles. Particles outside the compositional range of cosmic spherules [*Taylor et al.*, 2000] have been identified as micrometeorites on the basis of their texture.

other Antarctic and deep sea CSs [*Taylor et al.*, 2000]. This range is distinct from that of local volcanic rocks [*LeMasurier and Thomson*, 1990] and tephra [*Curzio et al.*, 2008]. Very minor fly ashes may be emitted in Antarctica from the activity of permanent stations (from welding, waste incineration, vehicles) or large ships, but our major Antarctic sampling site (TAM) was at >100 km from the coast or any permanent station. In the other sites care was taken to avoid pollution from the surface layers, and sampling sites were upwind from Antarctic stations. Despite the high-altitude injection of volcanic tephra from South American volcanoes in Antarctica, *Basile et al.* [2001] have shown that the maximum diameter for these particles is 50 μm. Therefore, the presence of fly ashes in our samples is highly improbable in the size range we studied. Characteristic surface features of MMs can be identified in whole particle SEM images (Figure 2, samples CSa–CSe). The volume has been estimated using whole particles SEM images, assuming that the semiminor axes are equal for spherules, or using a different geometry for particles with a noneven shape. SEM images of the polished sections enabled classification of the MMs into different categories. The main factor determining

Figure 2. Scanning electron microscope backscattered electron images of polished sections (except for the whole spherules when specified as secondary electron (SE)) of cosmic spherules. CSa is barred olivine cosmic spherule FRO2-007 (SE) with visible bars, CSb is cryptocrystalline cosmic spherule FRO2-006 (SE) with knobbly protrusions, CSc is porphyritic olivine cosmic spherule 03-40-17 (SE) with olivine microphenocrysts, CSd is I-type cosmic spherule FRO2-090 (SE), and CSe is G-type cosmic spherule FRO2-071 (SE). Barred olivine (BO) cosmic spherules. BOa is WAL-015, BOb is FRO2-013, BOc is FRO2-037, BOd is FRO2-113, and BOe is WAL-038. Porphyritic olivine (PO) cosmic spherules. POa is WAL-079, POb is FRO2-085, POc is FRO2-092, POd is FRO2-115, and POe is FRO2-075. Cryptocrystalline (CC) cosmic spherules. CCa is WAL-060, CCb is WAL-011, and CCc is WAL-119. V-type (V) cosmic spherules. Va is 03-40-06 and Vb is MIL-135. I-type (I) cosmic spherules. Ia is FRO2-028, Ib is FRO2-026, Ic is WAL-009, Id is FRO2-090, and Ie is FRO2-016. G-type (G) cosmic spherules. Ga is MIL-073, Gb is MIL-087, Gc is FRO2-071, Gd is WAL-059, and Ge is FRO2-039.

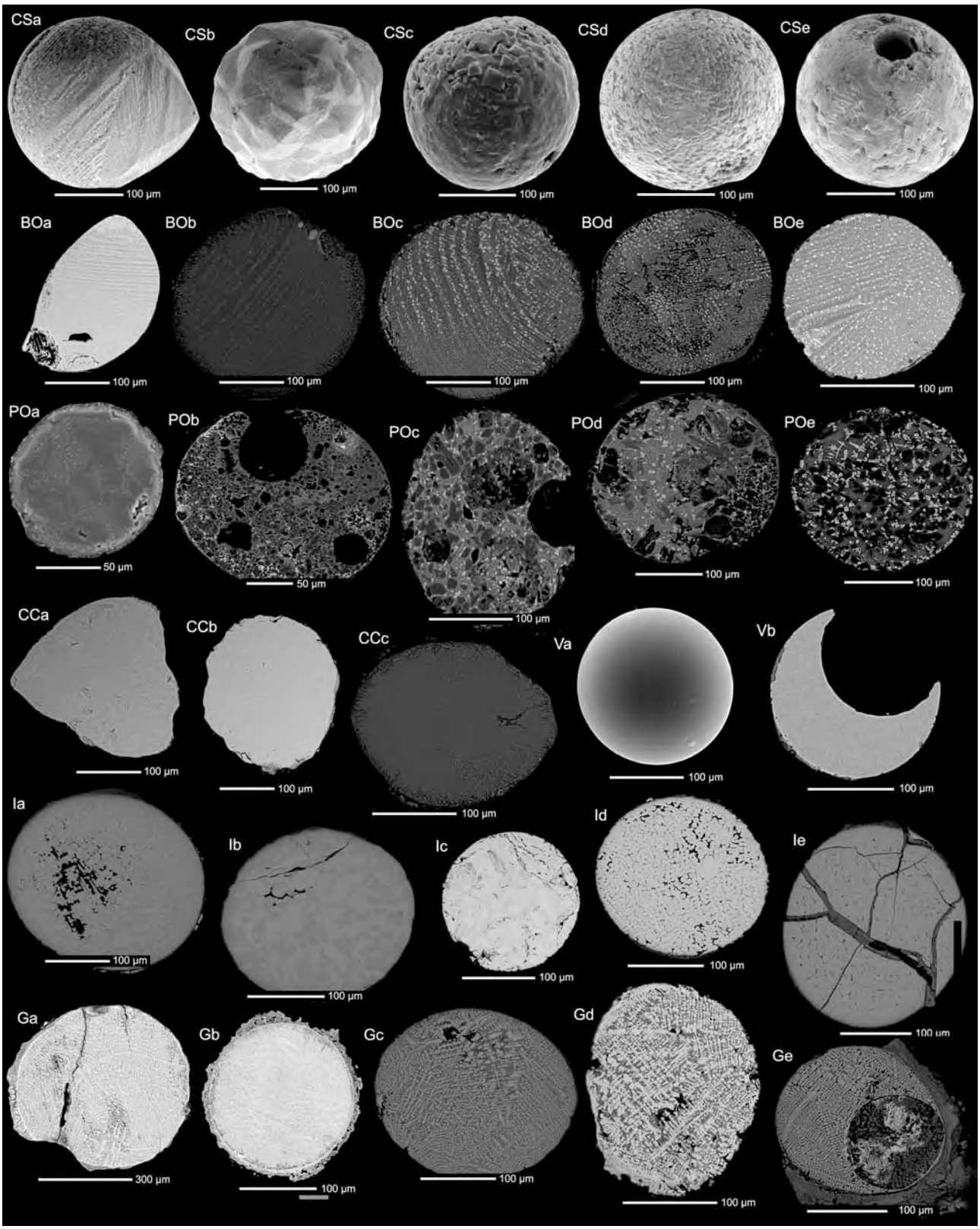
CSa
CSb
CSc
CSd
CSe
BOa
BOb
BOc
BOd
BOe
POa
POb
POc
POd
POe
CCa
CCb
CCc
Va
Vb
Ia
Ib
Ic
Id
Ie
Ga
Gb
Gc
Gd
Ge
100 µm
50 µm
300 µm

Figure 2

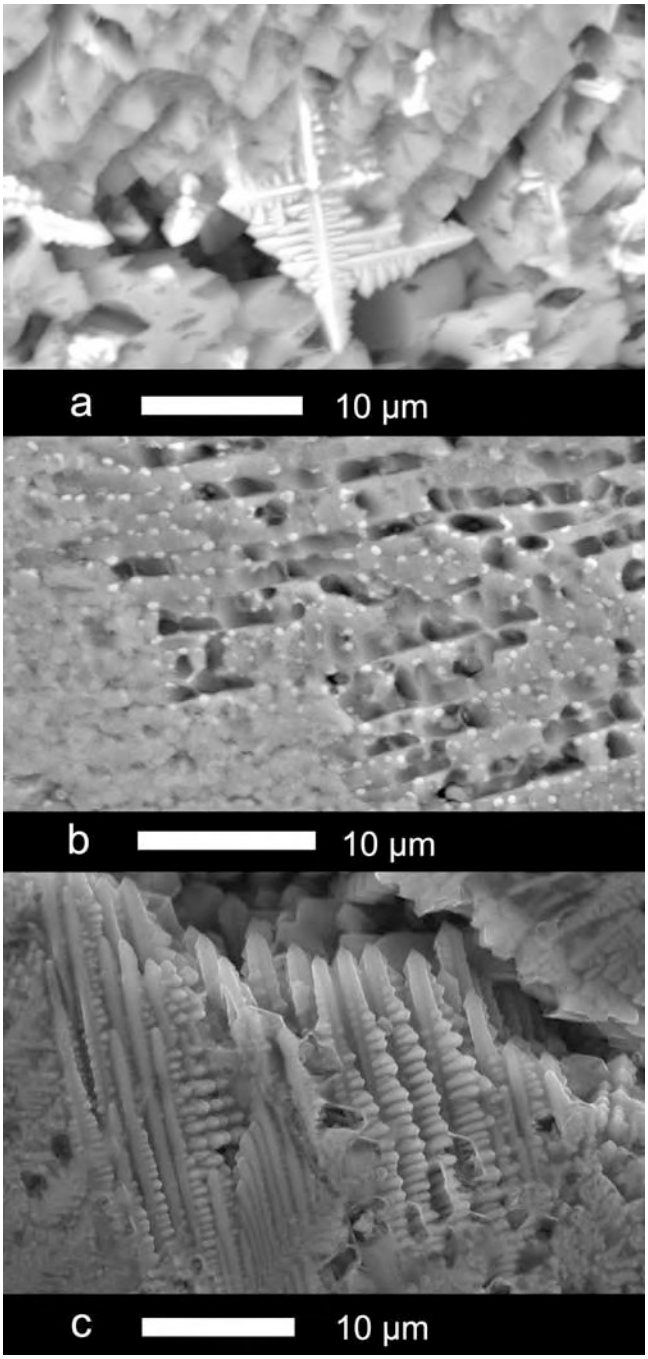

Figure 3. Close up scanning electron microscope backscattered electron images of magnetite grains on the surface of barred olivine cosmic spherules. (a) Magnetite dendrite. (b) Small magnetite grains (<1 μm). (c) Large magnetite dendrites (>10 μm).

the texture of micrometeorites is the extent of thermal reprocessing during atmospheric entry [*Genge et al.*, 2008].

[13] The most common CSs are S-type (stony). Their composition is broadly chondritic [*Genge et al.*, 2008]. They are dominated by olivine microphenocrysts, silicate glass and magnetite and/or chromite, and they can also contain relict grains that survived atmospheric entry. Depending on the texture, S-type CSs can be subdivided into subclasses. Barred olivine CSs (BO) are dominated by parallel growth olivine within a glassy mesostasis with magnetite (Figure 2, samples BOa–BOe). Porphyritic olivine CSs (PO) are dominated by olivine microphenocrysts within a glassy mesostasis with accessory magnetite/chromite, and relict olivine grains are commonly found (Figure 2, samples POa–POe). Cryptocrystalline CSs (CC) contain micron to submicron olivine crystals and magnetite grains (Figure 2, samples CCa–CCc). V-type (glass) CSs do not contain olivine microphenocrysts (Figure 2, samples Va and Vb). Figure 3 shows close up SEM images of magnetite grains at the surface of BO CSs. Dendrites of magnetite can have sizes up to a few tens of μm, whereas the smallest grains are <1 μm.

[14] I-type (iron) CSs contain iron oxides wüstite and magnetite [*Genge et al.*, 2008] (Figure 2, samples Ia–Ie). In rare cases metal cores have been described, but none were observed in this study or in that of *Marfaing et al.* [2008].

[15] G-type CSs are dominated by dendritic magnetite within a mesostasis of silicate glass [*Genge et al.*, 2008] (Figure 2, samples Ga–Ge).

[16] ScMMs are highly vesicular particles consisting mainly of microporphyritic olivine crystals in a silicate glass (Figure 4, samples SCa–SCe), often containing crystal and/or lithic relics. They are surrounded by a magnetite rim that is produced during the atmospheric entry.

[17] The most heated unmelted MMs also have a magnetite rim. Fine-grained micrometeorites (FgMMs) (Figure 4, samples FGa–FGd) are dominated by a groundmass similar to the fine-grained matrices of chondritic meteorites, whereas coarse-grained micrometeorites (CgMMs) (Figure 4, samples CGa–CGb) are dominated by anhydrous silicate grains larger than $\sim$1 μm.

[18] In order to check the presence of magnetic phases other than magnetite, one I-type CS and one S-type CS were studied through synchrotron X-Ray diffraction (Figure 5). Phase identification shows that the I-type particle is made of magnetite and minor wüstite, whereas the S-type particle is constituted of forsterite and minor magnetite. The possible presence of other magnetic phases was carefully checked but none were revealed. A Rietveld study (see Figure S1 in the auxiliary material) allowed us to determine the relative abundance of the identified phases, namely, not accounting for the presence of a possible amorphous component: the I-type spherule has a magnetite to wüstite ratio of 89:11, whereas the S-type particle has a forsterite to magnetite ratio of 97:3. The scrutiny of refined cell parameters allows us to get information on the crystal chemistry of the constituting phases. For the I-type particle, refined cell parameters for magnetite and wüstite are respectively $a = 8.404(1)$ Å and $a = 4.298(1)$ Å, which compare well with the literature data for these phases, indicating that both magnetite and wüstite are pure phases. For the S-type particle, the refined cell parameters for magnetite is $a = 8.382(1)$ Å, which is smaller than the value for pure magnetite. This indicates substitution of magnetite, but the substitution degree and the substitute elements cannot be deduced from these measurements.

5. Magnetic Properties

[19] In order to characterize MMs in terms of magnetic mineralogy, we measured the "S ratio" $S_{0.3}$ of 10 stony CS samples from Frontier Mountain: it is the IRM obtained

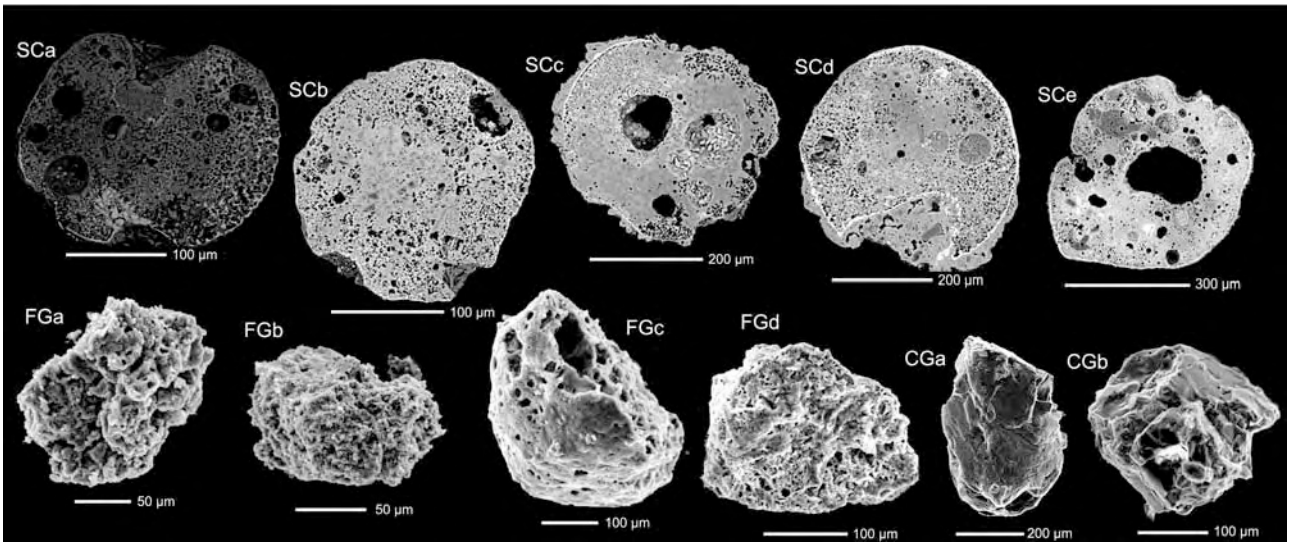

Figure 4. Scanning electron microscope backscattered electrons images of scoriaceous micrometeorites and secondary electron images of unmelted micrometeorites. Scoriaceous (SC) micrometeorites. SCa is FRO2-107, SCb is MIL-040, SCc is MIL-082, SCd is MIL-090, and SCe is MIL-144. Fine-grained (FG) unmelted micrometeorites. FGa is 05-37-02, FGb is 05-37-19, FGc is 05-37-10, and FGd is 05-37-23. Coarse-grained (CG) unmelted micrometeorites. CGa is 05-37-14 and CGb is 05-37-22.

after applying a 3 T field and then a back field of −0.3 T normalized to the 3 T IRM. The S ratios are in the range 0.94–1.00, with a mean value of 0.98. Such high values are typical of magnetite.

[20] Temperature-dependent magnetic susceptibility analyses performed on 6 Miller Butte CSs (Figure 6) allow us to estimate Curie temperatures (T_c). According to *Petrovský and Kapièka* [2006], the commonly used two-tangent method [*Grommé et al.*, 1969] overestimates T_c by up to a few tens of degrees. They recommend to define T_c as the intersect of the linear fit to inverse susceptibility and the temperature axis, when linear behavior of inverse susceptibility is observed. We estimated T_c with both methods (Table 1): the inverse susceptibility method yields values in the range of 517–552°C, whereas the two-tangent method yields values in the range of 500–585°C. The Curie temperatures for BO samples MIL-036, MIL-051, MIL-127 are ∼60°C below the 580°C expected for pure magnetite [*Dunlop and Özdemir*, 2001], which indicates that magnetite in these samples contains impurities. WDS bulk analyses indicate the presence of Ni, Cr and Ti. These elements can be substituted for Fe in magnetite. Unfortunately, we could not measure single magnetite grains with the microprobe, but we observed that measurements averaged on magnetite grains and silicate surrounding minerals reveal higher concentrations of these elements than measurements on silicates. *Robin et al.* [1992] analyzed single magnetite grains in micrometeorites using a SEM with energy dispersive spectrometer: the range is 0–3% for NiO, 0–20% for Cr_2O_3 and 0–1% for TiO. The Curie temperatures of BO samples MIL-118 and MIL-004, and G-type sample MIL-073 are closer to 580°C, which indicates that magnetite in these samples contains less impurities than for other samples. However, WDS bulk analyses do not reveal differences in the chemical composition of these samples.

[21] Thermal demagnetization of sIRM (Figure 7) measured on 13 CSs gives maximum blocking temperatures in

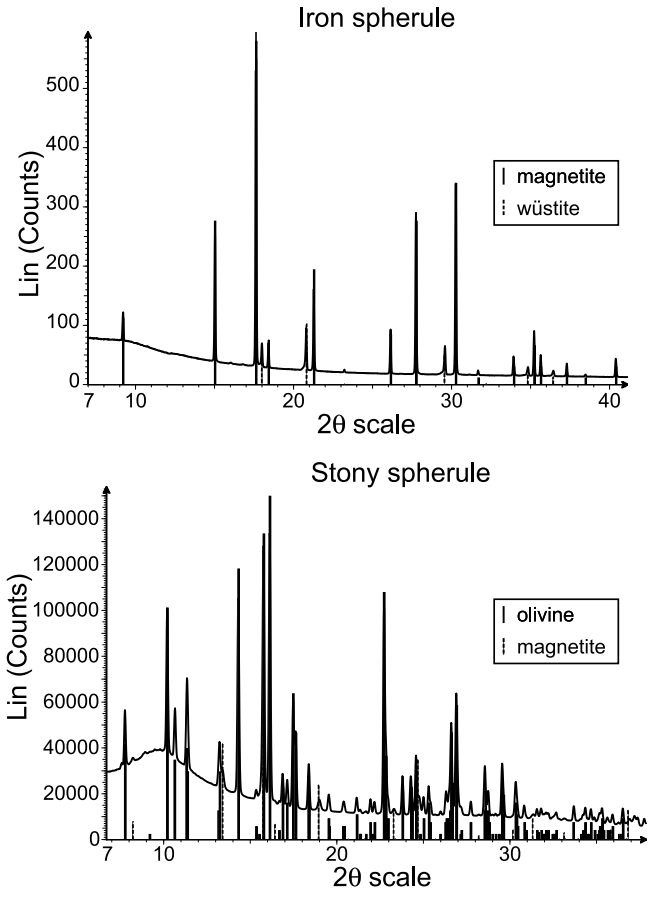

Figure 5. X-Ray diffraction pattern of iron and stony cosmic spherules, with superimposed patterns of diffracting phases: magnetite and wüstite.

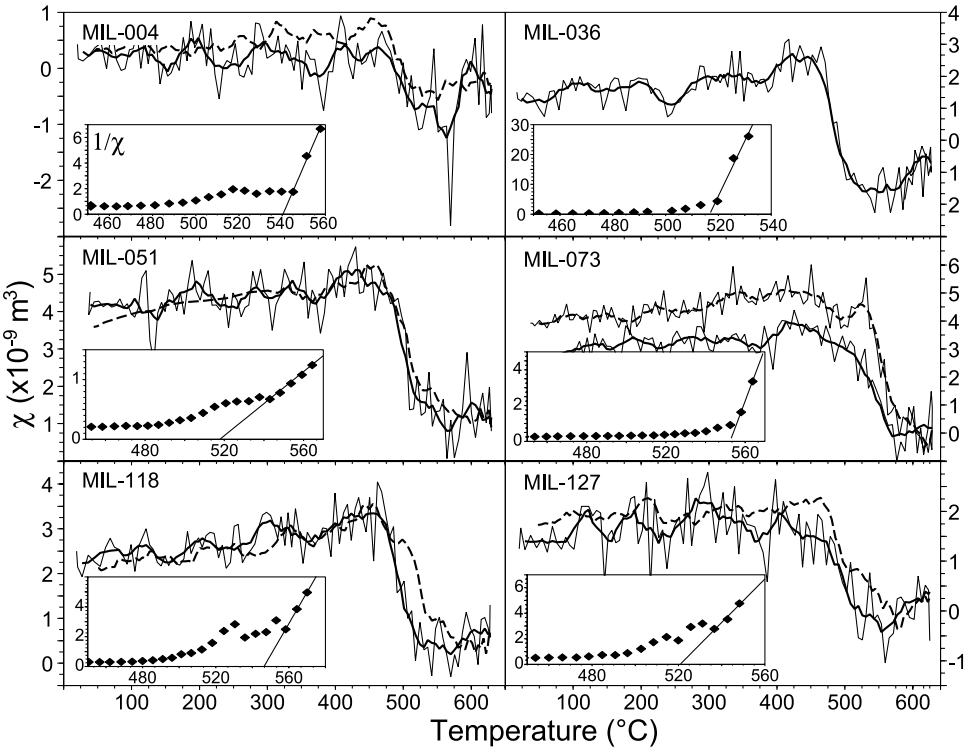

Figure 6. Temperature-dependent magnetic susceptibility (χ) analyses for selected micrometeorite samples. The Curie temperatures are estimated with the inverse susceptibility ($1/\chi$, compare inset) method [*Petrovský and Kapièka*, 2006]. The thick solid curve is a smoothed curve (moving average of 5 measurements) of the heating path. The dashed curve is smoothed curve of the cooling path (the cooling path was not measured for sample MIL-036).

the range of 555–585°C (Table 1). These temperatures are significantly higher than estimated T_c values. BO sample MIL-004 is the only particle for which both analyses were made. Its T_c is ~540°C (Table 1), and its maximum blocking temperature is 566 ± 5°C (Table 1). Most of the remanence is carried by small magnetite grains, whereas larger magnetite grains dominate the magnetic susceptibility (which was used to estimate T_c). The difference found between thermal demagnetization and temperature-dependent susceptibility analyses may indicate the presence

Table 1. Temperature Dependent Magnetic Susceptibility Analyses and Thermal Demagnetization of sIRM Results[a]

Sample	Type[b]	Mg	Al	Si	Ca	Ti	Cr	Mn	Fe	Ni	O	Sum	T_{cP}	T_{c2t}	MBT
MIL-004	PO	14.99	1.81	15.11	0.39	0.03	0.57	0.06	8.82	0.03	58.16	99.98	540	500 550	566 ± 5
MIL-013	S	NA	NA	NA	NA	NA	NA	NA	NA	NA	NA	NA			560 ± 5
MIL-019	V	16.71	1.29	16.30	0.99	0.03	0.04	0.13	6.05	0.00	58.49	100.02			564 ± 5
MIL-020	BO	15.48	1.49	14.20	1.03	0.06	0.10	0.05	9.88	0.16	57.53	99.97			565 ± 5
MIL-023	PO	19.25	0.61	14.53	0.47	0.01	0.09	0.07	7.46	0.05	57.44	99.96			568 ± 5
MIL-024	BO	16.01	0.90	14.59	1.23	0.04	0.03	0.08	9.55	0.00	57.55	99.98			569 ± 5
MIL-027	BO	16.49	1.36	16.20	1.22	0.02	0.10	0.09	6.01	0.02	58.48	100.00			565 ± 5
MIL-036	BO	11.85	2.28	17.49	1.39	0.03	0.07	0.10	7.33	0.02	59.30	99.85	517	510 550	
MIL-044	BO	15.28	1.40	16.49	0.20	0.02	0.11	0.08	7.75	0.00	58.63	99.97			562 ± 5
MIL-051	BO	15.87	1.24	14.23	0.69	0.05	0.19	0.09	9.62	0.49	57.49	99.96	518	510 550	
MIL-073	G	11.40	0.66	11.34	0.40	0.03	0.11	0.02	19.98	0.01	55.91	99.87	552	575 585	
MIL-118	BO	15.17	1.54	15.08	0.67	0.05	0.09	0.09	9.08	0.25	57.97	99.97	546	520 560	
MIL-120	BO	13.95	1.56	14.54	1.11	0.05	0.07	0.07	10.89	0.07	57.69	99.99			580 ± 5
MIL-127	BO	13.34	1.47	13.84	1.45	0.04	0.19	0.11	11.72	0.47	57.35	99.98	521	525 575	
MIL-157	CC	17.91	0.55	15.96	0.40	0.02	0.07	0.13	6.82	0.01	58.14	100.01			576 ± 5
MIL-158	BO	14.87	1.42	14.67	1.14	0.05	0.14	0.06	9.70	0.25	57.75	100.05			571 ± 5
MIL-160	BO	12.25	1.47	13.92	1.26	0.02	0.21	0.08	12.85	0.41	57.39	99.85			574 ± 5
MIL-161	CC	17.99	1.14	15.78	0.89	0.03	0.06	0.13	5.77	0.02	58.20	100.02			560 ± 5

[a]Bulk chemical analyses were obtained by averaging wavelength dispersive spectrometry measurements on a 30 × 20 μm window. They are given in atom percentage. T_{cP} is the Curie temperature (in °C) obtained with inverse susceptibility method [*Petrovský and Kapièka*, 2006], T_{c2t} is the Curie temperature (in °C) obtained with the two tangent method [*Grommé et al.*, 1969]. MBT is the maximum blocking temperature (in °C) obtained with the thermal demagnetization of sIRM.

[b]PO, porphyritic olivine cosmic spherule; S, stony cosmic spherule; V, glass cosmic spherule; BO, barred olivine cosmic spherule; G, G-type cosmic spherule; CC, cryptocrystalline cosmic spherule.

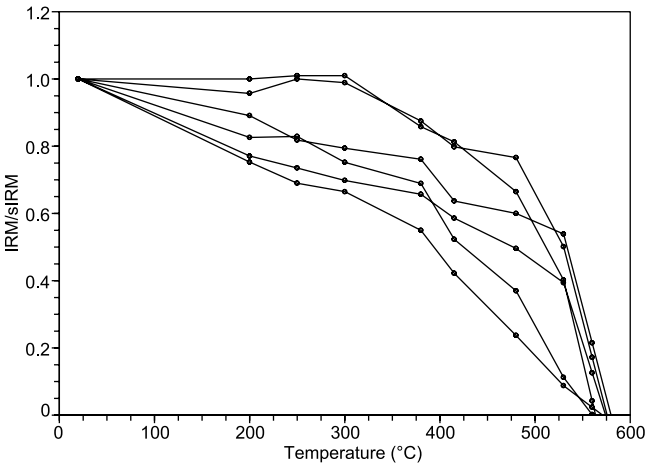

Figure 7. Stepwise thermal demagnetization of sIRM for selected cosmic spherules from Antarctica (Miller Butte sample).

of two populations of magnetite grains with different degrees of cation substitution within magnetite, the larger grains being more substituted. Within a single MM, magnetite grains could have different origins and grow in different redox and temperature conditions. Chemical analyses on individual magnetite grains would be necessary to confirm this hypothesis.

[22] Hysteresis loop measurements (Figure 8) give values for the coercive field B_c, saturation magnetization M_s, saturation remanent magnetization M_{rs}. A comparison between the value of M_{rs} determined using the AGM and the sIRM measured with the 2G Enterprises DC Squid cryogenic magnetometer reveals that the AGM does not give reliable absolute values for M_{rs} and M_s. Therefore, only their ratio is used in the following. The remanent coercive field B_{cr} was determined by DC backfield demagnetization of the sIRM using the AGM. The Day plot [*Day*, 1977] (Figure 9) indicates that the magnetic inclusions in BO, PO and CC CSs have pseudosingle domain (PSD) to single domain (SD) grain sizes. SEM images and hysteresis measurements are in agreement, with smaller magnetite grains being single domain and larger grains having multidomain (MD) behavior. For each CS type, samples with smaller magnetite grains (Figure 2, samples BOa–BOb, POa–POb, and CCa–CCb and Figure 8b) tend to have higher M_{rs}/M_s ratios whereas samples with larger magnetite grains (Figure 2, samples BOc–BOe, POc–POe, and CCc and Figures 8a and 8d) have lower ratios. One glass CS

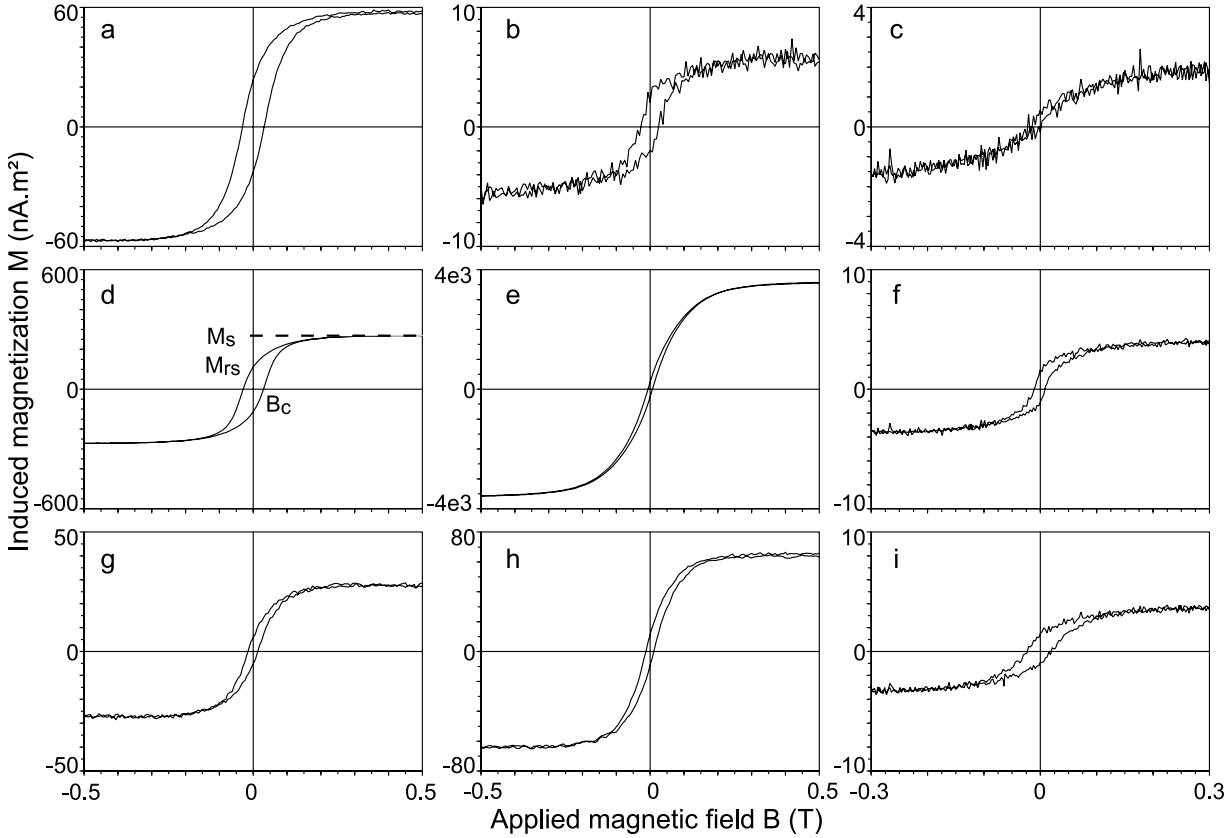

Figure 8. Hysteresis loops measured with a Princeton Measurements Corporation Alternating Field Magnetometer after correction of high-field slope (70% interval). (a) Barred olivine cosmic spherule WAL-085 (m = 24 μg). (b) Porphyritic olivine cosmic spherule WAL-079 (m = 29 μg). (c) Glass cosmic spherule 03-40-06 (mean diameter = 102 μm). (d) Cryptocrystalline cosmic spherule FRO2-001 (m = 53 μg). (e) I-type cosmic spherule FRO2-031 (m = 73 μg). (f) Fine-grained unmelted micrometeorite 05-37-23 (mean diameter = 204 μm). (g) Scoriaceous micrometeorite WAL-086 (m = 24 μg). (h) G-type cosmic spherule WAL-096 (m = 24 μg). (i) Coarse-grained unmelted micrometeorite 05-37-22 (mean diameter = 230 μm).

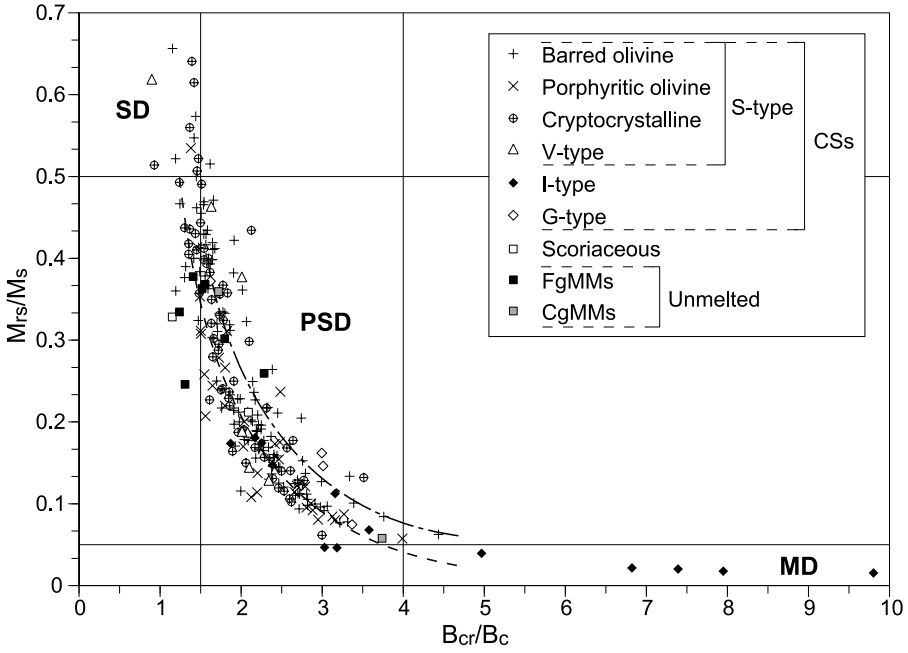

Figure 9. Day plot [*Day*, 1977] of the hysteresis parameters for different types of micrometeorites. The dashed and dashed-dotted curves are the mixing curves for a SD–MD mixture according to *Day* [1977] and *Dunlop* [2002], respectively.

sample (05-06-24) has SD magnetite inclusions, while other samples contain PSD magnetite (Figure 8c). Magnetite in I-type and G-type CSs has MD to PSD magnetic behavior. In I-type CSs with lower amounts of magnetite (Figure 1, Ia and Figure 8e) the magnetite is closer to a PSD domain state, whereas CSs with larger amounts of magnetite have higher B_{cr}/B_c ratios (Figure 2, samples Ib–Ie with increasing proportions of magnetite from Ib to Ie). Among G-type CSs, samples with bigger magnetite dendrites (Figure 2, samples Gd–Ge and Figure 8h) have lower M_{rs}/M_s ratios (closer to MD magnetite values), whereas samples with finer magnetite dendrites (Figure 2, samples Ga–Gc) have hysteresis parameters that are closer to those expected for SD magnetite. The two measured ScMMs (FRO2-107 and WAL-086, Figure 8g) and FgMM 05-37-23 (Figure 8f) have PSD magnetite inclusions. Although metal and sulphides can be present as minor primary phases in FgMMs, their contribution to the magnetic properties is not evidenced by our hysteresis data. Of the two measured CgMMs, one (05-37-22) has PSD magnetite and the other (05-37-14, Figure 8i) has magnetic properties that are close to the border between PSD and MD magnetite. *Xu et al.* [1994] measured hysteresis properties of magnetite spherules extracted from limestone. Most spherules they measured show MD magnetic characteristics. According to our measurements, most magnetic spherules of extraterrestrial origin in sediments would show PSD grain size.

[23] Measured low-field total magnetic susceptibility values for 337 CSs, 4 ScMMs, 1 FgMM and 1 CgMM fall in the range of 4×10^{-13}–1.1×10^{-10} m^3 (45 more MMs had susceptibilities below the noise level of the magnetic susceptibility meter used). The low-field volume magnetic susceptibility is represented as a function of particle diameter in Figure 10 for the Miller Butte, Frontier Mountain and Walcott Névé MMs. All of the data points above 1 SI are from I-type CSs. Owing to the sample bias caused by magnetic separation, these MMs are overrepresented in the Frontier Mountain sample. This bias and the fact that small diameter samples with low volume susceptibility are below the noise level of the magnetic susceptibility meter explain the apparent trend of increasing susceptibility with decreasing particle diameter. In order to scale the potential contribution of MMs to the susceptibility of sedimentary rocks in which they deposited, we calculated the limit above which the signal of a single MM exceeds that of a standard 8 cm^3 sediment sample used in rock magnetic studies. Only few of the measured MMs have a susceptibility approaching that of a 10^{-5} SI (low value for calcareous ooze or siliceous ooze) sediment sample (Figure 10). The probability for a sediment to have its magnetic susceptibility record biased by the presence of a MM is negligible for most sediments [*Suavet et al.*, 2008].

[24] The volume susceptibility distributions for different types of MMs are shown in Figure 11. Owing to the uncertainty in the estimation of the volume of samples, the volume susceptibilities we give have a reliability of ±10%. Comparison with the value for pure magnetite (~3 SI for a sphere) allows us to estimate the proportion of magnetite in the samples. As expected, there is a correlation between the volume susceptibility and the magnetite content observed on SEM images. Most BO and CC CSs have susceptibilities in the range of 0.03–0.8 SI. PO CSs have susceptibilities in the same range, but their peak is below 0.1 SI. Glass CSs have significantly lower volume susceptibilities, with the majority of samples in the range of 0.01–0.1 SI. I-type CSs all have volume susceptibilities greater than 0.57 SI, and the peak of their distribution is in the range of 1–2.9 SI. G-type CSs can also have susceptibilities above 1 SI, but most samples are in the range of 0.1–0.3 SI. ScMMs have susceptibilities in the range of 0.07–0.12 SI.

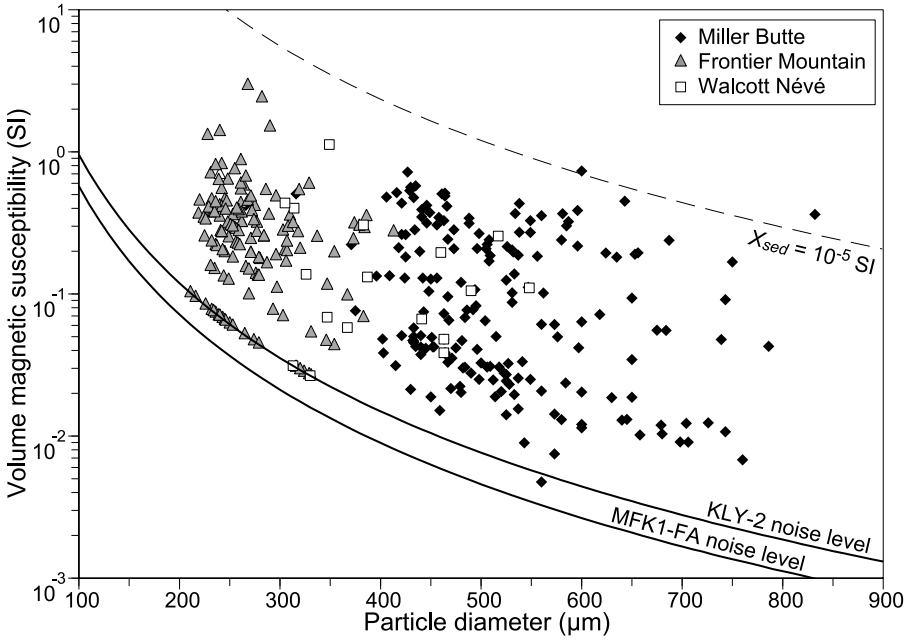

Figure 10. Volume magnetic susceptibility as a function of particle diameter for Miller Butte, Frontier Mountain, and Walcott Névé micrometeorites from Antarctica. The instrumental noise level is indicated with solid curves for the KLY 2 Kappabridge and MFK1-FA magnetic susceptibility meters, respectively. Samples that were below the noise level are represented on the noise level line. Dashed curves represent the limit above which the absolute susceptibility of a single micrometeorite exceeds that of an 8 cm^3 sediment sample with a volume susceptibility X_{sed} of 10^{-5} SI.

The 2 unmelted MMs measured, FgMM 05-37-23 and CgMM 05-37-14, have susceptibilities of 0.12 and 0.055 SI, respectively.

[25] The saturation magnetization M_s (either directly measured with the VSM or calculated from the ratio M_{rs}/M_s using the sIRM measured with the 2G Enterprises DC Squid cryogenic magnetometer) is plotted in Figure 12 as a function of the specific ferromagnetic susceptibility of MMs. The ferromagnetic susceptibility was obtained by subtracting the high-field susceptibility (the slope of the saturation moment in a hysteresis loop) from the total susceptibility (measured with KLY 2 or MFKA-FA magnetic susceptibility meters) [*Rochette*, 1987]. The data for most of the samples lie below the theoretically expected line for spheres of pure magnetite. This may be the consequence of two different effects: substitution in magnetite tends to reduce the value of M_s, and departure from sphericity increases the magnetic susceptibility, as shown with the theoretically expected line for elongated grains of pure magnetite [*Rochette et al.*, 2003].

[26] The anisotropy of magnetic susceptibility was measured for 13 of the largest Miller Butte CSs (Table 2). They have an anisotropy degree (ratio of maximum to minimum susceptibility) in the range of 1.15–1.64. The samples with the highest anisotropy degree (MIL-174 and MIL-022) are strongly anisometric samples (axial ratios of 1.79 and 1.35, respectively). The shape parameter T [*Jelinek*, 1981] indicates oblate fabrics for most BO CSs. Sample MIL-104, with the highest positive value for T, has parallel olivine bars. BO CSs with lower positive values for T either have less visible bars (MIL-020 and MIL-120) or more than one group of bars with different orientations (MIL-099). Sample MIL-036 has visible olivine bars, yet its fabrics are only weakly oblate. Sample MIL-035 has a prolate fabric and its texture is intermediate between barred olivine and microcrystalline. Sample MIL-024 also has a prolate fabric, this sample has at least 5 populations of bars among which 3 intersect on an axis. The estimated shape anisotropy, the anisotropy of an object of the same shape with isotropic

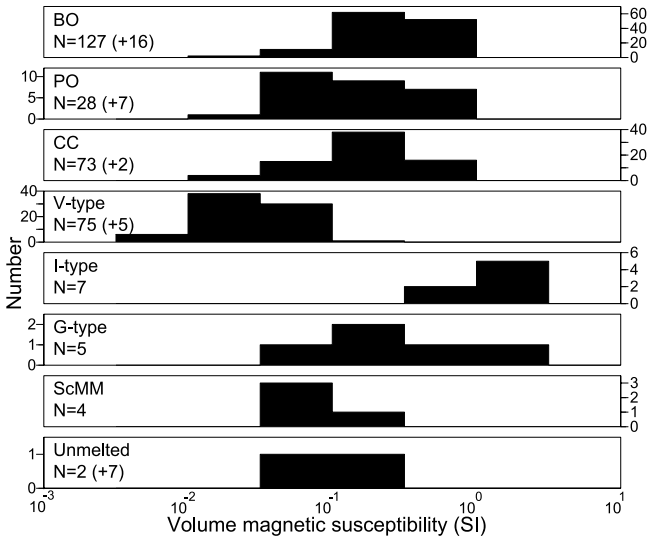

Figure 11. Volume magnetic susceptibility distributions for different types of micrometeorites. The bracketed numbers indicate how many samples were below the instrumental noise level.

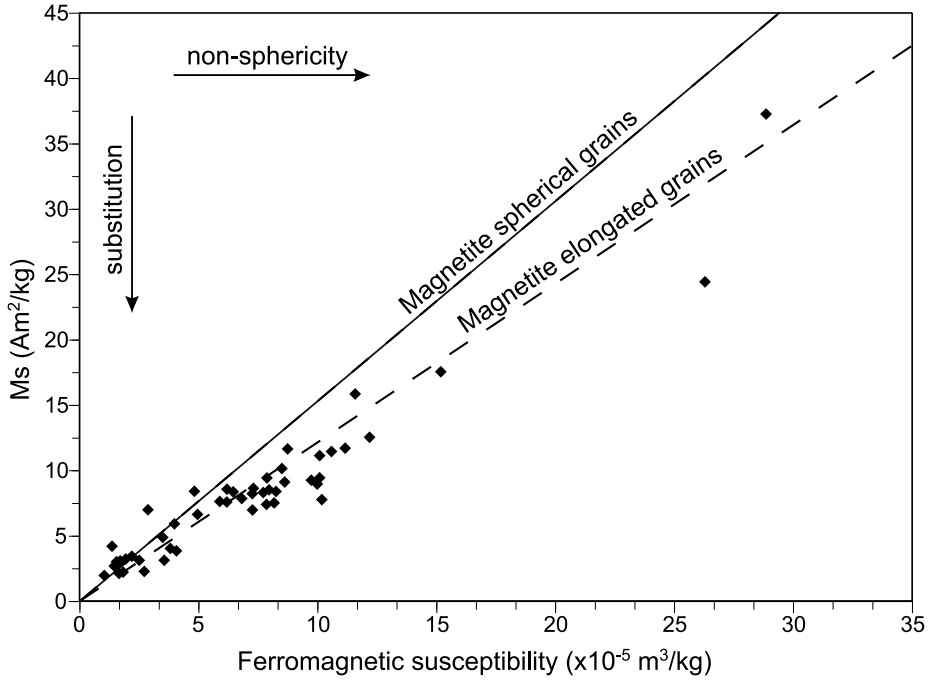

Figure 12. Saturation magnetization as a function of the mass ferromagnetic susceptibility. The theoretical curve for spheres of pure magnetite is given for comparison (slope = 1.53×10^5). The effects of substitution and departure from sphericity are shown with arrows. The dashed curve represents the theoretical slope for elongated grains of pure magnetite with an axial ratio of 2 [*Rochette*, 2003].

intrinsic susceptibility, is 1.07 for MIL-174, and 1.02 for MIL-022. This is much lower than their anisotropy degree P (1.64 and 1.44, respectively). Therefore, the anisotropy of magnetic susceptibility of these samples is dominated by the orientation and distribution of magnetite grains within the silicate matrix. Of the three PO CSs measured, one has a slightly oblate fabric (MIL-023) and two have a prolate fabric (MIL-004 and MIL-006). The only measured G-type CS has a strongly oblate fabric.

6. Natural Remanent Magnetization

[27] The NRM of 230 CSs, 4 ScMMs and 4 unmelted MMs was measured (only samples that were not subjected to magnetic extraction were analyzed). The NRM was below the noise level of the magnetometer for 53 CSs and for 1 ScMM. The sIRM was also measured for 76 of these CSs and for the 4 unmelted MMs. The NRM is in the range of $<10^{-10}$–1.6×10^{-7} Am^2. The volume magnetization is represented as a function of particle diameter in Figure 13 for the Miller Butte, Frontier Mountain, Walcott Névé and CONCORDIA collections. In order to scale the potential contribution of MMs to the NRM of sedimentary rocks in which they were deposited, we calculated the limit above which the NRM of a single MM exceeds that of a standard 8 cm^3 sediment sample for different sediment magnetization values. All samples with NRM intensity above the noise level of the magnetometer have a stronger moment than a sediment sample with a 10^{-5} A/m magnetization (lower range for siliceous/calcareous chalk or ooze), and some MMs have a moment exceeding that of a sediment sample with a 10^{-3} A/m magnetization (deep sea clays for instance)

Table 2. Anisotropy of Magnetic Susceptibility[a]

Sample	Type	χ_m (m^3)	Standard Error (%)	χ_{n1}	χ_{n2}	χ_{n3}	P	T
MIL-004	PO	3.27×10^{-11}	6.36	1.15 ± 0.05	0.96 ± 0.05	0.89 ± 0.05	1.29	0.41
MIL-006	PO	3.40×10^{-11}	9.17	1.12 ± 0.07	0.99 ± 0.07	0.90 ± 0.07	1.25	0.10
MIL-020	BO	2.38×10^{-11}	1.31	1.06 ± 0.01	1.01 ± 0.01	0.93 ± 0.01	1.15	0.24
MIL-022	BO	2.38×10^{-11}	7.22	1.18 ± 0.06	0.99 ± 0.06	0.82 ± 0.06	1.44	0.05
MIL-023	PO	1.99×10^{-11}	4.18	1.07 ± 0.03	1.00 ± 0.03	0.93 ± 0.03	1.16	0.05
MIL-024	BO	2.95×10^{-11}	3.06	1.09 ± 0.02	0.96 ± 0.02	0.94 ± 0.02	1.16	0.68
MIL-035	BO	4.87×10^{-11}	3.74	1.07 ± 0.03	0.99 ± 0.03	0.93 ± 0.03	1.15	0.22
MIL-036	BO	2.58×10^{-11}	4.42	1.12 ± 0.03	1.00 ± 0.03	0.88 ± 0.04	1.27	0.08
MIL-073	G	2.82×10^{-11}	8.34	1.11 ± 0.06	1.03 ± 0.06	0.86 ± 0.06	1.29	0.38
MIL-099	BO	2.92×10^{-11}	10.30	1.10 ± 0.08	1.07 ± 0.08	0.90 ± 0.08	1.22	0.14
MIL-104	BO	2.33×10^{-11}	1.94	1.13 ± 0.01	1.05 ± 0.02	0.83 ± 0.02	1.36	0.52
MIL-120	BO	2.91×10^{-11}	2.12	1.08 ± 0.02	1.00 ± 0.02	0.92 ± 0.01	1.17	0.10
MIL-174	BO	8.42×10^{-11}	10.37	1.26 ± 0.08	0.97 ± 0.08	0.77 ± 0.08	1.64	0.04

[a] χ_m is the mean susceptibility. χ_{n1}, χ_{n2}, and χ_{n3} are the normed principal susceptibilities. P is the anisotropy degree (ratio of maximum and minimum susceptibility). T is the shape parameter ($T < 0$ for prolate fabrics, $T > 0$ for oblate fabrics [*Jelinek*, 1981]).

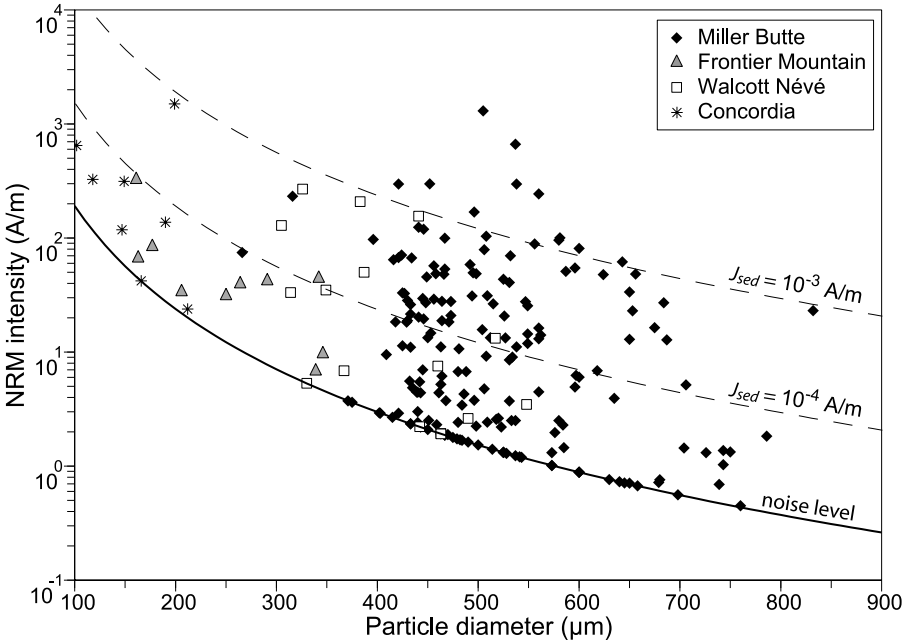

Figure 13. Natural remanent magnetization as a function of particle diameter for Miller Butte, Frontier Mountain, Walcott Névé, and CONCORDIA micrometeorites from Antarctica. The instrumental noise level is indicated with a solid curve. Samples that were below the noise level are represented on the noise level line. Dashed curves represent the limit above which the moment of a single micrometeorite exceeds that of an 8 cm^3 sediment sample with a volume magnetization J_{sed} of 10^{-4} A/m or 10^{-3} A/m, respectively.

(Figure 13). According to *Suavet et al.* [2008], the probability for a sediment to have its magnetization direction biased of >30° is not negligible (>1%) for sediments with magnetizations up to 5×10^{-3} A/m and sedimentation rates up to 10 cm/ka, and apparent reversals of polarity are possible (probability >1%) for sediments with low magnetizations ($<2 \times 10^{-4}$ A/m) and low sedimentation rates (<1 cm/ka). Although the Miller Butte and Frontier Mountain samples contain MMs with a terrestrial age of many tens of thousands of years, their magnetization range is not lower than that of 30–40 year old CONCORDIA MMs. The effect of terrestrial weathering on the magnetic properties of MMs therefore appears to be small. In particular, transformation of magnetite into maghemite does not seem to occur, as can be deduced from the reversible paths of temperature-dependent magnetic susceptibility analyses on Miller Butte samples (Figure 6).

[28] NRM intensity distributions for different types of CSs are shown in Figure 14. Owing to the uncertainty in the estimation of the volume of samples, the NRM intensities we give have a reliability of ±10%. BO and CC CSs have similar distributions, with a range of ∼1–300 A/m and a peak at 10–100 A/m. PO CSs have lower NRM intensities on average, with a range of 1–55 A/m and a peak below 10 A/m. Glass CSs have the lowest NRM intensities, most samples are in the range of 0.45–20 A/m. G-type CSs are in the range of 6.8–35 A/m. ScMMs have NRM intensities in the range of 3.7–16 A/m. The 3 FgMMs and CgMM 5-37-22 unmelted MMs have magnetization intensities among the highest values measured, with a range of 78–526 A/m. The NRM of the only analyzed I-type CS (16-160-1) is below the noise of the magnetometer because of its small volume.

[29] As CSs are quenched after melting during atmospheric entry, their NRM should be a thermal remanent magnetization (TRM) acquired in the Earth's magnetic field. Cap Prudhomme sample 05-13-01 and CONCORDIA sample 06-09-07 have NRM/sIRM [*Fuller*, 1974] ratios greater than 0.1. Such a high ratio is unexpected for a

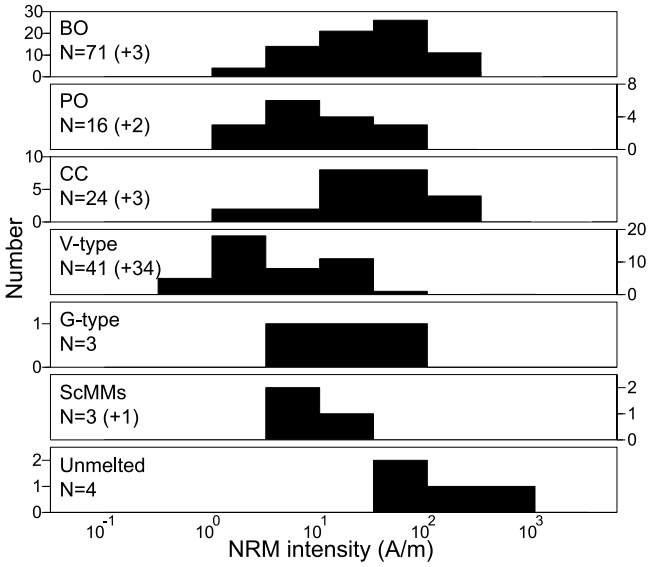

Figure 14. Natural remanent magnetization distributions for different types of micrometeorites. The numbers in parentheses indicate how many samples were below the instrumental noise level.

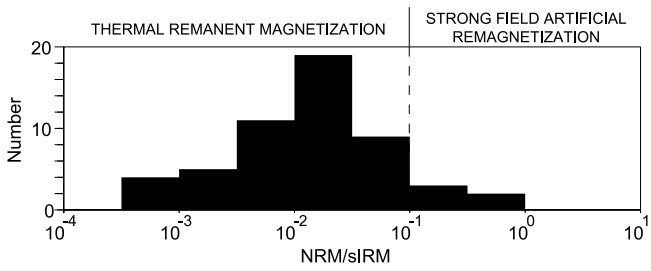

Figure 15. NRM/sIRM ratio distribution for all measured cosmic spherules. Ratios <0.1 are consistent with a thermal remanent magnetization acquired by quenching in the Earth's magnetic field during atmospheric entry. Ratios >0.1 may indicate that the samples have been remagnetized after entry by exposure to a strong (>mT) magnetic field.

TRM. It might indicate that these samples have been artificially remagnetized after their entry through the Earth's atmosphere by exposure to a strong (>mT) magnetic field. Figure 15 shows the distribution of NRM/sIRM ratios for all cosmic spherules we measured. All of the measured unmelted MMs from Cap Prudhomme collection also have NRM/sIRM ratios greater than 0.1. Remagnetization of these samples cannot be excluded, as they were collected many years ago without particular efforts to protect them from terrestrial and artificial magnetic fields, but most melted MMs from that collection have NRM/sIRM ratios below 0.1 (which indicates that they have not been artificially remagnetized). It is possible that the preatmospheric magnetization of unmelted MMs was not completely erased during atmospheric entry. Although temperature gradients are not supposed to develop in particles with diameter less than ~600 μm [*Love and Brownlee*, 1991], *Flynn* [2001] suggested that energy absorbing phases can allow temperature

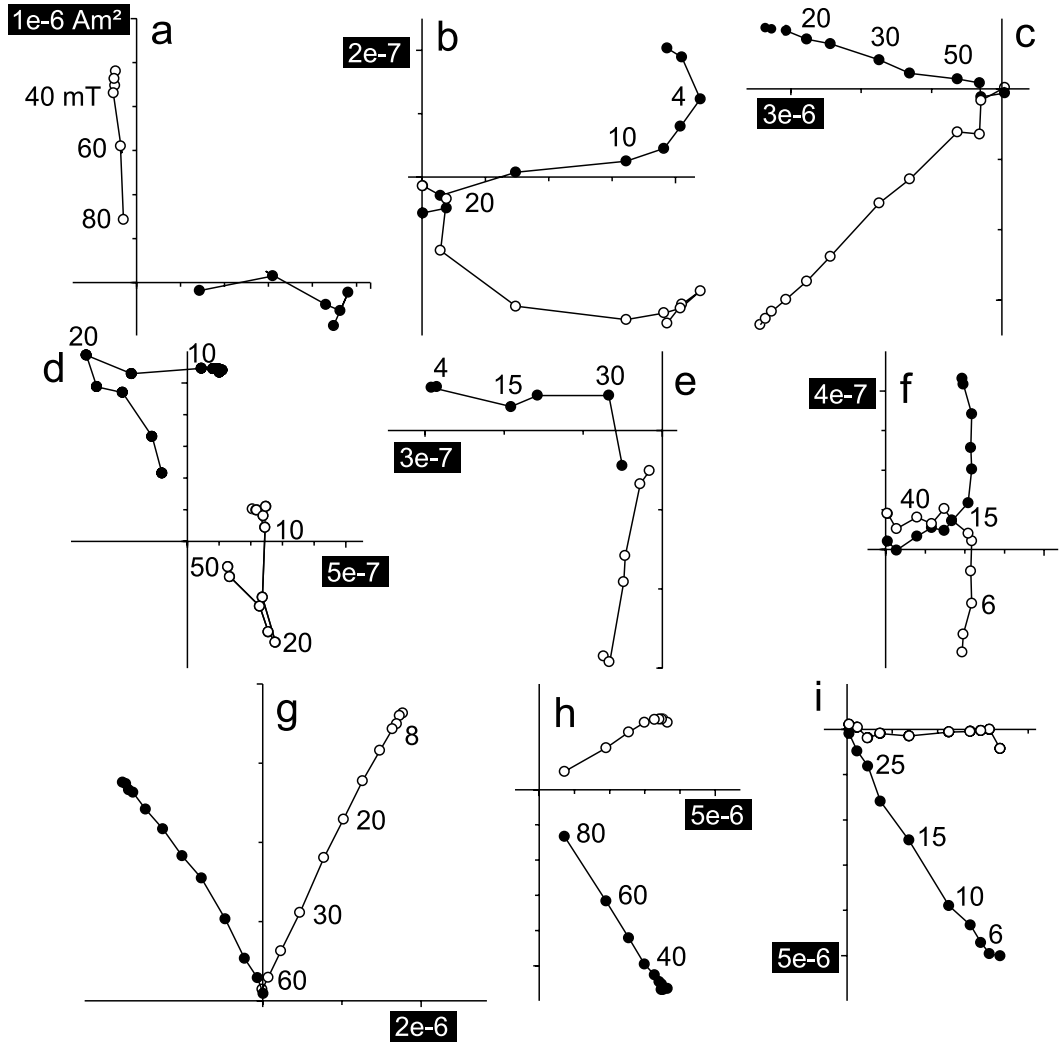

Figure 16. Orthogonal vector component plots of stepwise alternating field demagnetization data for the natural remanent magnetization of selected micrometeorites. (a) Glass cosmic spherule MIL-008. (b) Barred olivine cosmic spherule 06-09-33. (c) Cryptocrystalline cosmic spherule MIL-058. (d) Coarse-grained unmelted micrometeorite 05-37-22. (e) Fine-grained micrometeorite 05-37-19. (f) Barred olivine cosmic spherule FRO5-01. (g) Barred olivine cosmic spherule WAL-004. (h) Cryptocrystalline cosmic spherule WAL-011. (i) Porphyritic olivine cosmic spherule MIL-004.

gradients to develop in smaller particles. He calculated that about 50% of the total mass (before entry and ablation) of particles in the 10–100 μg mass range is not heated above 600°C during atmospheric entry. Conservation of the preatmospheric magnetization therefore seems to be possible in unmelted MMs. This magnetization could be carried by primary magnetite, as hysteresis data points toward magnetite as the main carrier of magnetization.

[30] Alternating field demagnetization of NRM and sIRM was carried out for 39 CSs and 4 unmelted MMs. Orthogonal vector component plots of demagnetization data for CSs often have a single magnetization component (Figures 16a and 16c and 16g–16i), but curved demagnetization trajectories are sometimes visible (Figures 16b and 16f). This curvature might indicate that the MM was rotating during atmospheric entry while cooling in the Earth's field. In order to further investigate the nature of the magnetization, we used a different normalization technique, the normalization by isothermal remanent magnetization derivative vs. alternating field: REM′ = (dNRM/dAF)/(dIRM/dAF) [*Gattacceca and Rochette*, 2004] are in the range of 10^{-3}–10^{-1}, which is consistent with the magnetization being a TRM acquired in the Earth's field. Coarse-grained unmelted sample 05-37-22 (Figure 16d) has a two-component magnetization. As this sample has well-defined components different from the typical curvature observed in samples that have been remagnetized through contact with artificial magnets [*Gattacceca and Rochette*, 2004], it is unlikely that this sample was remagnetized after collection, unless one invokes two successive applications of magnets with decreasing strength. The two components have REM'>0.3, so the sample cannot have had a TRM acquired in the Earth's magnetic field during atmospheric entry. Fine-grained unmelted sample 05-37-19 (Figure 16e) has a poorly determined single-component magnetization. The high coercivity components in samples with two-component magnetizations could represent preatmospheric magnetizations: the magnetization could be a remanent magnetization acquired in the early history of the protoplanetary disk in a strong field generated by the Sun (T Tauri phase) or by lightning discharging, or a TRM acquired on the asteroid parent body in a dynamo field, or a shock magnetization (see discussion in the work by, e.g., *Gattacceca and Rochette* [2004]).

7. Conclusions

[31] Magnetic measurements on melted cosmic spherules of different types allowed correlation of magnetic properties with the grain size of magnetite observed using electron microscopy. The volume magnetic susceptibility of cosmic spherules is in the range of 0.005–2.9 SI. Anisotropy of magnetic susceptibility is in the range of 15–64%, with most samples having oblate fabrics. The natural remanent magnetization of the cosmic spherules is a stable thermal remanent magnetization that was acquired during cooling in the Earth's magnetic field after melting in the atmosphere. The volume magnetization is in the range of 0.45–300 A/m. Curie temperatures deduced from susceptibility measurements at different temperatures are in the range of 485–544°C; maximum blocking temperatures determined from thermal demagnetization of micrometeorites have higher values in the range of 560–580°C. The difference between these temperature estimations may be related to the presence of different populations of magnetite grains with different degrees of cation substitution.

[32] Measurements on scoriaceous micrometeorites, and on fine-grained and coarse-grained micrometeorites, gave susceptibilities in the range of 0.06–0.12 SI. The magnetization of scoriaceous micrometeorites is in the range of 3.8–16 A/m. Unmelted micrometeorites have high magnetization intensities (78–525 A/m) that could represent preatmospheric remanent magnetizations (acquired in a strong field in the early Solar System, in the dynamo field of the asteroid parent body, or by shock magnetization), or remagnetizations that occurred after atmospheric entry of the samples.

[33] Micrometeorites are tiny objects, but their high magnetite content gives them higher magnetic susceptibility and magnetization than most terrestrial rocks. Therefore, a single micrometeorite deposited in a sediment may induce a significant bias in the magnetic properties of the sedimentary rock at the scale of samples used for paleomagnetic studies [*Suavet et al.*, 2008].

[34] **Acknowledgments.** We would like to thank S. Gilder, A. Roberts, J. Gee, S. Brachfeld, and T. von Dobeneck for their comments on this work and C. Engrand for providing micrometeorites from the CONCORDIA, Cap Prudhomme, and Greenland collections. This work was supported by the French Agence Nationale de la Recherche (project ANR-05-JCJC-0133).

References

Basile, I., J. R. Petit, S. Touron, F. E. Grousset, and N. Barkor (2001), Volcanic layers in Antarctic (Vostok) ice cores: Source identification and atmospheric implications, *J. Geophys. Res.*, *106*, 31,915–31,931.

Curzio, P., L. Folco, M. A. Laurenzi, M. Mellini, and A. Zeoli (2008), A tephra chronostratigraphic framework for the Frontier Mountain blue-ice field (northern Victoria Land, Antartctica), *Quat. Sci. Rev.*, *27*, 602–620.

Day, R. (1977), Hysteresis properties of titanomagnetites: Grain-size and compositional dependance, *Phys. Earth Planet. Inter.*, *13*, 260–267.

Dunlop, D. (2002), Theory and application of the Day plot (M_{rs}/M_s versus H_{cr}/H_c): 1. Theoretical curves and tests using titanomagnetite data, *J. Geophys. Res.*, *107*(B3), 2056, doi:10.1029/2001JB000486.

Dunlop, D. J., and Ö. Özdemir (2001), *Rock Magnetism: Fundamentals and Frontiers*, *Cambridge Stud. Magn.*, vol. 3, 596 pp., Cambridge Univ. Press, Cambridge, U. K.

Duprat, J., C. Engrand, M. Maurette, G. Kurat, M. Gounelle, and C. Hammer (2007), Micrometeorites from central Antarctic snow: The CONCORDIA collection, *Adv. Space Res.*, *392*, 605–611, doi:10.1016/j.asr.2006.05.029.

Flynn, G. J. (2001), Atmospheric entry heating of interplanetary dust, in *Accretion of Extraterrestrial Matter Throughout Earth's History*, edited by B. Peucker-Ehrenbrink and B. Schmitz, pp. 107–127, Kluwer Acad., New York.

Folco, L., P. Rochette, N. Perchiazzi, M. D'Orazio, M. A. Laurenzi, and M. Tiepolo (2008), Microtektites from Victoria Land Transantarctic Mountains, *Geology*, *36*, 291–294, doi:10.1130/G24528A.1.

Fuller, M. (1974), Lunar magnetism, *Rev. Geophys.*, *12*, 23–70.

Gattacceca, J., and P. Rochette (2004), Toward a robust normalized magnetic paleointensity method applied to meteorites, *Earth Planet. Sci. Lett.*, *227*, 377–393, doi:10.1016/j.epsl.2004.09.013.

Genge, M. J., C. Engrand, M. Gounelle, and S. Taylor (2008), The classification of micrometeorites, *Meteorit. Planet. Sci.*, *43*, 497–515.

Grommé, C. S., T. L. Wright, and D. L. Peck (1969), Magnetic properties and oxidation of iron-titanium oxide minerals in Alae and Makaopuhi lava lakes, Hawaii, *J. Geophys. Res.*, *74*, 5277–5294.

Hammersley, A. P. (1997), FIT2D: An introduction and overview, *ESRF Internal Rep. ESRF97HA02T*, Eur. Synchrotron Radiat. Facil., Grenoble, France.

Harvey, R. P., and M. Maurette (1991), The origin and significance of cosmic dust from the Walcott Névé, Antarctica, *Proc. Lunar Planet. Sci. Conf.*, *21*, 569–578.

Jelinek, V. (1981), Characterization of the magnetic fabric of rocks, *Tectonophysics*, *79*, 63–67.

LeMasurier, W. E., and J. W. Thomson (1990), *Volcanoes of the Antarctic Plate and Southern Oceans*, *Antarct. Res. Ser.*, vol. 48, 487 pp., AGU, Washington, D.C.

Love, S. G., and D. E. Brownlee (1991), Heating and thermal transformation of micrometeoroids entering the Earth's atmosphere, *Icarus*, *89*, 26 43.

Love, S. G., and D. E. Brownlee (1993), A direct measurement of the terrestrial mass accretion rate of cosmic dust, *Science*, *262*, 550 553.

Marfaing, J., P. Rochette, J. Pellerey, P. Chaurand, C. Suavet, and L. Folco (2008), Study of a set of micrometeorites from Antarctica using magnetic and ESR methods coupled with micro-XRF, *J. Magn. Magn. Mater.*, *320*, 1687 1695, doi:10.1016/j.jmmm.2008.01.037.

Maurette, M., C. Hammer, D. E. Brownlee, N. Reeh, and H. H. Thomsen (1986), Placers of cosmic dust in the blue lakes of Greenland, *Science*, *233*, 869 872.

Maurette, M., C. Olinger, M. Christophe Michel-Levy, G. Kurat, M. Pourchet, F. Brandstätter, and M. Bourot-Denise (1991), A collection of diverse micrometeorites recovered from 100 tonnes of Antarctic blue ice, *Nature*, *351*, 44 46.

McManus, D. A., et al. (1970), Site 38, *Initial Rep. Deep Sea Drill. Proj.*, *5*, 255 296.

Petrovský, E., and A. Kapièka (2006), On determination of the Curie point from thermomagnetic curves, *J. Geophys. Res.*, *111*, B12S27, doi:10.1029/2006JB004507.

Robin, E., P. Bonth, L. Froget, C. Jhanno, and R. Rocchia (1992), Formation of spinels in cosmic objects during atmospheric entry: A clue to the Cretaceous-Tertiary boundary event, *Earth Planet. Sci. Lett.*, *108*, 181 190.

Rochette, P. (1987), Magnetic susceptibility of the rock matrix related to magnetic fabric studies, *J. Struct. Geol.*, *9*, 1015 1020.

Rochette, P., L. Sagnotti, G. Consolmagno, M. Denise, L. Folco, J. Gattacceca, M. Osete, and L. Pesonen (2003), Magnetic classification of stony meteorites: 1. Ordinary chondrites, *Meteorit. Planet. Sci.*, *38*, 251 268.

Rochette, P., et al. (2008a), Magnetic classification of stony meteorites: 2. Non-ordinary chondrites, *Meteorit. Planet. Sci.*, *43*, 959 980.

Rochette, P., L. Folco, C. Suavet, M. van Ginneken, J. Gattacceca, N. Perchiazzi, R. Braucher, and R. P. Harvey (2008b), Micrometeorites from the Transantarctic Mountains, *Proc. Natl. Acad. Sci. U. S. A.*, *105*, 18,206 18,211, doi:10.1073/pnas.0806049105.

Suavet, C., P. Rochette, J. Gattacceca, and L. Folco (2008), Micrometeorites: A possible bias on the sedimentary magnetic record, *Geochem. Geophys. Geosyst.*, *9*, Q11002, doi:10.1029/2008GC002160.

Taylor, S., and J. H. Lever (2001), Seeking unbiased collections of modern and ancient micrometeorites, in *Accretion of Extraterrestrial Matter Throughout Earth's History*, edited by B. Peucker-Ehrenbrink and B. Schmitz, pp. 205 219, Kluwer Acad., New York.

Taylor, S., J. H. Lever, and R. P. Harvey (1998), Accretion rate of cosmic spherules measured at the South Pole, *Nature*, *392*, 899 903.

Taylor, S., J. H. Lever, and R. P. Harvey (2000), Numbers, types and composition of an unbiased collection of cosmic spherules, *Meteorit. Planet. Sci.*, *35*, 651 666.

Toppani, A., and G. Libourel (2003), Factors controlling compositions of cosmic spinels: Application to atmospheric entry conditions of meteoritic materials, *Geochim. Cosmochim. Acta*, *67*, 4621 4638.

Toppani, A., G. Libourel, C. Engrand, and M. Maurette (2001), Experimental simulation of atmospheric entry of micrometeorites, *Meteorit. Planet. Sci.*, *36*, 1377 1396.

van Andel, T. H., et al. (1973), Site 160, *Initial Rep. Deep Sea Drill. Proj.*, *16*, 265 299.

Xu, W., R. van der Voo, and D. R. Peacor (1994), Are magnetite spherules capable of carrying stable magnetizations?, *Geophys. Res. Lett.*, *21*, 517 520.

J. Duprat, CSNSM, Batiment 104, F-91406 Orsay, France.

L. Folco, Museo Nazionale dell'Antartide, Universit di Siena, Via Laterina 8, I-53100 Siena, Italy.

J. Gattacceca, P. Rochette, and C. Suavet, CEREGE, Aix-Marseille Université, CNRS, Europôle Médipteraléen de l'Arbois, BP 80, F-13545 Aix-en-Provence, CEDEX 04, France. (suavet@cerege.fr)

R. P. Harvey, Department of Geological Sciences, Case Western Reserve University, Cleveland, OH 44106, USA.

N. Perchiazzi, Dipartimento di Scienze della Terra, Università di Pisa, Via S. Maria 53, I-56126 Pisa, Italy.

Chapitre 6

Micrométéorites et propriétés magnétiques des sédiments

6.1 Article *Suavet et al., Geophysics, Geochemistry, Geosystems*, 2008

Contribution de C. Suavet : Conception et programmation du modèle numérique. Analyse des résultats. Ecriture de l'article.

Geochemistry Geophysics Geosystems G3
AN ELECTRONIC JOURNAL OF THE EARTH SCIENCES
Published by AGU and the Geochemical Society

Research Letter
Volume 9, Number 11
8 November 2008
Q11002, doi:10.1029/2008GC002160
ISSN: 1525 2027

Click Here for Full Article

Micrometeorites: A possible bias on the sedimentary magnetic record

C. Suavet, P. Rochette, and J. Gattacceca
CEREGE, Aix-Marseille Université, CNRS, F-13545 Aix-en-Provence, France (suavet@cerege.fr)

L. Folco
Museo Nazionale dell'Antartide, Via del Laterino 8, I-53100 Siena, Italy

[1] Micrometeorites are strongly magnetic and continuously accumulate at the Earth's surface. On the basis of previously acquired magnetic data, we investigated at which conditions micrometeorites can bias the sedimentary palaeomagnetic and rock magnetic record. We calculated the probabilities for a sediment sample (discrete samples or U-channel samples) to have its detrital remanent magnetization deviated by the presence of a micrometeorite. Our model shows that direction anomalies >5° caused by micrometeorites may be rather frequent (more than 1% of measured samples), even for sediments with typical values of sedimentation rate (up to 10 cm/kyr) and remanent magnetization (up to 5×10^{-3} A/m). Excursions >30° caused by micrometeorites have probabilities >1% in sediments with remanent magnetization $<10^{-3}$ A/m and sedimentation rate <10 cm/ka. Reversals caused by micrometeorites have probabilities >1% for sediments with remanent magnetization $<2 \times 10^{-4}$ A/m and sedimentation rate <1 cm/ka. On the other hand, only sediments with magnetic susceptibilities $<10^{-5}$ SI and sedimentation rates <1 cm/ka can be significantly affected by the presence of micrometeorites.

Components: 2648 words, 8 figures.

Keywords: micrometeorites; sedimentary magnetic record.

Index Terms: 1599 Geomagnetism and Paleomagnetism: General or miscellaneous; 3005 Marine Geology and Geophysics: Marine magnetics and paleomagnetics (1550); 6015 Planetary Sciences: Comets and Small Bodies: Dust.

Received 8 July 2008; **Revised** 9 September 2008; **Accepted** 25 September 2008; **Published** 8 November 2008.

Suavet, C., P. Rochette, J. Gattacceca, and L. Folco (2008), Micrometeorites: A possible bias on the sedimentary magnetic record, *Geochem. Geophys. Geosyst.*, *9*, Q11002, doi:10.1029/2008GC002160.

1. Introduction

[2] Micrometeorites are terrestrially collected extraterrestrial particles smaller than about 1 mm. They constitute the main part of the mass flux of extraterrestrial matter accreted on Earth [*Love and Brownlee*, 1993; *Taylor et al.*, 1998]. No significant variability of this flux with time is detectable from marine osmium isotope records [*Peucker-Ehrenbrink*, 1996]. Micrometeorites have been found in deep-sea sediments, in Greenland seasonal lakes, in Antarctic aeolian sedimentary traps, ice and snow, and in continental sands (see *Taylor and Lever* [2001] for a review). The majority of micrometeorites are strongly magnetic due to a high magnetite content. On the basis of the measurement of the magnetization and magnetic susceptibility of Antarctic micrometeorites (C. Suavet et al., Magnetic properties of micrometeorites, sub-

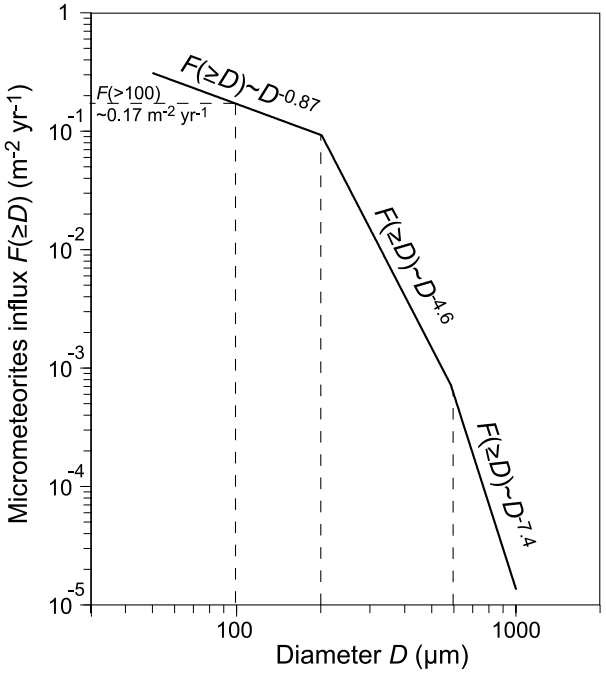

Figure 1. Cumulative size flux distribution of micrometeorites used in the calculations.

mitted to *Journal of Geophysical Research*, 2008), we investigate the possibility that under certain conditions the influx of micrometeorites may contribute significantly to the magnetization and/or the magnetic properties of sediments and bias their palaeomagnetic record.

2. Potential Effect on the Natural Remanent Magnetization

[3] In order to estimate the contribution of micrometeorites to the natural remanent magnetization (NRM) of sediments, we calculate the probability P_d for a standard sediment sample used in palaeomagnetic studies to have its detrital remanent magnetization (DRM) deviated of an angle $\delta \geq d$ by a micrometeorite. Small-diameter micrometeorites may be present in large numbers but they contribute to the background noise only: they do not induce anomalies. In the following, we study the cases $d = 5°$ (small disturbance of the palaeomagnetic signal), $d = 30°$ (critical value defining geomagnetic excursions), and $d = 90°$ (reversed polarity) and their associated probabilities P_5, P_{30} and P_{90}. In the case of standard U-channels (with a square section of 2×2 cm^2), the volume measured by magnetometers is about 16 cm^3. For discrete standard palaeomagnetic cores, the volume is 10.8 cm^3. In the following calculation, a sediment volume $V_{sed} = 10$ cm^3 is used. We have checked that using any V_{sed} value in the range 8–16 cm^3 induces only slight differences in P_d values, so that the results are valid for all types of sediment samples used in paleomagnetic studies.

[4] The parameters controlling the value of P_d for a given sediment are as follows:

[5] 1. The sedimentation rate Sr (m/a). We consider sedimentation rates in the range of 10^{-6}–10^{-4} m/a (0.1–10 cm/ka).

[6] 2. The background DRM of the sediment J_{sed} (A/m). We consider sediment DRM in the range of 10^{-6}–10^{-2} A/m.

[7] 3. The flux and size frequency distribution of micrometeorites. The cumulative size frequency distribution we use (Figure 1) is based on Antarctic micrometeorites collections: the 2000 South Pole collection [*Taylor et al.*, 2005], Frontier Mountain, and Miller Butte collections [*Rochette et al.*, 2008]. The size frequency distribution follows a power law with exponent slopes of −0.87 for diameters $D \leq 200$ μm, −4.6 for $200 < D \leq 600$ μm and −7.4 for $D > 600$ μm. The micrometeorites influx (number of micrometeorites with mean diameter $\geq D$(m) falling per year per square meter) deduced from these parameters is

$$F(\geq D) = \begin{cases} a_1 D^{b_1} = 6 \times 10^{-5} D^{-0.87} \\ \text{if} \quad D \leq 2 \times 10^{-4}\,\text{m} \\ a_2 D^{b_2} = 10^{-18} D^{-4.6} \\ \text{if} \quad 2 \times 10^{-4} < D \leq 6 \times 10^{-4}\,\text{m} \\ a_3 D^{b_3} = 9 \times 10^{-28} D^{-7.4} \\ \text{if} \quad D > 6 \times 10^{-4}\,\text{m} \end{cases} \quad (1)$$

In the following, we write $F(\geq D) = a\,D^b$; (a_i, b_i), $i = \{1, 2, 3\}$ must be substituted to (a, b) according to the diameter range. If we note t the sediment sample collection duration (the time it takes to deposit a height h (m) of sediment, in years) and A the collection surface area (in square meters), we have $t = h/S_r$ and $V_{sed} = h\,A$. The average number of micrometeorites of diameter $\geq D$ in the sediment sample is $N(\geq D) = AtF(\geq D) = (V_{sed}/S_r)aD^b$.

[8] 4. The NRM of micrometeorites J_m (A/m). We use the NRM distribution of Miller Butte micrometeorites collection [*Rochette et al.*, 2008; Suavet et al., submitted manuscript, 2008]. There is no correlation between the NRM and the diameter of micrometeorites. The NRM of micrometeorites (180 measured) ranges from 10^{-1} to more than 100 A/m, with a mode value of 10 A/m. The

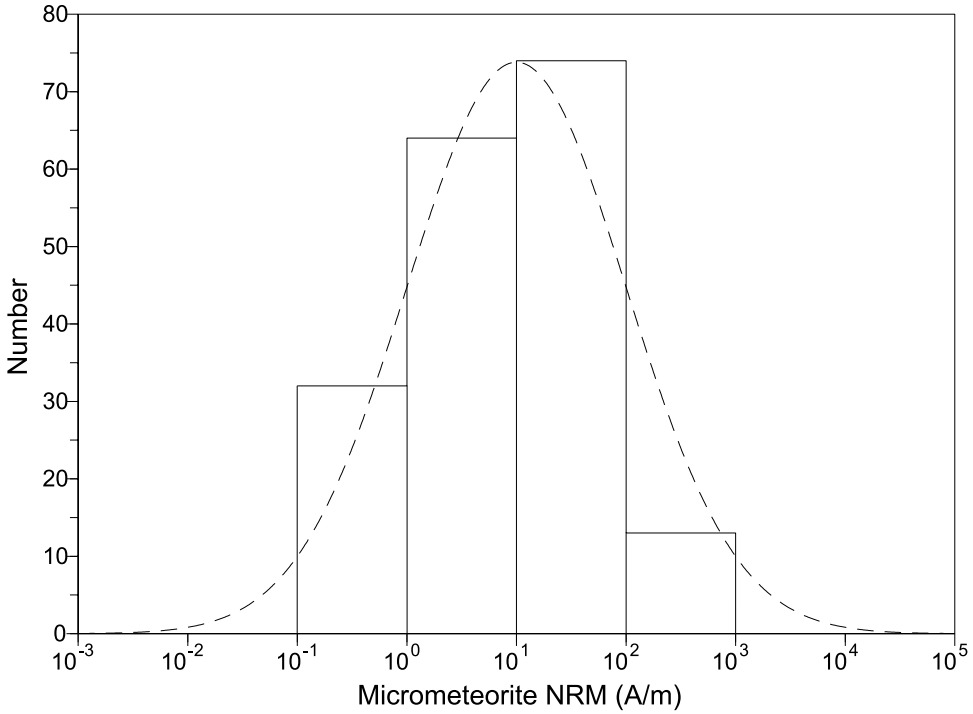

Figure 2. Natural remanent magnetization distribution for Miller Butte micrometeorite collection [*Rochette et al.*, 2008] and approximation by a log-normal distribution (mode is 10 A/m; standard deviation is 1).

distribution is approximated by a log-normal distribution $n(J_m)$ (Figure 2).

[9] The angular deviation due to the addition of the magnetization vector of one micrometeorite **M** to the coherent vector of the bulk sediment **S** is

$$\delta = \arccos\left(\frac{\mathbf{S}\cdot(\mathbf{S}+\mathbf{M})}{\|\mathbf{S}\|\,\|\mathbf{S}+\mathbf{M}\|}\right) \tag{2}$$

if we note $\alpha = \|\mathbf{M}\|/\|\mathbf{S}\|$ and θ the angle between the two vectors, equation (2) becomes

$$\begin{aligned}\delta &= \arccos\left(\frac{\|\mathbf{S}\|^2 + \|\mathbf{S}\|\,\|\mathbf{M}\|\cos\theta}{\|\mathbf{S}\|\,\sqrt{\|\mathbf{S}\|^2 + \|\mathbf{M}\|^2 + 2\|\mathbf{M}\|\,\|\mathbf{S}\|\cos\theta}}\right)\\ \delta &= \arccos\left(\frac{\|\mathbf{S}\|^2 + \alpha\,\|\mathbf{S}\|^2\cos\theta}{\|\mathbf{S}\|\,\sqrt{\|\mathbf{S}\|^2 + \alpha^2\,\|\mathbf{S}\|^2 + 2\alpha\,\|\mathbf{S}\|^2\cos\theta}}\right)\\ \delta &= \arccos\left(\frac{1+\alpha\cos\theta}{\sqrt{1+\alpha^2+2\alpha\cos\theta}}\right)\end{aligned} \tag{3}$$

The maximum deviation $\delta_{\max}(\alpha)$ is

$$\delta_{\max}(\alpha) = \begin{cases}\arcsin(\alpha) & \text{if } \alpha \le 1\\ \pi & \text{if } \alpha > 1\end{cases} \tag{4}$$

[10] Assuming that micrometeorites are randomly oriented when they get trapped in the sediment, which is realistic considering the size of the particles as surface forces dominate the magnetic couple, we calculate the average deviation $\overline{\delta}(\alpha)$ by integration on a spherical uniform distribution.

$$\overline{\delta}(\alpha) = \frac{\int_0^\pi \delta(\alpha,\theta)\,\sin\theta\,\mathrm{d}\theta}{\int_0^\pi \sin\theta\,\mathrm{d}\theta} = \frac{1}{2}\int_0^\pi \delta(\alpha,\theta)\,\sin\theta\,\mathrm{d}\theta \tag{5}$$

[11] The intensity anomaly induced by the presence of a micrometeorite is estimated with the ratio I_a of the resulting and background intensities.

$$\begin{aligned}I_a &= \frac{\|\mathbf{S}+\mathbf{M}\|}{\|\mathbf{S}\|} = \frac{\sqrt{\|\mathbf{S}\|^2 + \alpha^2\,\|\mathbf{S}\|^2 + 2\alpha\,\|\mathbf{S}\|^2\cos\theta}}{\|\mathbf{S}\|}\\ I_a &= \sqrt{1+\alpha^2+2\alpha\cos\theta}\end{aligned} \tag{6}$$

Figure 3 shows the value of I_a as a function of α and θ: for a given α, the anomaly is positive for low values of θ and becomes negative for increasingly high values of θ as α becomes higher. Hence positive intensity anomalies induced by micrometeorites are more frequent than negative anomalies. This last comment is important as geomagnetic excursions are generally associated with a lower magnetization intensity.[12] The volume of the micrometeorite is V_m (m^3).

$$\|\mathbf{M}\| = \alpha\,\|\mathbf{S}\| \Leftrightarrow J_m\,V_m = \alpha\,J_{sed}\,V_{sed} \Leftrightarrow D = \sqrt[3]{\frac{6}{\pi}\frac{\alpha\,J_{sed}V_{sed}}{J_m}} \tag{7}$$

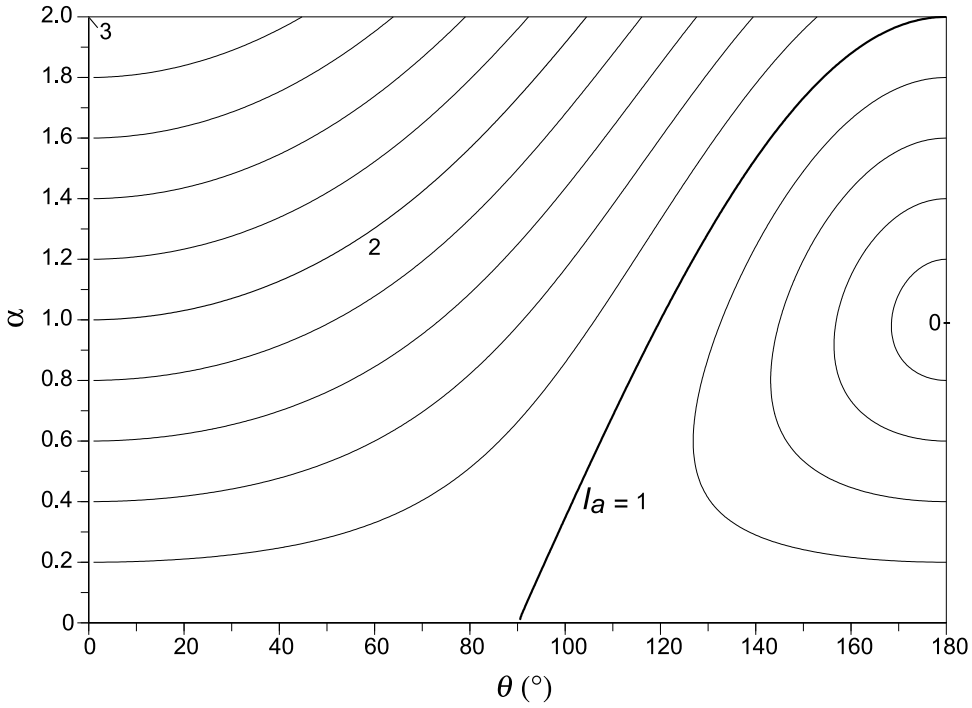

Figure 3. Contour lines of the ratio of resulting and background intensities I_a as a function of the ratio of the micrometeorite and sediment magnetizations α and the angle between the magnetizations θ.

[13] The average number of micrometeorites with a diameter in the range D_1–D_2 ($D_1 < D_2$) in the sediment sample is $[N(\geq D_1) - N(\geq D_2)]$, so the probability of presence of a micrometeorite with $\alpha\|\mathbf{S}\| \leq \|\mathbf{M}\| < (\alpha + \mathrm{d}\alpha)\ \|\mathbf{S}\|$ is $Q(\alpha)\mathrm{d}\alpha = \mathrm{d}N$. $Q(\alpha)$ is the density function for the probability of presence of a micrometeorite with $\|\mathbf{M}\| = \alpha\ \|\mathbf{S}\|$

$$Q(\alpha) = \frac{\mathrm{d}N}{\mathrm{d}\alpha} \tag{8}$$

[14] The probability R_d for a randomly oriented micrometeorite with a magnetization $\|\mathbf{M}\| = \alpha\ \|\mathbf{S}\|$ to induce an angular deviation $\delta \geq d$ in a sediment sample is

$$R_d(\alpha) = \frac{\int_0^\pi f(\alpha,\theta)\sin(\theta)\,\mathrm{d}\theta}{\int_0^\pi \sin(\theta)\,\mathrm{d}\theta}$$
$$R_d(\alpha) = \frac{1}{2}\int_0^\pi f(\alpha,\theta)\sin(\theta)\,\mathrm{d}\theta \tag{9}$$

with

$$f(\alpha,\theta) = \begin{cases} 0 & \text{if } \mathrm{d(a,q)} < \mathrm{d} \\ 1 & \text{if } \mathrm{d(a,q)} \geq \mathrm{d} \end{cases}$$

P_d is obtained by a double integration on α and J_m.

$$P_d(J_{sed}, S_r) = \iint Q(\alpha, J_m)\, R_d(\alpha)\, n(J_m)\,\mathrm{d}\alpha\,\mathrm{d}J_m \tag{10}$$

[15] We compute P_5, P_{30}, and P_{90} numerically. Figures 4, 5, and 6 show contour lines of P_5, P_{30}, and P_{90} for sedimentation rates in the range of 0.1–10 cm/ka and sediment DRM intensities in the range of 10^{-6}–10^{-2} A/m.

3. Potential Effect on the Magnetic Susceptibility

[16] The magnetic susceptibility of sediments is a commonly measured property. We tried to estimate if the presence of a micrometeorite in a sediment sample can induce a significant susceptibility anomaly. The case of diamagnetic sediments, with negative susceptibility, has not been studied specifically, but the occurrence of susceptibility anomalies in these sediments can be estimated by using the absolute value of susceptibility.

[17] Although micrometeorites with diameter <100 μm (most of them unmelted) that are present in much larger number than large micrometeorites contribute to the magnetic susceptibility of the sediment, their contribution is continuous: they do not induce anomalies. It is not necessary to include them in the calculation as they only change the background susceptibility signal. Only micrometeorites that fall less frequently are likely to

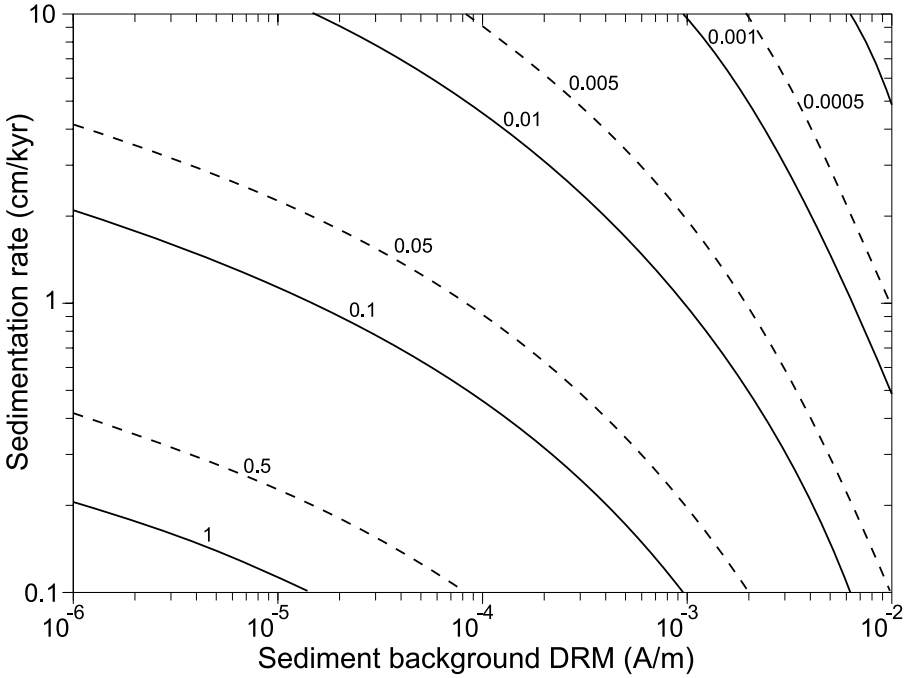

Figure 4. Probability for a 10 cm^3 sediment sample to have its detrital remanent magnetization deviated of an angle $\delta \geq 5°$ by a micrometeorite.

induce a detectable anomaly in the magnetic susceptibility record.

[18] We consider that a micrometeorite of total susceptibility $X_m(m^3)$ (volume susceptibility κ_m(SI)) in a sediment sample of total susceptibility $X_{sed}(m^3)$ (volume susceptibility κ_{sed}(SI)) induces a significant susceptibility anomaly if

$$\frac{X_m}{X_{sed}} \geq \beta_{\min} \Leftrightarrow \kappa_m V_m \geq \beta_{\min} \kappa_{sed} V_{sed} \qquad (11)$$

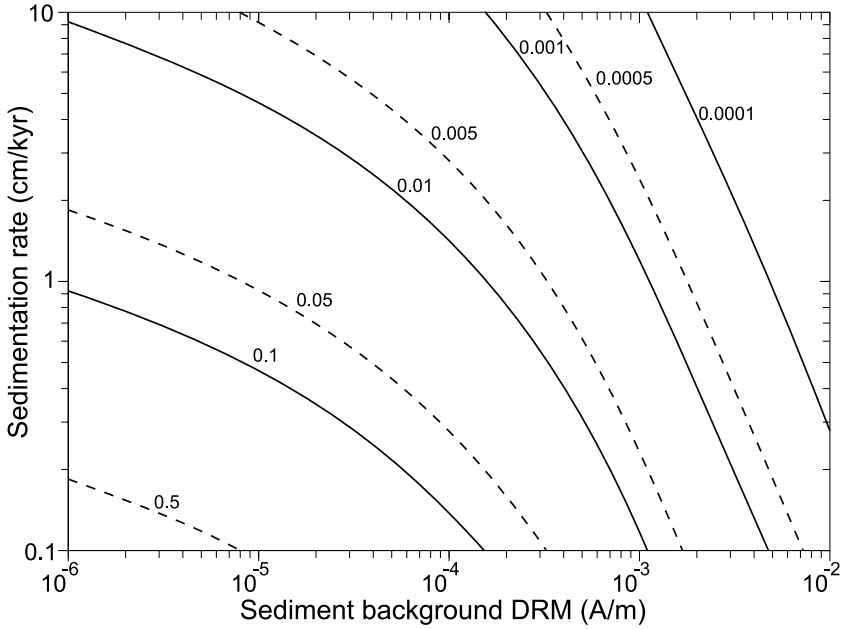

Figure 5. Probability for a 10 cm^3 sediment sample to have its detrital remanent magnetization deviated of an angle $\delta \geq 30°$ by a micrometeorite.

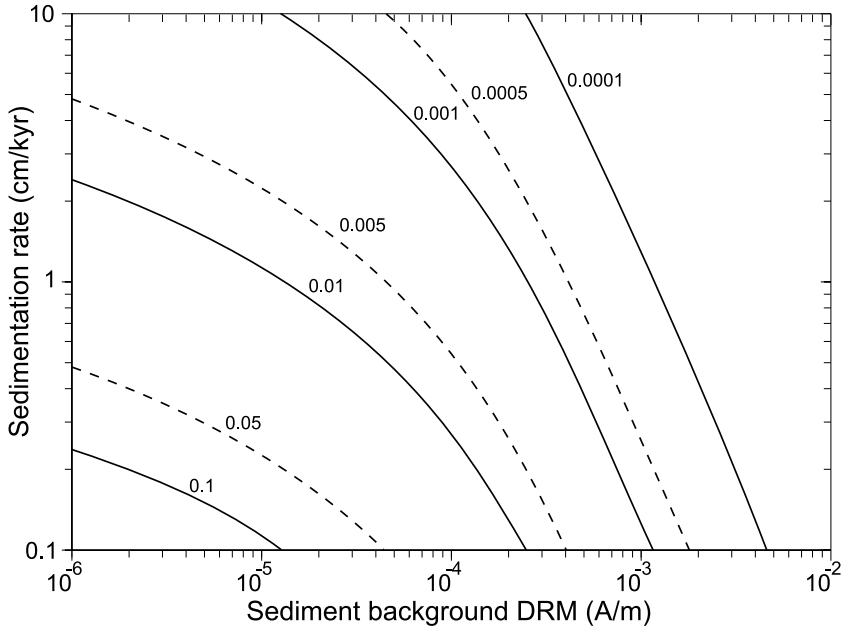

Figure 6. Probability for a 10 cm^3 sediment sample to have its detrital remanent magnetization deviated of an angle $\delta \geq 90°$ by a micrometeorite.

This is true for

$$D \geq D_{\min} = \sqrt{[3]}\frac{6}{\pi}\frac{\beta_{\min}\kappa_{sed}V_{sed}}{\kappa_m} \quad (12)$$

[19] We selected two critical values for $\beta_{\min}$ in the calculation: $\beta_{\min 1} = 1$ (anomaly of 100% of the background susceptibility) and $\beta_{\min 2} = 1/10$ (anomaly of 10% of the background susceptibility).

[20] The average number (equivalent to the probability of presence) of micrometeorites with a sufficient size to induce a magnetic susceptibility anomaly in a sediment sample is

$$P_\beta(\geq D_{\min}) = AtF(\geq D_{\min}) = \frac{V_{sed}}{Sr}a(D_{\min})^b$$
$$P_\beta(\geq D_{\min})\frac{a\,V_{sed}}{S_r}\left(\frac{6}{\pi}\frac{\beta_{\min}\kappa_{sed}V_{sed}}{\kappa_m}\right)^{\frac{b}{3}} \quad (13)$$

[21] According to magnetic susceptibility measurements of micrometeorites collected at Miller Butte (Antarctica) [*Rochette et al.*, 2008; Suavet et al., submitted manuscript, 2008], there is no correlation between the volume susceptibility and the diameter of micrometeorites. The measurement of 185 micrometeorites yields values ranging from 10^{-3} to 10 SI. We combine equation (13) with the volume susceptibility distribution of Miller Butte collection approximated by a log-normal distribution (Figure 7) to obtain the probability of presence of a micrometeorite of a sufficient size to induce a susceptibility anomaly in a sediment sample (Figure 8).

4. Discussion

[22] The validity of this model can be tested with micrometeorites recovered from deep-sea sediments. According to equation (5), micrometeorites recovered from zeolitic clays cored in the Pacific Ocean: 5–38–1 and 5–38–2 (diameters: 210 and 140 μm), with NRM $>10^{-10}$ Am^2 (Suavet et al., submitted manuscript, 2008), would induce an average deviation of 30° on a sediment sample with a DRM of $\sim 2 \times 10^{-5}$ A/m and an average deviation of 5° on a sediment sample with a DRM of $\sim 10^{-4}$ A/m. These DRM values are common for most sediments (siliceous/calcareous chalk or ooze usually have DRM in the range of 10^{-5}–10^{-3} A/m, as can be seen in ODP/IODP Initial Reports). However, these micrometeorites would not induce significant direction anomalies in deep-sea clays, as their DRM is usually above 10^{-3} A/m.

[23] Figures 4 and 5 show that even for sediments with a DRM of $\sim 10^{-3}$ A/m and a sedimentation rate of $\sim$1 cm/ka, the probability to have a deviation of the DRM $\geq$30° ($\geq$5°) is $\sim$0.5% (1%). This means that the measurement of 4 m of U-channel samples taken from such a sediment (covering a time span of 400 ka) with a typical step of 2 cm would show approximately one $\geq$30° excursion

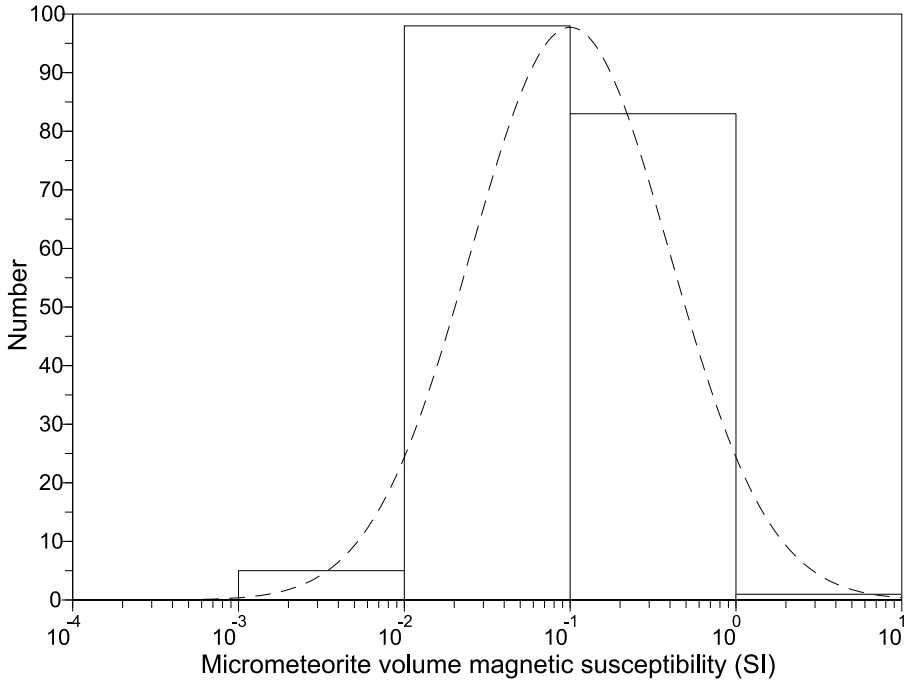

Figure 7. Volume magnetic susceptibility distribution for Miller Butte micrometeorite collection [*Rochette et al.*, 2008] and approximation by a log-normal distribution (mode is 0.1 SI; standard deviation is 0.6).

and approximately two $\geq 5°$ direction anomalies. Figure 6 shows that the probability for a sediment sample to show a magnetic reversal due to a micrometeorite is $\geq 1\%$ for sediments DRM $< 10^{-4}$ A/m and sedimentation rate <1 cm/ka.

[24] Anomalies caused by micrometeorites in the magnetic susceptibility record are much less likely than DRM direction anomalies. The probability for sediment samples to contain a micrometeorite of a sufficient size to induce an anomaly of 100% (10%) of the background susceptibility in a sediment with

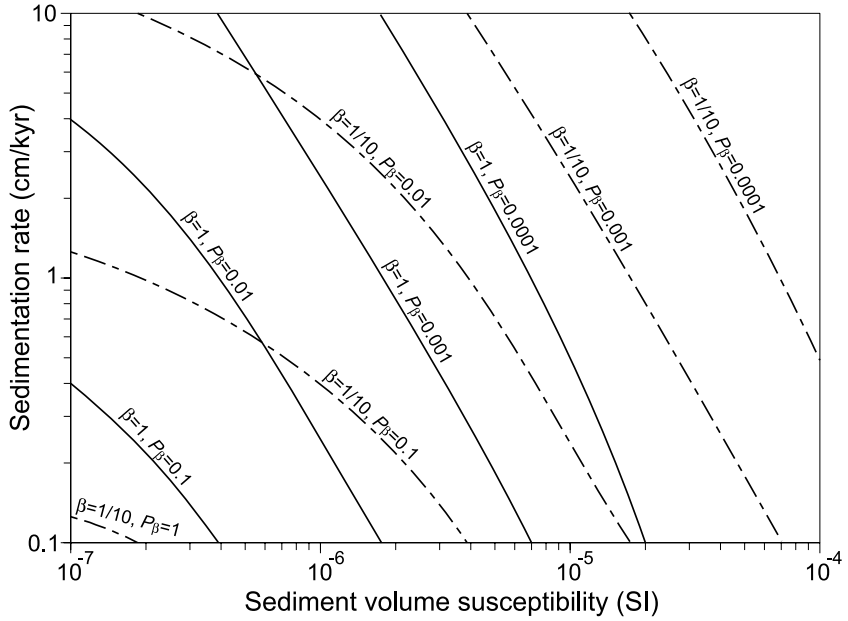

Figure 8. Probability P_β of presence of micrometeorites with a susceptibility at least equal to βX_{sed} in a 10 cm^3 sediment sample of total susceptibility X_{sed} for different sediment mass susceptibilities and sedimentation rates.

a volume susceptibility of $\sim 10^{-5}$ SI (low value for calcareous ooze or siliceous ooze) and a sedimentation rate of 1 cm/ka is only 0.0001 (0.001).

[25] Looking for micrometeorites in sediment samples with a direction and/or magnetic susceptibility anomaly should only be attempted if the probability P_d is high enough. For example, this is the case for the Cretaceous pelagic limestones studied by *Cronin et al.* [2001]. Interestingly, these authors reported single sample excursional directions (about 1.5% of the total number of samples) that could be accounted for by our model. The sedimentation rate of 0.8 cm/ka and sediment DRM in the range of $\sim 5 \times 10^{-5}$–2×10^{-3} A/m yield a probability of excursions $\geq 30°$ induced by a micrometeorite of ~0.5–2%, well in agreement with the number of excursions observed by *Cronin et al.* [2001]. These authors proposed that their excursional directions are of rock magnetic rather than geomagnetic origin. Their interpretation, based on an anomalous magnetic fabric, was that these samples were affected by "cryptoslumping." One way to prove our alternative explanation would be to recover the micrometeorite responsible for the directional excursion in a given sample. Recovery of the micrometeorite could be done by cutting the sediment sample in two parts and measuring the NRM (however this operation must be performed before demagnetization) or the magnetic susceptibility to identify in which half the micrometeorite is. This operation can be repeated until the volume is small enough to be searched by gentle crushing and magnetic separation.

[26] If thermal or alternating field demagnetization is performed, a blocking temperature outside the range 560–580°C or a median destructive field outside the range 10–60 mT, that are characteristic of micrometeorites (Suavet et al., submitted manuscript, 2008), would discard micrometeorites as a possible cause for direction anomaly. Anisotropy of magnetic susceptibility is also expected to be strong when a micrometeorite is the cause for the anomaly (micrometeorites have anisotropy degrees in the range of 1.15–1.64 (Suavet et al., submitted manuscript, 2008)).

5. Conclusion

[27] Our model shows that magnetization direction anomalies >5° caused by micrometeorites may be rather frequent (more than 1% of measured samples), even for sediments with typical values of sedimentation rate (up to 10 cm/ka) and remanent magnetization (up to 5×10^{-3} A/m). The calculation of the probability P_d for a 10 cm^3 sediment sample to have its detrital remanent magnetization deviated of an angle $\delta \geq d$ by a micrometeorite gives: P_{30} >1% for sediments with magnetizations $<10^{-3}$ A/m and sedimentation rates <10 cm/ka, and P_{90} >1% for sediments with magnetizations $<2 \times 10^{-4}$ A/m and sedimentation rates <2 cm/ka. Care should be taken when interpreting anomalous directions as possible geomagnetic excursions in such sediments. Conversely, the magnetic susceptibility record is less likely to exhibit anomalies caused by a single micrometeorite, but this possibility cannot be excluded for very low susceptibility sediments ($<10^{-5}$ SI).

Acknowledgments

[28] We would like to thank J. Tarduno, M. Jackson, and L. Lanci for reviewing this work; S. Brachfeld, T. von Dobeneck, and S. Gilder for their comments on the preliminary version of this work; and J. Duprat, R. P. Harvey, and C. Engrand for providing samples and advice. This work was supported by the French Agence Nationale pour la Recherche (project ANR 05 JCJC 0133 01).

References

Cronin, M., L. Tauxe, C. Constable, P. Selkin, and T. Pick (2001), Noise in the quiet zone, *Earth Planet. Sci. Lett.*, *190*, 13 30.

Love, S. G., and D. E. Brownlee (1993), A direct measurement of the terrestrial mass accretion rate of cosmic dust, *Science*, *262*, 550 553.

Peucker Ehrenbrink, B. (1996), Accretion of extraterrestrial matter during the last 80 million years and its effect on the marine osmium isotope record, *Geochim. Cosmichim. Acta*, *60*, 3187 3196.

Rochette, P., L. Folco, C. Suavet, M. van Ginneken, J. Gattacceca, N. Perchiazzi, R. Braucher, and R. P. Harvey (2008), Micro meteorites from the Transantarctic Mountains, *Proc. Natl. Acad. Sci. USA*, in press.

Taylor, S., and J. H. Lever (2001), Seeking unbiased collec tions of modern and ancient micrometeorites, in *Accretion of Extraterrestrial Matter Throughout Earth's History*, edited by B. Peucker Ehrenbrink and B. Schmitz, pp. 205 219, Kluwer Acad., New York.

Taylor, S., J. H. Lever, and R. P. Harvey (1998), Accretion rate of cosmic spherules measured at the South Pole, *Nature*, *392*, 899 903.

Taylor, S., G. Matrajt, J. H. Lever, D. J. Joswiak, and D. E. Brownlee (2005), Size distribution of Antarctic microme teorites, paper presented at Workshop on Dust in Planetary Systems, NASA, Kaua'i, Hawaii.

Chapitre 7

Annexe : Analyses en résonance de spin électronique

Available online at www.sciencedirect.com
ScienceDirect
Journal of Magnetism and Magnetic Materials 320 (2008) 1687–1695
Journal of magnetism and magnetic materials
www.elsevier.com/locate/jmmm

Study of a set of micrometeorites from Antarctica using magnetic and ESR methods coupled with micro-XRF

J. Marfaing[a,*], P. Rochette[b], J. Pellerey[b], P. Chaurand[b], C. Suavet[b], L. Folco[c]

[a]*Aix Marseille Université, CNRS, Institut Matériaux Microélectronique Nanoscience de Provence UMR 6242, Case 142, Faculté des Sciences et Techniques, F 13397 Marseille Cedex 20, France.*
[b]*Aix Marseille Université, CNRS, CEREGE , Europôle de l'Arbois, BP 80, F 13545 Aix en Provence, Cedex 4, France*
[c]*Museo Nazionale dell'Antartide, Siena, Italy*

Received 4 July 2007; received in revised form 7 December 2007
Available online 30 January 2008

Abstract

A collection of iron rich micrometeorites from Antarctica have been investigated using electron spin resonance (ESR) and conventional magnetic methods to establish a complete magnetic codification of their specific characteristics. Due to the high selectivity of the ESR, the spectra show that the amount and nature of the magnetic impurities contained in these tiny sized samples, mainly Ni and Cr ions, significantly modify their ESR responses. This result provides a criterion, the Ni/Cr content (identified by spectroscopy), useful for a faithful classification of this class of extraterrestrial particles with close magnetic properties. We attempt to separate the contribution of the different magnetic ions in the ESR response. This method can be easily extended to other magnetic impurities.

Keywords: Iron rich micrometeorite; Electron spin resonance; Conventional magnetic method; Micro XRF spectroscopy; Ni and Cr impurities

1. Introduction

Micrometeorites are extraterrestrial particles found on the Earth's surface, of diameter below 1 mm, that have suffered variable alteration due to atmospheric entry heating. They range from unmelted and partially melted particles, retaining much of their original mineralogy, to totally melted cosmic spherules (CS). According to Engrand and Maurette [1], micrometeorites form a unique family of the primitive solar material; they are mineralogically different from larger meteorites and probably originate in comets. On the other hand, Genge et al. [2] have challenged this view and shown that some micrometeorites are alike chondritic meteorites. Micrometeorites constitute in mass the vast majority of the extraterrestrial matter flux, with typically about one micrometeorite larger than 100 μm falling every year per square meter. However, large collections of these materials are difficult to find due to destruction of particles by weathering and highly variable concentrating processes in terrestrial environments. Antarctica is an ideal place to look for pristine micrometeorite, because the material in this region suffers little, if any, chemical or physical weathering and there is very little contamination. There are only a few minerals found in melted micrometeorites (CS) and these are determined both by the composition of the particle and by the degree of heating each particle sustained when entering the earth's atmosphere. There is no definite system of classification for CS, the most elaborate one being proposed by Taylor et al. [3]. They can, however, be grouped on the basis of their composition and of their texture. Most CS are Si-rich (glassy or crystalline with near olivine composition). However, a few percent are iron rich. Little is known on the origin of these Fe-rich CS, besides the assumption that they should derive from atmospheric oxidation of meteoritic metal [4]. A distinctive faithful codification can also be attempted through their magnetic behavior. In the magnetic domain, usually more conventional magnetic techniques are coupled with Mössbauer spectroscopy or electron spin resonance (ESR) spectroscopy. Diluted as well as concentrated ferro- or

*Corresponding author. Tel.: +33 0491 288 752; fax: +33 0491 288 775.
E mail address: jannie.marfaing@l2mp.fr (J. Marfaing).

0304 8853/$ see front matter
doi:10.1016/j.jmmm.2008.01.037

ferri-magnetic compounds with unpaired electrons are characterized by ESR spectroscopy, respectively, as electron paramagnetic resonance (EPR) or ferromagnetic resonance (FMR) showing a defined resonance with an incident monochromatic microwave radiation. This technique, non-destructive and rapid, is now fairly active and fructuous for magnetic materials [5], and is easy to couple with the conventional magnetic methods.

The present work, concerning a study of a series of 14 iron-rich CS from Antarctica, has been motivated by two main reasons: (i) the CS are largely uncharacterized because of the difficulty caused by their tiny size for studying their physical properties; (ii) because of their great number, their dispersion in various areas, their history and origin, it is useful to establish some diagnostic tools through all the magnetic techniques to define pertinent distinctive parameters allowing an easy and rapid comparison of their properties with the aim to enlarge the criteria for an accurate classification. To do so, we plan to investigate the magnetic properties of some micrometeorites from Antarctica using the conventional magnetic techniques and the ESR methodology. However, due to the complexity of the Fe oxides, main components of these samples, the analysis of the ESR signals is not trivial. We attempt to give an adequate description of the magnetic response of this class of CS, in relation with the specificity of the samples and their chemical characteristics, specifically their impurity contents, identified by micro-X-ray fluorescence spectroscopy (micro-XRF).

2. Samples and non-magnetic characterization

We selected strongly magnetic CS within the 100–200 μm fraction of sample 3 from the Frontier Mountain micrometeorite trap [6]. The most magnetic fraction was extracted in several steps using a hand magnet. The powder was submitted to alternating field demagnetization (to avoid clumping the grain together) and ultrasonic cleaning. About 100 CS were aligned on a scotch double-faced tape covering a glass slide.

2.1. Chemical analysis by micro-XRF

Micro-XRF measurements were carried out on a HORIBA XGT-5000 microscope equipped with an X-ray guide tube producing a focused and high-intensity beam with a 100 μm spot size. The X-ray beam is generated with an Rh X-ray tube at an accelerating voltage of 30 kV with a current of 1 mA. X-ray emission from the irradiated sample is detected with an energy-dispersive X-ray (EDX) spectrometer equipped with a liquid-nitrogen-cooled high-purity Si detector (resolution of 145 eV at the MnKα emission line).

14 CS selected among the most iron-rich were aligned on a scotch double-faced tape covering a glass slide. The focused incident X-ray beam was pointed on the center of each CS, and XRF spectra were recorded with a counting time of 200 s.

Compared with SEM-EDX, this technique is much more sensitive for heavy elements (e.g. Cr and Ni detection limit of 100 mg/kg) and provides bulk chemical analysis (probing over a several tens of μm depth according to the element analyzed) because the X-ray beam penetrates within the sample. Fig. 1 exemplifies our detection sensitivity of trace elements such as Cr and Ni in micrometeorites, whose compositions are given in Table 1. Thus, this technique presents the advantage to be less interfered by the crust of the secondary products (at the surface of the CS analyzed). On the other hand, the CS support (scotch double-face tape and glass slide) can affect the CS chemical analysis. The support contains mainly Si, S, K and Ca.

Therefore, elements of interest are only Fe, Ni and Cr, exclusively present in the CS core (with a possible minor contribution from secondary crust for Fe): Fe being the major element (the Fe at% are high, comprised between 60% and 98%) and Ni and Cr present at trace level (Table 1). Other elements detected are Al, Si, K, P, S, Ca, Ti and Mn likely coming from the secondary crust or from the support (note that C and O are not detected by this technique). We can note that most of the selected CS are Si-poor (<4 at%). We consider that the Si analyzed comes from the support or the crust. Only two CS (CS s-15 and s-47) present higher Si content, respectively, around 7 and 21 at% (Table 1), which can be partly attributed to CS. CS s-47 corresponds to the group of the 100 CS studied, i.e. magnetite bearing barred-olivine. The intermediate CS s-15 is likely a g-type [3]. A theoretical approach based on fundamental parameter (FP) and standard-less methods [7] was used as an easy and rapid way of extracting semi-quantitative analysis from micro-XRF spectra (results presented in Table 1). The use of this standard-less method and the sample geometry (quasi-spherical shape) induce errors on the semi-quantitative results. Relative precision on Ni and Cr is estimated to be 5%, with a detection limit

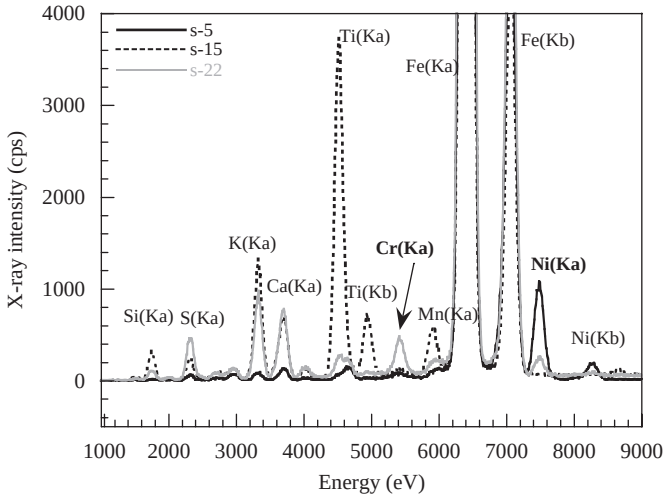

Fig. 1. Micro XRF spectra of three CS (s 15; s 22; and s 5) with different Ni/Cr at% contents (respectively, 0.7, 2.7 and 113).

Table 1
Measured parameters and chemical analyses of the set of CS

Sample	Size (μm)	Mass (μg)	Density	M_s (Am^2/kg)	M_s/M_s^*	Fe[a] at%	Si[a] at%	Ni[a] at%	Cr[a] at%	Ni/Cr ratio	Relative error on Ni/Cr ratio (%)	g_{eff}
s 15	**120**	**4**	**4.9**	**20**	**0.21**	**72**	**7**	**0.06**	**0.08**	**0.7**	**22**	**2.39**
s 47	**180**	**6**	**1.9**	**2.8**	**0.03**	**61**	**21**	**1.8**	**1.7**	**1.0**	**10**	**2.37**
s 22	125	1	1.0	(97)	**(1)**	86	<4	1.1	0.4	2.7	**10**	2.71
s 24	**131**	**4**	**3.4**	**10**	**0.1**	**81**	<4	**1.7**	**0.5**	**3.4**	**10**	**2.54**
s 21	**129**	**7**	**6.3**	**21**	**0.22**	**98**	**<4**	**1.4**	**0.2**	**7**	**10**	**2.84**
s 38	177	15	5.2	61	0.66	94	<4	1.9	0.2	9	**10**	2.93
s 33	202	20	4.7	53	0.58	88	<4	5.6	0.2	28	**10**	2.78
s 58	195	15	3.9	77	0.83	93	<4	2.5	0.06	42	**22**	2.90
s 5	140	4	2.8	49	0.53	90	<4	6.8	0.06	113	**22**	3.30
s 40	182	16	5.1	43	0.46	87	<4	5.0	0.04	125	**30**	2.77
s 65	134	6	4.7	53	0.58	87	<4	6.5	0.05	130	**25**	2.78
s 18	132	6	5			93	<4	4.6	0.03	153	**38**	3.09
s 6	146	9	5.5	46	0.50	91	<4	7.4	0.03	243	**38**	2.87
s 30	126	7	6.7	34	0.37	84	<4	8.8	0.01	880	**105**	3.06

Relative precision on Ni and Cr is estimated to be 5%, with a detection limit of 100 ppm. These values were used to compute the relative error on the Ni/Cr ratio. Bold values correspond to magnetite poor CS.
[a]Semi quantitative results obtained by micro XRF.

of 100 ppm. These values were used to compute the relative error on the Ni/Cr ratio. However, a high precision is not required because the objective is to identify a pertinent criterion to establish a faithful classification of these CS, based on coupled chemical and magnetic analyses.

All selected Fe-rich CS contain Ni at low content, between 1 and 9 at%, except CS s-15, which is practically Ni-free. Cr is also present at trace level (<0.5 at%) except CS s-47, which presents a higher Cr content around 1.7 at%. Based on these results, the selected Fe-rich CS were separated in three ranks according to the Ni/Cr at% ratio: low ratio (<7), intermediate ratio (between 9 and 50) and high ratio (>100). Moreover, this ratio appears to be the most relevant parameter in the ESR spectra analysis (Table 1).

2.2. SEM observations

Then CS were observed by scanning electron microscopy (SEM) to measure shape, dimension and image surface structures. Diameters are reported in Table 1. The most studied CS are nearly spherical, but some may show a slight ellipsoidal shape (see Fig. 11). CS surfaces show some secondary incrusting minerals formed during the stay of the CS within granitic detriti [6]. However, most surfaces are clean and show crystalline structures suggesting that the grain interior, although polycrystalline, may show some coherence in crystallite orientation. Some holes are visible indicating connection with the surface of a likely spherical cavity that erupted an immiscible phase (gas, sulfide). Sectioning and polishing an iron CS from the same collection indeed show such a spherical cavity. Apart from such a cavity, the interior of iron CS may show some central voids since thermal contraction during crystallization and cooling of the melted droplets were impeded by the rigid external spherical shell formed by quenching. Sectioning also reveals the polycrystalline state with intermixed wustite and magnetite crystals of nearly 10 μm size (as revealed by backscattered images).

2.3. Specific gravity

CS were individually weighted using a Mettler microbalance. Masses range from 1 to 20 μg and repeated weighing showed an uncertainty of near 1 μg (Table 1). Combining mass and diameter allows to estimate CS specific gravity, and to compare it with pure minerals: olivine (3.2–3.5), magnetite (5.2), wustite (5.88). The two silicates bearing CS yield a specific gravity of 4.9 and 1.9. The first (likely g-type) agrees with a majority of magnetite with minor olivine, the second (likely barred olivine) agrees with majority of olivine and large porosity. The nearly pure iron CS exhibits specific gravity in the range 2.8–6.7 (except CS s-22 at 2). Considering the large uncertainty on specific gravity, we cannot infer securely that the two values exceeding pure magnetite–wustite mixtures (CS s-21 and s-30) actually contain nuggets of denser material (metallic iron or PGE, as described in Ref. [8]). However, it is a hypothesis worth considering. For CS s-6, s-33, s-38, s-40, s-65, specific gravity values suggest pure magnetite–wustite mixture with small porosities, while larger porosities are expected in CS s-22 (hollow sample as demonstrated by later breaking), CS s-5, s-24, s-58.

3. Results and discussion

3.1. Magnetic measurements

Hysteresis loops up to 0.6 T of individual particles were obtained using an alternating gradient force magnetometer

(Micromag), and corrected from sample holder. A moderate high field slope was corrected by assuming saturation at 0.5 T (linear behavior is achieved near 0.3 T). Saturation magnetization (M_s) varies from 2 to 115×10^{-8} A m^2, while sample holder Ms was a few 10^{-9} Am^2 (see Ref. [9] for examples of hysteresis loops obtained with this instrument). Precision on specific M_s is mainly linked to the precision on mass (1 μg). Iron spherules are typically a mixture of magnetite and other weakly magnetic or paramagnetic iron oxides (wustite or eventually hematite). FeNi metal has also rarely been reported in some iron spherules. Generally Ni is in substitution in magnetite or wustite and M_s measurement is mainly due to the presence of the magnetite phase in the samples.

Ratio between the CS magnetization, M_s, and the pure magnetite's one, $M_s^* = 92$ A m^2/kg can be related to an estimated percentage of Fe ions in the samples, taking for 1 the total number of Fe^{3+} and Fe^{2+} ions in magnetite. This approach allows a determination of the CS which are of poor- or rich-magnetite type according to whether the ratio M_s/M_s^* is low (<0.25) or high, respectively. Table 1 shows that the four magnetite-poor CS are among the Ni-poor and those having the lowest Ni/Cr at% ratio.

CS s-22 stands out with a high magnetite amount (100%) and low Ni content ($\approx$1 at%); however, this sample is extremely light (weight measured: 1 μg) and therefore the magnetite percent is practically undefined. For the other CS the computed magnetite proportion is between 40% and 80%. Precision on this amount has to be weighted by the CS mass and range from 5% to 20%. If present, the metal should be a minor component as it would show up in CS Ms values exceeding the one of the magnetite. When possible (large enough M_s) hysteresis parameters were derived. They revealed that magnetic grains were very soft ($M_{rs}/M_s<0.1$, $H_c<10$ mT), indicating multidomain magnetite. This rough classification can be completed by the ESR study.

3.2. ESR spectra

The ESR experiments were carried out using a Bruker EMX 10/12 spectrometer operating at $\nu_0 = 9.63$ GHz. The cavity, excited on the TE_{102} mode, was irradiated with a microwave power of 1 mW. The static field B was modulated sinusoidally at a frequency $\nu_m = 100$ kHz with an amplitude of 5×10^{-4} T. For $\nu_0 = 9.63$ GHz, the resonance for $g = 2$ (free spin) occurs at $B_r \approx 0.3464$ T. The spectra have been recorded at room temperature under identical conditions, from $B = 0$ up to 1 T with a resolution of 1024 points. Due to the small mass of some CS, to extract the specific signal of the meteorites, signal of the cavity and the sample holder have been subtracted. Each spectrum was normalized to the spectrometer gain and sample mass.

As already said, in the following, the Ni/Cr content in the CS is taken as a pertinent parameter for comparing the ESR response of the CS.

3.2.1. Derivative signals FMR response of the CS

The CS s-15 and s-47 are two poor-magnetite-like phases, especially s-47 with a minimal Ni/Cr ratio. Their ESR spectra presented in Fig. 2 can be regarded as reference for the ESR study of this kind of samples. The signal is broad and shows an anisotropic shape, characteristic of FMR resonance. No specific additive line of dispersed Fe^{3+} ions has been detected, at about $B = 160$ mT ($g = 4.3$), as sometimes seen in several glasses [10,11], clay minerals [12–15], tephra [16,17] and magnetofossils [18] which also present a large signal. The derivative lines give a direct access to the g-value at zero-crossing, which can be considered as the effective g-value of the samples, g_{eff}. If the lines are very narrow, as observed in samples of high crystal quality, the g-value is well related to a single magnetic ion in its crystallographic configuration inside the sample. The interpretation of large lines (case of multicrystals or powder) is more uneasy, as the broadening is mainly due to (i) the spin–spin interactions, in concentrated systems, whether of a same element or of different types of ions; (ii) the anisotropy due to the sample shape.

As CS s-15 and s-47 present a strong ferrosilicate character and minimal values of the Ni/Cr ratio, their FMR response can be compared with that of a ferrosilicate tephra, free of Ni and Cr ions, largely studied under similar conditions in a previous work [16,17] (see Fig. 2). The spectra show similarities, a regular and asymmetric line shape; however, the linewidth and the asymmetry are more important in the case of the CS responses, mainly due to the different Fe ions content in the samples. Even if s-15 contains a very low amount of Cr and Ni as the RX of Fig. 1 shows, the ESR spectrum is revealing this small amount of impurity as the corresponding lineshape (position of the maximum and g_{eff} value 2.39) is very

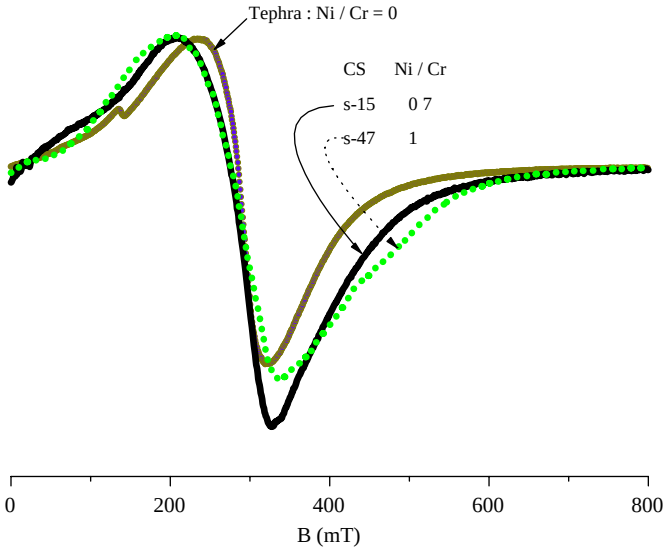

Fig. 2. FMR response of a ferrosilicate tephra, free of Ni and Cr ions (tephra 711), and two CS, magnetite like, which present a low Ni/Cr at% ratio, respectively 0.7 and 1 for CS s 15 and 1 for CS s 47.

similar to the s-47 one in comparison with the fully free one of Ni/Cr tephra (g_{eff} value = 2.14); this substantiates the sensibility of the ESR technique, which can identify with a great accuracy if impurities exist or not in the sample.

In the series, CS s-15 and s-21, which are characterized by a very similar M_s/M_s^* and so suggest comparable ferro-oxide phases in the CS, present a different Ni/Cr ratio, higher in the case of s-21. Their line shapes differ, as Fig. 3 shows; the broadening of the s-21 line can be attributed to the spin–spin interactions between Ni–Ni or Fe–Ni ions as the concentration of Ni ions in s-21 is around seven times more than in s-15. In parallel, the double integration of their derivative lines, which is proportional to the magnetic susceptibility of each CS, shows a higher magnetic susceptibility for s-21 than for s-15, suggesting that Ni ions substitute for the Fe sites. Let us consider now the case of CS s-38 and s-21: they present a similar Fe at% content (slightly superior for s-21) and a comparable number of magnetic impurities (Ni/Cr at% similar ratio), but an M_s/M_s^* ratio 3 times higher for s-38 than for s-21. Fig. 4 displays that the type of ferroxides present in the CS influences the FMR spectra. Their line shape is broad, asymmetric, with a close g_{eff} value. However, the s-38 spectrum exhibits several structures in the range 300–500 mT. These additive lines are also present in the FMR signature of CS, presenting a Ni/Cr at% ratio in the range $9 < \text{Ni/Cr at\%} < 50$. Fig. 5 presents the responses of 3 CS, with Ni/Cr at% ratios of 9, 28 and 42 (s-38, s-33 and s-58, respectively). These CS are of rich-magnetite type (high M_s/M_s^* ratio) and the increasing quantity of magnetic dopants, mainly due to the Ni ions, has the tendency to develop several peculiar interactions, which can be detected by the set of lines existing at high field. However, it is not excluded that these additive lines can be partially due to the shape anisotropy of samples due to the eventual presence of holes in the samples capable of appreciably modifying the external field orientation.

Other CS contain a high Ni/Cr at% ratio (>100), and for this class the FMR response is similar: the lines are regular and very broad (more than 200 mT), as seen in Fig. 6, and the g-values are higher ($2.78 < g_{eff} < 3.3$) than for CS, presenting the lowest Ni/Cr at% ratio ($g_{eff} = 2.39$ for CS s-15). In this group, CS s-30 contains a quasi-zero Cr ions content (0.01 at%) and a maximal Ni ions amount ($\approx$9 at%). Several ferroxides are present in this CS (as the M_s/M_s^* ratio attests), and its line is significantly representative of the magnetic interactions induced by the Ni ions in substitution with the Fe-oxides in comparison with the Fe–Fe interactions that can exist in CS containing a very low content of impurities, as it is the case for s-15 (Fig. 2). The evolution of the FMR line shape with the increasing amount of Ni ions, from CS containing a very few number

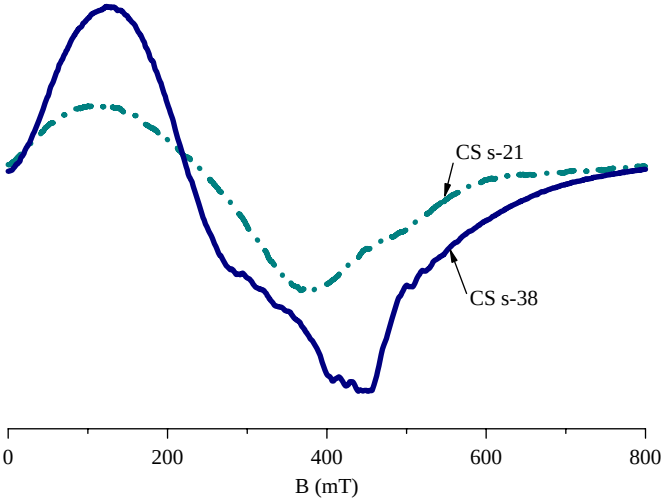

Fig. 4. Spectra of CS presenting a similar impurity ratio and different ferro oxide phases.

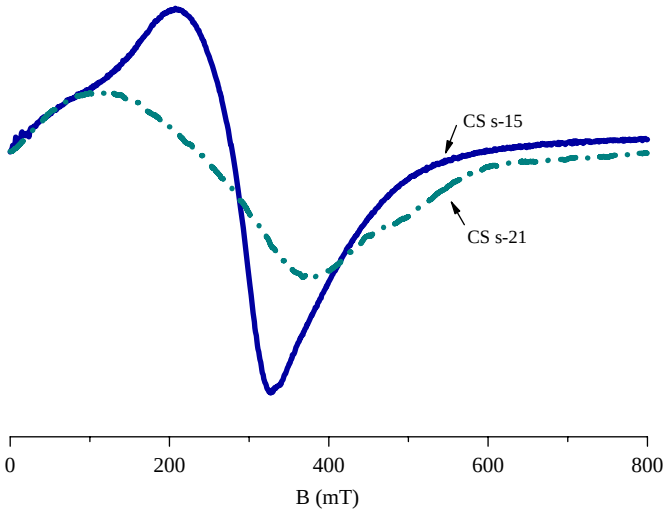

Fig. 3. Influence of the increased quantity of Ni ions for two poor magnetite type CS: broadening of the line and decreasing of the amplitude.

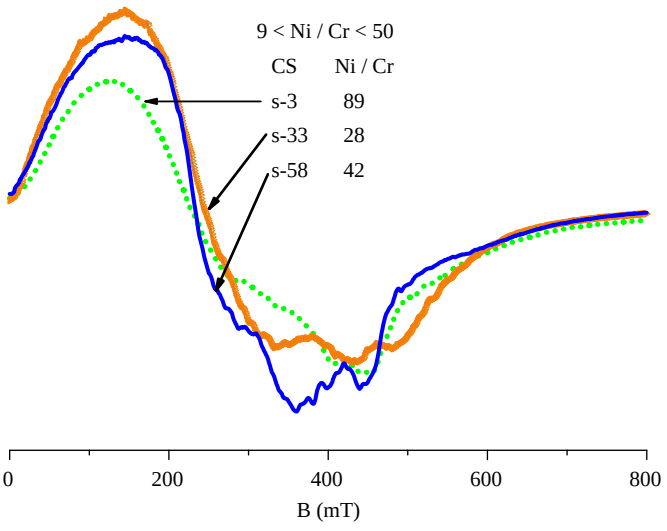

Fig. 5. FMR responses of three rich magnetite type CS with Ni/Cr ratios of 9, 28 and 42 (CS s 38, s 33 and s 58, respectively).

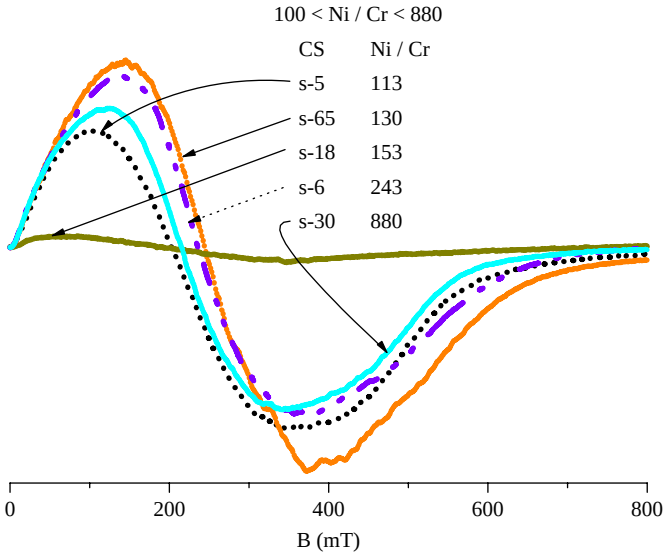

Fig. 6. FMR responses of CS with high Ni/Cr ratio (Ni/Cr > 100).

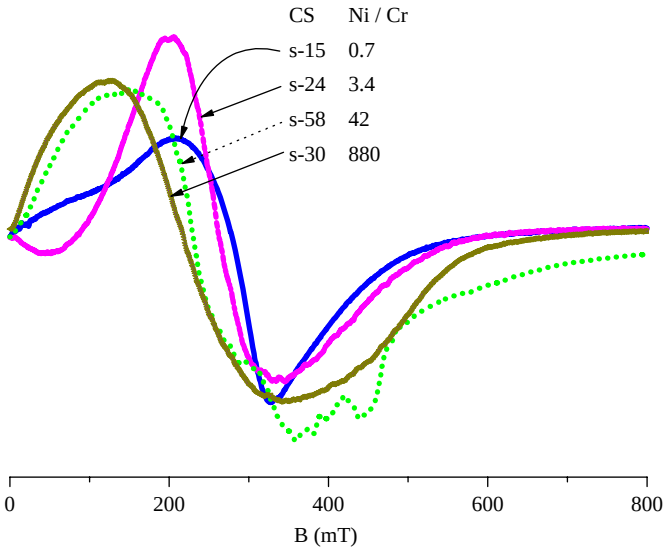

Fig. 7. Change of the FMR responses of CS with increasing Ni/Cr ratios showing the broadening of the line and the g_{eff} shift towards low field in the range [0 1 T].

of Ni and Cr ions (s-15) to CS mainly containing a high quantity of Ni ions (s-30), is presented in Fig. 7. Whatever the type of Fe phases is, poor- or rich-magnetite type (respectively, s-15 and 24 or s-58 and 30), the increase of Ni ions in the samples induces the broadening of the FMR line and the shift of the g_{eff} value towards low field.

3.2.2. Differential signals role of the impurities

In soil samples, Ni and Cr impurities are rarely detected via EPR. In general, only Ni^{2+} ion is EPR active and hence can be detected as impurity when Fe metal is quenched in the presence of oxygen giving a (Fe,Ni)O component [19]. In the presence of Cr and Ni impurities, a more complex system can be formed: whether a $(Fe,Ni,Cr)_3O_4$ oxide exists in which the charge of the ions can be Fe^{2+} or Fe^{3+}, Ni^{2+}, Cr^{3+}, or a multiphase material is formed with typically the thermodynamically stable $NiFe_2O_4$ (or $(Ni,Fe)Fe_2O_4$ and mainly $FeCr_2O_4$, $(Fe,Cr)_2O_3$, Cr_2O_3–FeO, $Cr_2(FeO_2)_6$ phases (database JCPDS). This scenario can be different in the case of micrometeorites as their formation is achieved under non-equilibrium conditions.

As the Ni/Cr at% ratio of the CS greatly modifies the EPR lines, the challenge is to attempt the EPR identification of the Ni and Cr roles in these samples.

3.2.2.1. Role of Ni. The Ni influence on the FMR signature can be evaluated because CS s-15 is quasi-free of Ni and Cr ions and so can be taken as a reference of the FMR absorption of Fe ions. The fact that all the CS are Cr-poor reinforces this approach. Each CS can be compared with CS s-15 by subtracting their spectra. This difference line is useful to evaluate the Ni increasing content, which can be regarded by this way in two cases, when the CS are of poor-or rich-magnetite type. More, using the difference of signals tends to reduce the Fe ions magnetic response.

In the first case (poor-magnetite type), the difference between the two signals of s-15 and s-21 traduces the influence of both residual Fe and Ni ions, EPR active in s-21 (Fig. 8a). In the second case (Fig. 8b), s-38 is of rich-magnetite type with a Ni/Cr at% ratio very close to that of s-21 (poor-magnetite type) and the difference line is comparable to the precedent one. So, whatever the type of the sample is, the difference line shows two distinct signals, due to FMR active ions. The signal at low field varies in position and amplitude when the sample is of poor-or rich-magnetite type, suggesting that it could be due to the different number of Fe^{2+} or Fe^{3+} present in the

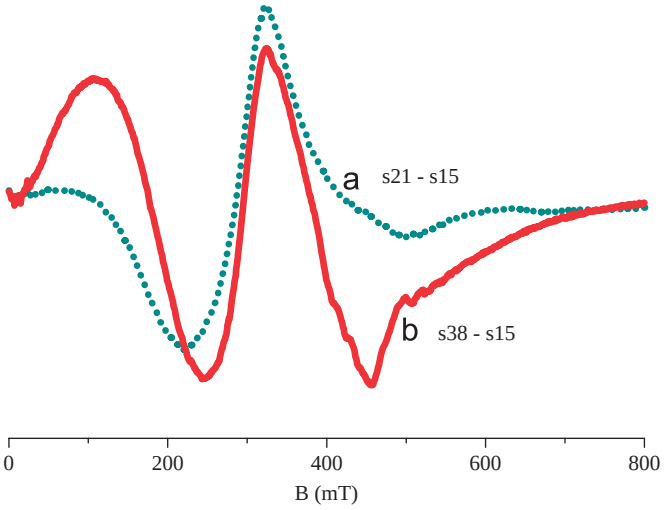

Fig. 8. (a) Difference of FMR spectra between two poor magnetite type samples, CS s 21 and CS s 15, but presenting different Ni /Cr ratios 7 and 0.7, respectively, showing the influence of the Ni ions in the sample. (b) Difference of FMR spectra between one rich magnetite type sample, CS s 38 (having similar Ni/Cr ratio as CS s 21), and a poor magnetite type sample, CS s 15 (Ni /Cr ratio 0.7), also showing the influence of the Ni ions in the sample.

samples. On the contrary, the signal near the high field is independent of the type of the sample and could be correlated to the presence of the Ni ions (see also further).

As usual in EPR study, complementary knowledge can be obtained using a Lorentzian–Dysonian fit of the lines, which takes into account the asymmetry of the signal. The best fit of Fig. 8b is obtained in Fig. 9 with three different absorption lines. The g values used in the fit are $g_{fit} = 3.61$, 2.14, and 1.68. Referring to the literature, only $g_{fit} = 2.14$ is comparable with $g_{Ni} = 2.19$ [20] measured for Ni^{2+} ion in different environments.

The other g_{fit} values could be due to the presence of Fe ions, while their state charge is not so clear. This result is not so surprising as the meteorites are of unknown origin and consequently some unexpected results can emerge if diverse oxidation states of the constitutive elements exist. In space, oxidation state is transformed (but not totally reset, as shown by the observation of metal inclusions by other studies) by the atmospheric entry oxidation, and eventually by slow oxidation on the Earth surface. Fe ions are assumed Ni substituted in the samples, but their oxidation state can be different from the classical Fe^{2+} and Fe^{3+} generally obtained in the soils, in relation with the melting conditions of the CS during its formation. Indeed, it has been tested [21] that a hypothetical candidate for the Martian oxidant is the Fe^{6+} ion, which is paramagnetic and EPR active, as non-oriented powder samples containing this ion display a singlet EPR spectrum at $g = 1.99$. This concrete possibility is testable by the near-term missions of the Mars program and could give new possibilities for the understanding of the Ni EPR response in the CS, in relation to the hypothesis of a Fe–Ni substitution process.

3.2.2.2. Role of Cr. Attempt to extract the Cr influence is more tricky as the Cr ion concentration is very low. However, two poor-magnetite-like samples (s-47 and s-24) present a comparable Ni at% amount but a different Cr ion concentration, around three times higher in s-47 than in s-24. By subtracting their derivative spectra, the role of Cr ions is evidenced in Fig. 10. We verify that difference between s-47 and s-22 gives a similar signature of the presence of Cr ions.

The best fit of the line is obtained (Fig. 10) with three different absorption lines, with g values of $g_{fit} = 4.38$, 2.71, and 2.22. In soil samples, Cr ions which can have various charges depending on the environment can observed via EPR around $1.90 < g < 2$.

While this approach is debatable, the complete analysis of the FMR spectra elicits the presence of specific Ni and Cr clues in the Fe oxidized CS. By a pertinent choice of the samples (according to their chemical components in Table 1), the difference of their EPR lines, shown in Fig. 11, independently evidences the EPR features of

- Fe ions (in low field range) in curve a (circles) concerning s-21–s-15 and b (triangles) related to s-47–s-24;
- Cr ions in curve c (full line) representative of s-33–s-40 and b;
- Ni ions in curve a.

No Fe-oxidized signal is detected in curve *c* as the two CS, s-40 and s-33, present very close at% Fe; in the same way, the presence of Cr and Ni ions is not detected in curve *a* and *b*, respectively.

However, independently of the various magnetic ions which can modify the EPR signal of one CS, the main feature of its representative line is characteristic of FMR absorption. By analogy with the FMR spectra of interacting spherical magnetic particles in soil or volcanic samples [22,23], the CS lines can be due to the interaction of the constitutive phases of the joined geometric microcrystals of the CS. Indeed, Fig. 12a shows the general pavement

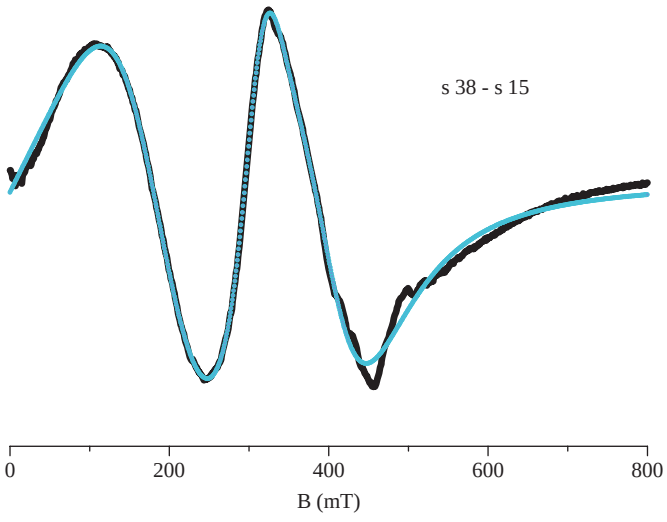

Fig. 9. The best fit of Fig. 8b obtained with three different absorption lines, located at 185, 312 and 399 mT.

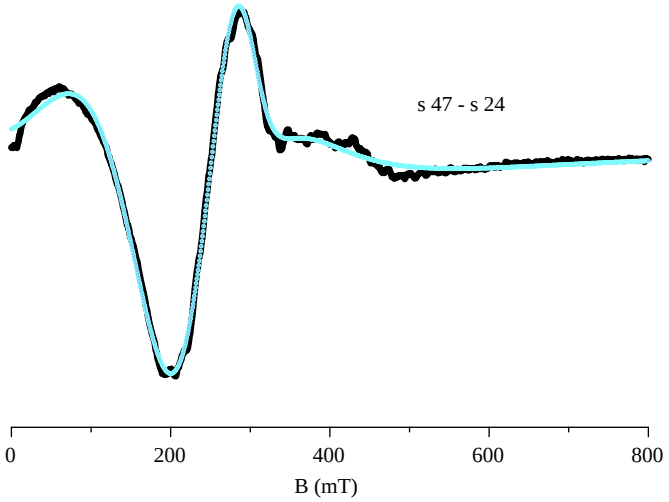

Fig. 10. Line obtained by difference of signals of CS s 47 and CS s 24) showing the influence of Cr ions (a solid line: experimental difference) and fit with three lines (dotted line).

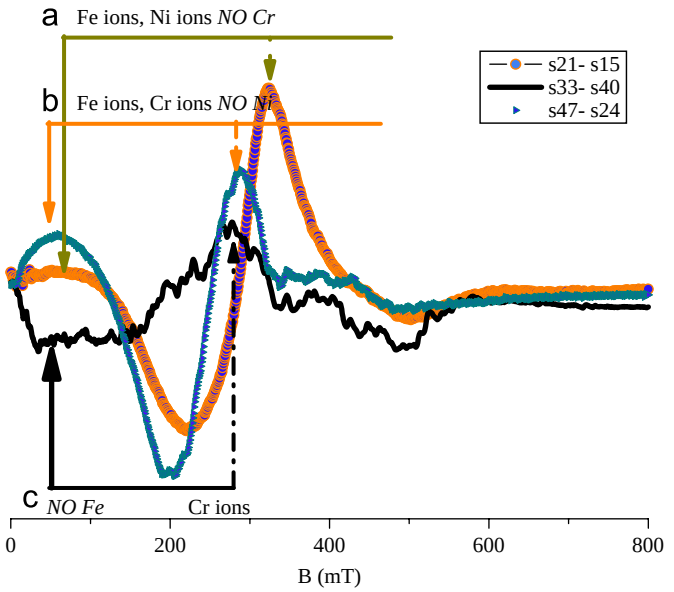

Fig. 11. Due to the chemical composition of each CS, the difference of their FMR spectra evidences the magnetic signals. (a) (circles): this difference s 21 s 15 shows the signal of Fe oxide and Ni ions; (b) (triangles): difference s 47 s 24, two poor magnetite type CS, shows the presence of Fe and Cr ions; (c) (full line): this difference for two CS with close Fe and Ni at%, s 33 s 40, shows the presence of Cr ions.

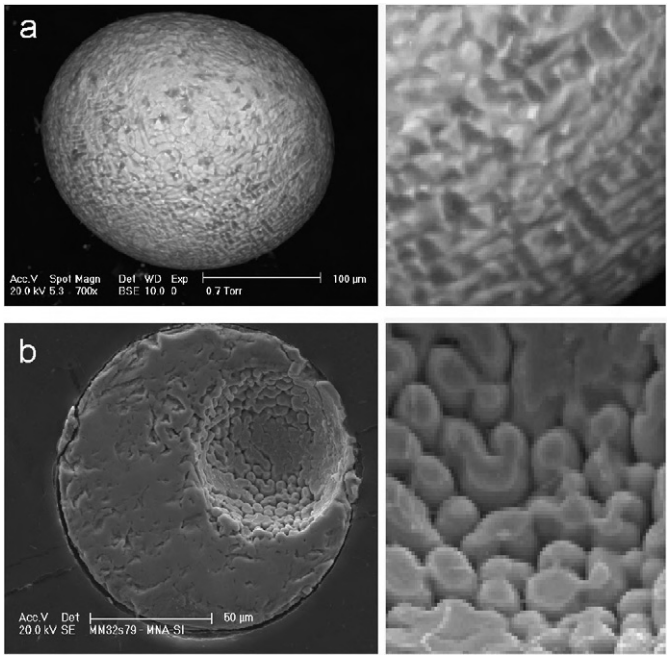

Fig. 12. (a) Pavement of the surface of CS (CS s 31b) with external details showing triangular and parallelepipedic shapes of the microcrystals. (b) Half of the CS with a hole inside the sample evidenced after cutting and polishing; details inside the hole of the ellipsoidal joined microstructures constituting the sample which are not modified by polishing can be appreciated with the links between the particles.

of surface for one CS, resulting from the juxtaposition of triangular-, parallelepiped- or square-shaped microcrystals (see zoom on the right). Some CS present more spherical/ellipsoidal microstructures and contain inside holes as evidenced in Fig. 12b by cutting and polishing. It is known that polishing affects the microstructures' shape, whose original shape is seen inside the hole, in the zoom pattern. But, whatever the microstructure model and the presence or not of hole are, the inter-linked particles, assumed to have a (ferro-) ferrimagnetic character, magnetically interact, and the resulting magnetic signature of CS is a main broad and asymmetric FMR signal.

The long-range ferromagnetic correlation extends across the grain boundaries and can induce a notable additional anisotropy seen in the spectra. This point is not elucidated because the anisotropy can also result from the pairing between the outside (surface) and inside (volume) grains; the surface contribution is important, as for these tiny samples the surface/volume ratio is high, and the oxidation degree of the Fe ions can be different at the surface and in the volume of the CS. It is known from recent studies that nanograins [24–27] are often considered as composed of two phases—core and shell—each of which exhibits different properties; this model can be kept for the meteorites, which are in some cases more or less empty, in regard with their density.

4. Conclusion

This paper has described the magnetic response of micrometeorites from the Antarctica obtained via conventional and ESR techniques with the goal to define pertinent distinctive parameters allowing an accurate classification as the magnetic results for such a class of materials are not numerous. The main difficulty for these CS is related to the complexity of their Fe oxide components. Beyond the chemical and magnetic parameters, which give a rudimentary knowledge of the magnetic characteristics for the CS, due to the small quantity of material, we show that the non-destructive ESR technique greatly contributes to accurate information for a useful classification. These CS are mainly Fe-rich, with variable Ni and Cr impurity contents, and present a FMR resonance with a signature very sensitive to the number and type of included or substituted magnetic impurities.

Whatever the magnetite type of the CS is, even poor-or rich-magnetite-like material, a pertinent parameter used in the classification of the studied set of samples has been the Ni/Cr at% ratio. The main result of the study is the evidence of a large evolution of the spectra, detected when the Ni/Cr at% ratio increases in the meteorites, from low to high g-factor as the Ni/Cr ions content rises. The long-range ferromagnetic correlation between Ni–Ni or Ni–Fe or Ni–Cr–Fe ions extends across the grain boundaries of the microcrystals constituting the samples and traduces the multiple interactions between magnetic ions differently sized and charged. For high Ni/Cr ions content, the FMR line shape stabilizes in a regular signal, broader than in the case of medium or low Ni/Cr at% ratio, showing that the maximum of the absorption is shifted towards low field,

due to the Ni ions' influence. Attempt to experimentally separate the two contributions of Ni and Cr ions included in the Fe-oxidized meteorites has been undertaken for poor- or rich-magnetite-like micrometeorites.

Acknowledgment

We are grateful to Prof. A. Stepanov for useful discussions. Sampling in Antarctica was supported by the Italian Programma Nazionale delle Ricerche in Antartide (PNRA) and by the French polar program Institut Paul Emile Victor (IPEV). Analyses were supported by ANR 05-JCJC-0133-01 and INSU/PNP programs.

References

[1] C. Engrand, M. Maurette, Meteoritics Planet. Sci. 33 (1998) 565.
[2] M.J. Genge, A. Gileski, M.M. Grady, Meteoritics Planet. Sci. 40 (2005) 225.
[3] S. Taylor, J.H. Lever, R.P. Harvey, Meteoritics Planet. Sci. 35 (2000) 651.
[4] V.M. Dekov, G.M. Molin, M. Dimova, C. Griggio, I. Rajta, I. Uzonyi, N. Jb. Miner. Abh. 183 (2007) 269.
[5] M.S. Seehra, D.L. Huber, Magnetism and magnetic materials, in: C.D. Graham Jr., G.H. Lander, J. J Rhyne (Eds.), AIP Conference Proceedings No. 24, AIP, New York, 1975, (1974 and references therein).
[6] L. Folco, P. Rochette, C. Suavet, J. Gattacceca, Meteoritics Planet. Sci. 41 (2005) 5201.
[7] D.K. G de Boer, P.N. Brouwer, Adv. X ray Anal. 33 (1990) 237.
[8] H. Feng, K.W. Jones, S. Tomov, B. Stewart, G.F. Herzog, C. Schnabel, D.E. Brownlee, Meteoritics Planet. Sci. 40 (2005) 195.
[9] Z. Djouadi, J. Gattacceca, L. d'Hendecourt, P. Rochette, A.P. Jones, C. Davoisne, H. Leroux, H. Borg, J. Astron. Astrophys. 468 (2007) L9 L12.
[10] C.M. Schlinger, D. Griscom, G.C. Papaefthymiou, D.R. Veblen, J. Geophys. Res. 93 (1988) 9137.
[11] A. Pawse, S. Breske Diehl, S.A. Marshall, Geophys. J. Int. 132 (1998) 712.
[12] J.C.J. Bart, N. Burriesci, F. Cariati, S. Cavallaro, N. Giordano, M. Petrera, Bull. Minéral. 105 (1982) 43.
[13] D. Bonnin, S. Muller, G. Calas, Bull. Minéral. 105 (1982) 467.
[14] J.M. Palias, S. Kichner, R.J. Delmas, Ann. Glaciol. 14 (1990) 216.
[15] E. Balan, T. Allard, B. Bouzot, G. Morin, J.P. Muller, Clays Clay Miner. 47 (1999) 605.
[16] B. Ananou, S. Regnier, Y. Ksari, J. Marfaing, A. Stepanov, Y. Touchard, P. Rochette, Geophys. J. Int. 155 (2003) 341.
[17] B. Ananou, A. Baronnet, Y. Ksari, J. Marfaing, S. Regnier, P. Rochette, A. Sulpice, A. Stepanov, J. Magn. Magn. Mater. 293 (2005) 816.
[18] B.P. Weiss, et al., Earth Planet. Sci. Lett. 224 (2004) 73.
[19] A. Kosakevitch, J.R. Disnar, Geochim. Cosmochim. Acta 61 (1997) 1073.
[20] A. Abragam, B. Bleany, Electron paramagnetic resonance of transition ions, in: W. Marshall, D.H. Wilkinson (Eds.), International Series of Monographs on Physics, Clarendon Press, Oxford, 1970.
[21] A.I. Tsapin, M.G. Goldfeld, G.D. McDonald, K.H. Nealson, B. Moskovitz, P. Solheid, K.M. KeCSer, S.D. Kelly, K.A. Orlandini, Icarus 147 (2000) 68.
[22] D.L. Griscom, J. Non Cryst. Solids 42 (1980) 287.
[23] C.M. Schlinger, D. Griscom, et al., J. Geophys. Res. 93 (1988) 9137.
[24] X. Battle, A. Labarta, J. Phys. D: Appl. Phys. 35 (2002) R15.
[25] F. Bodker, S. Morup, S. Linderoth, Phys. Rev. Lett. 72 (1994) 282.
[26] L. Del Bianco, A. Hernando, E. Bonetti, E. Navarro, Phys. Rev. B 56 (1997) 8894.
[27] L. Del Bianco, D. Fioani, A.M. Testa, E. Bonetti, L. Signorini, Phys. Rev. B 66 (2002) 174418.

Troisième partie

Rapports isotopiques de l'oxygène des micrométéorites

Chapitre 8

Identification des corps parents des micrométéorites

8.1 Manuscrit en préparation

Contribution de C. Suavet : Photographies au microscope électronique à balayage et pesée des micrométéorites. Analyses chimiques XRF. Mesures magnétiques. Mesure des rapports isotopiques de l'oxygène des micrométéorites et des standards par fluorination laser et spectrométrie de masse. Analyse des données. Ecriture de l'article.

Solving the parent bodies of micrometeorites with high-precision oxygen isotope ratios

Clément Suavet[1], Anne Alexandre[1], Ian A. Franchi[2], Jérôme Gattacceca[1], Corinne Sonzogni[1], Richard C. Greenwood[2], Luigi Folco[3], Pierre Rochette[1]

[1]CEREGE, Aix-Marseille Université, CNRS, Aix-en-Provence, France.
[2]Planetary and Space Science Research Institute, Open University, Milton Keynes, France.
[3]Museo Nazionale dell'Antartide, Università di Siena, Siena, Italy.

Abstract

Oxygen isotopic compositions allow identification of potential parent bodies of extraterrestrial materials. We measured oxygen isotope ratios of 33 large (diameter >500 μm) melted micrometeorites (cosmic spherules) from Antarctica using IR-laser fluorination coupled with mass spectrometry. Our results question the paradigm of carbonaceous chondrite-like parent bodies for all micrometeorites : as ∼30% of measured samples have oxygen isotope ratios lying above the terrestrial fractionation line, they may be related to ordinary chondrites or other, as yet, unsampled parent bodies. Therefore, a major part of the interplanetary dust accreted by the Earth originates from ordinary chondrite-related asteroids.

Article

Micrometeorites are extraterrestrial particles smaller than about 2 mm collected on the Earth's surface. Based on petrographic and chemical investigation of small unmelted micrometeorites (diameter ∼150–250 μm), previous studies (*1*) have concluded that 99% of them come from carbonaceous, possibly cometary parent bodies (CM/CR related), although evidence for ordinary chondrite-related micrometeorites was recently put forward (*2*, *3*). This argument has generated the credo that micrometeorites sample different objects than macroscopic meteorites. This credo has been explained invoking friable parent bodies that would produce small particles upon collision rather than big chunks of rocks.

Subsequent ion probe oxygen isotopic analyses, mostly on melted micrometeorites (cosmic spherules : CSs) (*4*, *5*, *6*), have confirmed this argument as all samples had oxygen isotope ratios below the terrestrial fractionation line (TFL), except for a few samples that indicated ratios on the TFL within analytical uncertainties. The typical analytical uncertainties of the ion probe ($\pm$1–2.75‰ on δ^{18}O, $\pm$0.7–1.7‰ on δ^{17}O, and $\pm$0.6–1.7‰ on Δ^{17}O for individual analyses (*4*, *5*), including the statistical uncertainty associated with the measurement of the sample as well as the uncertainty associated with the instrumental fractionation correction derived from repeated analyses of the standard mineral) make it difficult to resolve signatures indicating a potential ordinary chondrite parent body (Δ^{17}O $\approx$ 0.5–1.5‰) from terrestrial values. Consequently, the near-TFL values were interpreted as terrestrial contamination of carbonaceous chondrite material. IR-laser fluorination coupled with mass spectrometry has a much better precision, by one to two orders of magnitude : the reproducibility on quartz standards at CEREGE (Aix-en-Provence, France) is $\pm$0.15‰ for δ^{18}O (n = 76) (*7*), $\pm$0.11‰ and $\pm$0.034‰ for δ^{17}O and Δ^{17}O, respectively (n = 37) ; and at the Open University (Milton Keynes, United Kingdom) the reproducibility is $\pm$0.08‰ and $\pm$0.04‰ for δ^{18}O and δ^{17}O, respectively (measured on obsidian standard, n = 31), and $\pm$0.024‰ for Δ^{17}O (measured on terrestrial whole rocks and mineral separates, n = 47) (*8*). Measurements of δ^{18}O are possible on masses as small as 0.3 mg at CEREGE (*9*), and 0.2 mg at Open University (*10*), although such capability still limits analyses to the largest micrometeorites. The discovery of the Transantarctic Mountains micrometeorite collection (*3*) – in traps that collected micrometeorites by direct infall for hundreds of thousands of years – made available hundreds of CSs with a sufficient mass to allow IR-laser fluorination. In this study, we performed oxygen isotope measurements of 33 large (diameter >500 μm) silicate ("stony") CSs from the Transantarctic Mountains collection using IR-laser fluorination/mass spectrometry at CEREGE and Open University.

Figure 8.1 features our δ^{18}O and δ^{17}O single micrometeorite IR-laser fluorination data,

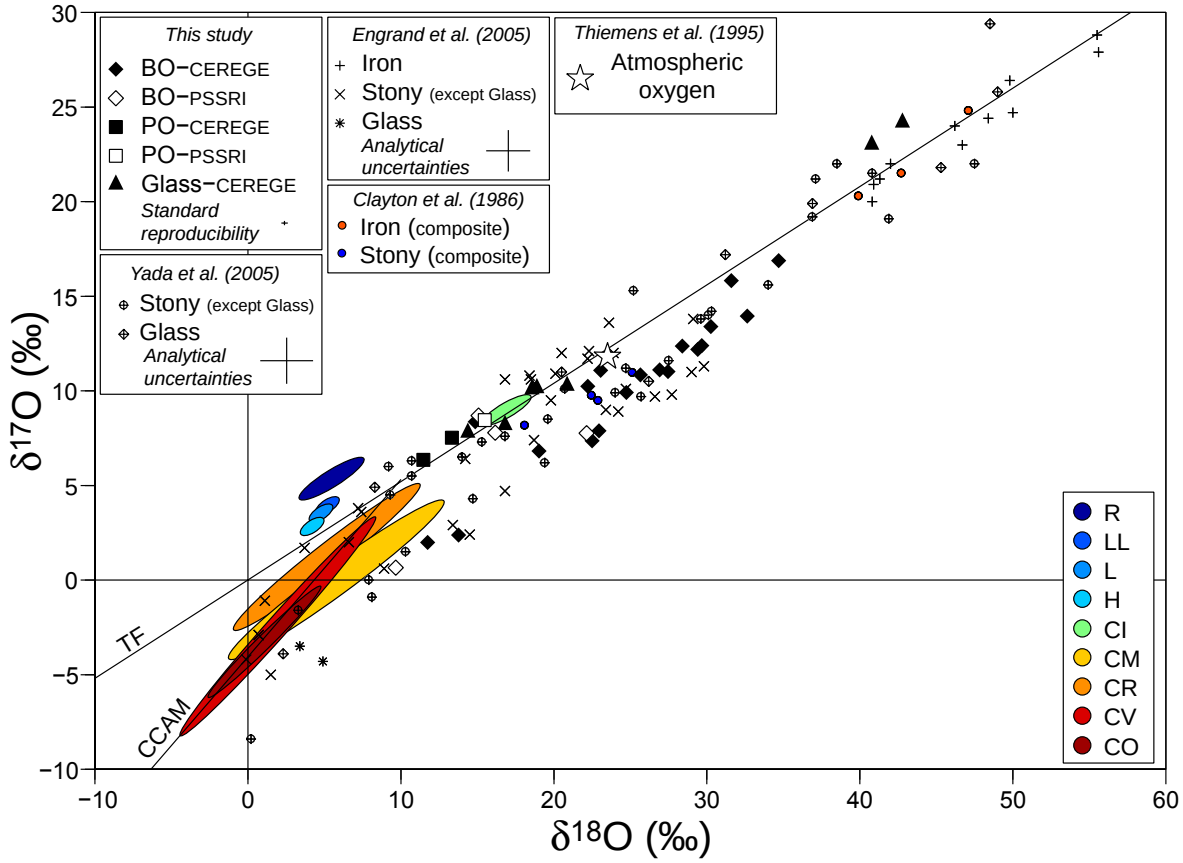

FIG. 8.1 – Oxygen isotopic compositions of cosmic spherules (in ‰ vs. V-SMOW) measured : 1) at CEREGE and PSSRI using the IR-laser fluorination/mass spectrometry technique (typical San Carlos olivine standard reproducibility obtained at CEREGE is represented : ±0.40‰ for δ^{18}O, ±0.20‰ for δ^{17}O, n = 22) ; 2) by Clayton et al. (1986) using the conventional fluorination technique on batches of cosmic spherules ; 3) by Engrand et al. (2005) and Yada et al. (2005) using ion probe (typical analytical uncertainties for individual analyses are represented). Fields for CO, CV, CR, CM, CI, H, L, LL and R chondrites are represented (Clayton et al., 1991 ; Clayton and Mayeda, 1999). The solid line labeled TF is the terrestrial fractionation line (approximated $\delta^{17}O = 0.52\times\delta^{18}O$), and the solid line labeled CCAM is the carbonaceous chondrite anhydrous minerals line (approximated $\delta^{17}O = 0.938\times\delta^{18}O - 4.06$) (Clayton and Mayeda, 1999).

with data obtained for previous studies by fluorination of composite samples (*11*) and ion probe data measured on Antarctic CSs (*4*, *5*) together with bulk isotopic compositions of meteorites (*12*, *13*). Our data covers the spectrum of δ^{18}O and δ^{17}O values obtained by previous studies on stony CSs, with a much better precision. Furthermore, data obtained in both laboratories are in good agreement. It is possible to roughly distinguish 4 groups

of isotopic signatures in our data (Table 1).

Group 1 (samples A1–A16, 48% of the total) : most CSs with barred olivine (BO) textures (16/23) have $\Delta^{17}O \approx -3$ to $-5‰$ and $\delta^{18}O$ in the 10–30‰ range.

Group 2 (samples B1–B7, 21% of the total) : five BO CSs and 2 glass CSs have $\Delta^{17}O \approx -1‰$ and $\delta^{18}O$ in the 15–35‰ range.

Group 3 (samples C1–C8, 24% of the total) : two BO CSs, all 3 CSs with porphyritic olivine (PO) texture, and 3 glass CSs have $\Delta^{17}O \approx 0.4$ to $0.8‰$ and $\delta^{18}O$ in the 10–20‰ range.

Group 4 (samples D1–D2, 6% of the total) : 2 glass CSs have $\Delta^{17}O \approx 1.8‰$ and $\delta^{18}O \approx 41‰$, which is near to the value found for three glass CSs in a previous study (*5*).

Figure 8.2 represents $\Delta^{17}O$ as a function of $\delta^{18}O$ for our samples, with possible parent bodies : carbonaceous chondrites CO, CV, CM, CR, CI ; ordinary chondrites H, L, LL ; and R chondrites (*12*, *13*). The isotopic signature of micrometeorites depends on the signature of the parent body, and of two processes : contamination by atmospheric oxygen, and mass-dependent fractionation during atmospheric entry (*4*). When micrometeoroids enter the atmosphere, they melt at an altitude of 85–90 km, and they are quenched in a few seconds (*14*). When the particle is melted, oxygen is exchanged with the atmosphere. Atmospheric oxygen at these altitudes has a $\delta^{18}O \approx 23.5‰$ and a $\delta^{17}O \approx 11.8‰$ (*15*). The heating of the particles also causes loss of material by evaporation, mainly of iron, which induces a mass-dependent fractionation of the oxygen (*4*).

These two processes may have various contributions to the measured isotopic signature. Starting from a parent material, we can define a domain of possible values for the isotopic signature of micrometeorites bounded by a line parallel to the TFL along which mass-dependent fractionation occurs, and a line connecting the value of the parent material to that of atmospheric oxygen, along which pure contamination by terrestrial oxygen occurs.

Iron CSs, derived from particles made entirely of metal grains, provide a direct test of this model as they do not contain oxygen before melting and therefore the oxygen

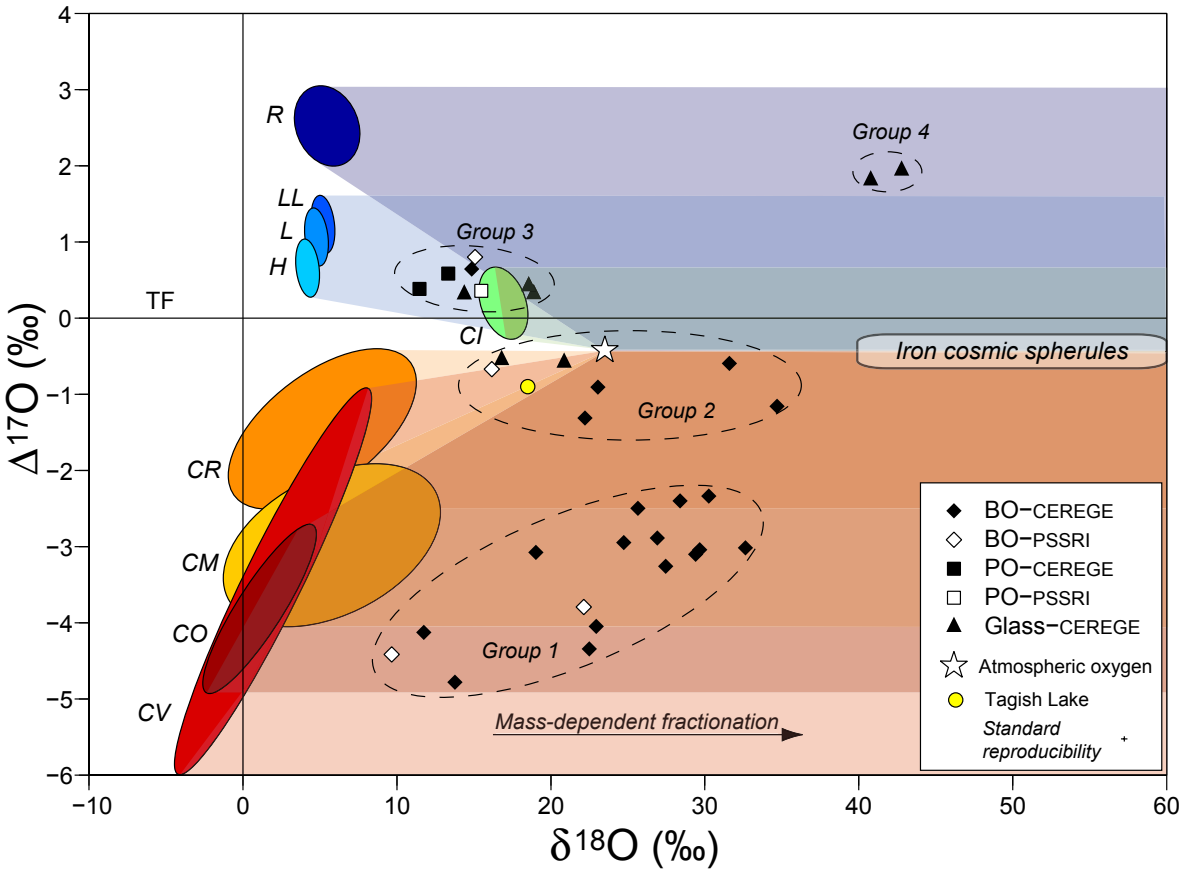

FIG. 8.2 – $\Delta^{17}O$ vs. $\delta^{18}O$ values (in ‰ vs. V-SMOW) of individual cosmic spherules measured by IR-laser fluorination/mass spectrometry (typical San Carlos olivine standard reproducibility obtained at CEREGE is represented : ±0.40‰ for $\delta^{18}O$, ±0.032‰ for $\Delta^{17}O$, n = 22). Potential parent bodies are displayed by colored domains (Clayton et al., 1991 ; Clayton and Mayeda, 1999). The whole rock isotopic composition of Tagish Lake meteorite (Brown et al., 2000) is also represented. The range of possible values of $\Delta^{17}O$ and $\delta^{18}O$ for a micrometeorite from a given parent body is represented with a shaded area.

they contain now is derived entirely from the atmosphere. Their $\Delta^{17}O$ is indeed close to the atmospheric value (*4*, *11*), with $\delta^{18}O$ in the 40–60‰ range (Fig. 1). Therefore, the oxygen isotopic signature of CSs is expected to lie between an extraterrestrial end-member composition – that may be a known meteorite group or an unknown parent body – and an "atmospheric entry end-member" that is exemplified by the iron CSs.

CSs from *Group 1* and *Group 2* are thus clearly related to carbonaceous chondrites,

with the dry (CO, CV) and hydrated (CM, CR) end-members. Atmospheric entry results in a 25–75% shift from extraterrestrial end-member composition to "atmospheric entry end-member" composition. Although most of these CSs could originate from any type of carbonaceous chondrite, the 5 micrometeorites with $\Delta^{17}O < -4$ cannot be related to CM/CR parent bodies, and therefore have a dry carbonaceous chondrite-related (CO/CV) parent body. The isotopic composition of the 2 glass CSs and one BO CS from *Group 2* (B5) can only be explained by a CR parent body. *Group 2* CSs could also be related to the parent body of the Tagish Lake meteorite (*16*).

CSs from *Group 3* seem to have an ordinary chondrite-related parent body. Although glass micrometeorites from this group are closer to the CI chondrite domain, a CI parent body is not consistent with these results once atmospheric effects are considered. Indeed, the sequence of textures with increasing heating and evaporation of Fe : PO<BO<glass (*17*) is also found in the increasing $\delta^{18}O$ (fractionation) and decreasing $\Delta^{17}O$ (contamination by atmospheric oxygen) for micrometeorites of *Group 3*. This is consistent with PO CSs retaining pristine oxygen isotopic composition in relict grains (*18*).

The only known parent material for glass CSs of *Group 4* could be the R chondrites, or the high $\Delta^{17}O$ component observed in the magnetites (*19*) and the mesostasis of unequilibrated ordinary chondrites (*20*). Enrichments in ^{17}O and ^{18}O are known for some atmospheric components (*15*) and therefore a possible atmospheric effect in these glass spherules with very high $\delta^{18}O$ cannot be entirely ruled out. These specimens may also be related to three cryptocrystalline CSs with very large ^{17}O enrichments previously reported (*5*).

Magnetic measurements (Fig. 3) give more insight into the key mineral controlled by heating during atmospheric entry : magnetite. As magnetite is the only significant carrier of magnetization in melted micrometeorites (*21*), the value of the saturation magnetization M_s is directly proportional to the amount of magnetite in the micrometeorite (the magnetite wt% is $M_s/0.92$ (*22*)). A trend of higher magnetite content for CSs with hi-

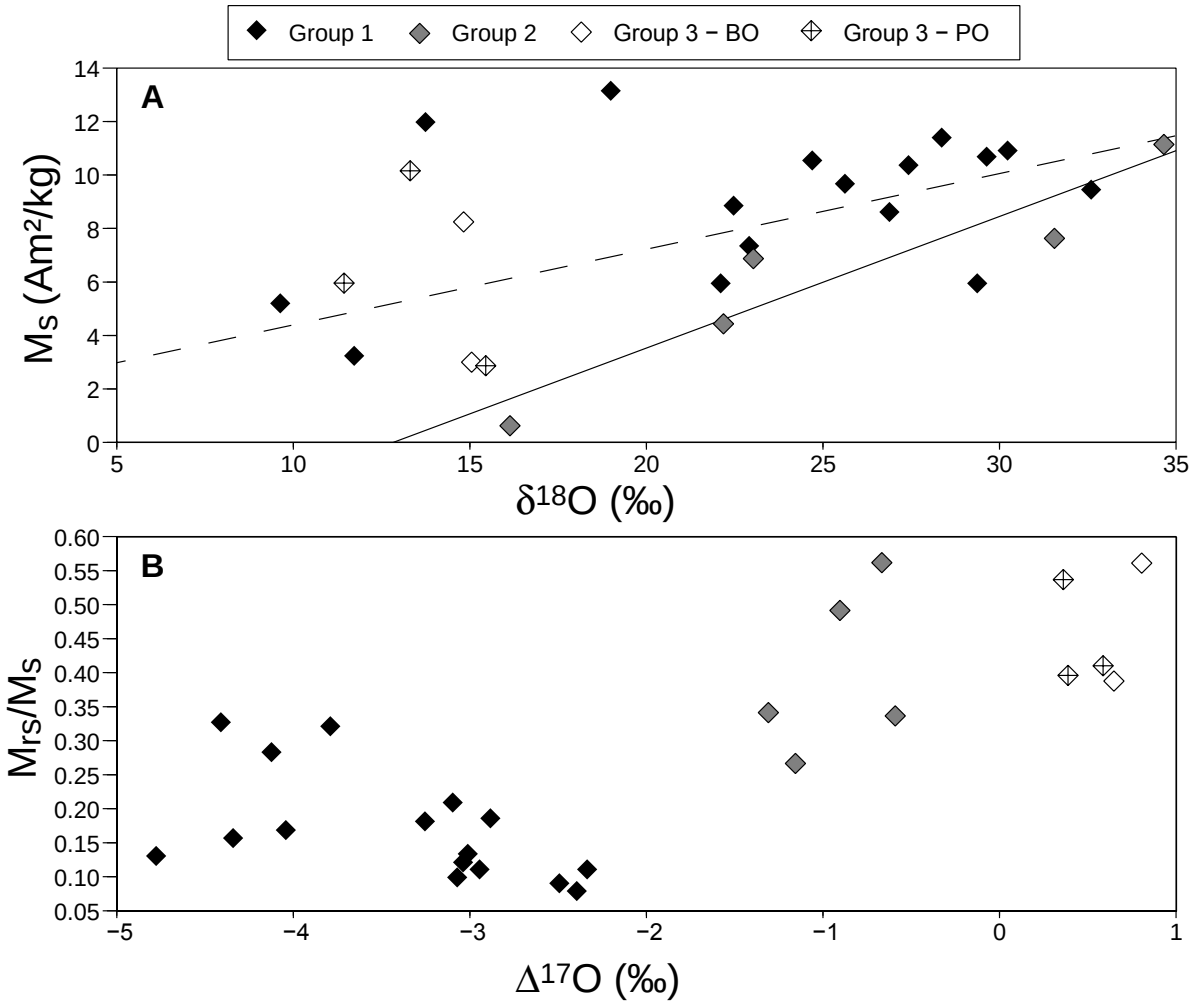

FIG. 8.3 – Magnetic properties of micrometeorites
from Isotopic *Groups 1, 2* (barred olivine (BO) texture only) and *3* (BO and porphyritic olivine (PO) textures). (**A**) Saturation magnetization M_s as a function of δ^{18}O (‰ vs. V-SMOW). Correlation lines are drawn for *Group 1* (dashed line, $R^2 = 0.56$ excluding two outliers) and *Group 2* (solid line, $R^2 = 0.88$). (**B**) Ratios of saturation remanent magnetization M_{rs} and saturation magnetization M_s as a function of Δ^{17}O (‰ vs. V-SMOW).

gher δ^{18}O is visible in *Group 2*. The positive correlation of magnetite amount with δ^{18}O is consistent with the processes of oxidation by high-δ^{18}O atmospheric oxygen and mass-dependent fractionation for particles that experience more heating. Magnetite amount may essentially trace the amount of oxidation of Fe^{2+} in the melt of olivine composition. *Group*

1 seems to have a similar trend, although two outliers have uncorrelated high M_s values that may indicate presence of magnetite before atmospheric entry. Based on the observed correlation, the preatmospheric entry end-member composition can be predicted for $M_s = 0$ at $\delta^{18}O \approx 13‰$ for *Group 2* and $\delta^{18}O \approx -5$ for *Group 1* (if we exclude the two outliers), which is roughly in agreement with the inferred CM and CO-CV carbonaceous chondrite compositions (*13*). The value of the ratio of saturation remanent magnetization M_{rs} and saturation magnetization M_s gives an estimate of the magnetite grain-size (*22*). Higher ratios correspond to smaller grain-size. Micrometeorites from *Group 1* seem to have larger magnetite grains than *Group 2* and *Group 3*. As magnetite is formed by oxidation of iron bearing phases, the magnetite grain-size differences probably reflect differences in composition of the parent minerals (especially fayalite mole percent (Fa%) in olivine), although differences in heating kinetics – as the entry velocity and angle vary for particles of different origins (*14*) – could also cause them. Larger grain sizes are expected for the oxidation of high Fa% olivine. This is in agreement with the lower Fa% observed in H and L chondrites (*Group 3*) with respect to average carbonaceous chondrites (*Group 1*).

Our finding of 30% of micrometeorites above the TFL, while previous studies by ion probe found none (*1*, *23*) or 6% (*5*), may be related to the lower precision of the ion probe (e.g. not allowing to decipher the ordinary chondrite related samples from the TFL). It could also indicate a higher proportion of ordinary chondrite related material in our large (diameter >500 μm) CSs, that may show an intermediate proportion between meteorites (80% above TFL) and small micrometeorites (0–6% above TFL). Recent petrogeochemical investigations of coarse grained unmelted micrometeorites suggest that about 20% of all micrometeorites would be ordinary chondrite-related (*2*), which is in agreement with our results. Impact destruction experiments (*24*) on hydrous (CM) and anhydrous (ordinary chondrite) targets have shown an order of magnitude increase of dust production in the 30–300 μm size range for the hydrous target. This may explain why previous authors, who studied mainly the 150–250 μm size fraction, have concluded for an overwhelming domi-

nance of CM parent body related micrometeorites while the large (our study) or small (IDPs) fractions may give a more representative sample of dust particles in Earth-crossing orbits. Our results could also reflect a variation of the composition of the flux of extra-terrestrial materials to the Earth : micrometeorites from the Transantarctic Mountains sample this influx at the hundreds of thousands of years timescale, whereas other studies were made on samples accreted in the last few thousands of years.

The discovery of significant numbers of ordinary chondrite-related CSs changes the paradigm that all micrometeorites derive from carbonaceous chondrite-related – possibly cometary – parent bodies : it demonstrates that they also derive from the parent body of ordinary chondrites. Important consequences are that ordinary chondrite-related asteroids produce dust, and that interplanetary dust in the Earth-crossing orbit partly originates from these objects. The availability of the TAM micrometeorite collection, and of IR-fluorination/mass spectroscopy for high precision oxygen isotope measurements, is a great opportunity for the characterization of the extraterrestrial dust flux entering Earth's atmosphere over the million-year time scale (*3*, *25*, *26*).

TAB. 8.1 – $\delta^{18}O$, $\delta^{17}O$ and $\Delta^{17}O$ values (in ‰ vs. V-SMOW) obtained for individual stony cosmic spherules using the IR-laser fluorination/mass spectrometry technique.

Name	Lab.	Type	Mass (μg)	$\delta^{18}O$	$\delta^{17}O$	$\Delta^{17}O$
A1	*C*	BO	439	28.39	12.37	−2.398
A2	*C*	BO	420	22.50	7.36	−4.344
A3	*C*	BO	350	32.63	13.95	−3.015
A4	*C*	BO	276	19.02	6.82	−3.075
A5	*C*	BO	501	25.65	10.84	−2.497
A6	*C*	BO	458	30.26	13.40	−2.338
A7	*C*	BO	262	11.75	1.99	−4.126
A8	*C*	BO	282	27.45	11.02	−3.258
A9	*P*	BO	660	22.13	7.76	−3.793
A10	*P*	BO	404	9.66	0.66	−4.414
A11	*C*	BO	556	29.40	12.19	−3.100
A12	*C*	BO	690	22.94	7.89	−4.046
A13	*C*	BO	386	24.73	9.91	−2.948
A14	*C*	BO	528	26.91	11.11	−2.887
A15	*C*	BO	330	13.77	2.38	−4.780
A16	*C*	BO	445	29.67	12.39	−3.041
B1	*C*	BO	395	31.59	15.83	−0.593
B2	*C*	BO	590	34.69	16.88	−1.158
B3	*C*	V	444	16.80	8.19	−0.551
B4	*C*	V	559	20.86	10.26	−0.584
B5	*P*	BO	466	16.17	7.78	−0.669
B6	*C*	BO	314	23.06	11.08	−0.907
B7	*C*	BO	353	22.22	10.24	−1.312
C1	*C*	PO	392	13.34	7.52	0.584
C2	*C*	BO	541	14.86	8.37	0.645
C3	*C*	V	438	18.89	10.14	0.316
C4	*C*	V	393	18.56	10.07	0.417
C5	*C*	V	481	14.37	7.78	0.311
C6	*C*	PO	728	11.46	6.35	0.385
C7	*P*	BO	636	15.08	8.69	0.802
C8	*P*	PO	877	15.48	8.45	0.359
D1	*C*	V	302	42.78	24.18	1.938
D2	*C*	V	314	40.77	23.01	1.807

Lab. : *C* = CEREGE, *P* = PSSRI. Type : BO = barred olivine, PO = porphyritic olivine, V = glass.

References and Notes

1. Engrand C., Maurette M., *Meteoritics & Planet. Sci.* **33**, 565 (1998).
2. Genge M. J., *Geology*, doi :10.1130/G24493A.1 (2008).
3. Rochette P., Folco L., Suavet C., van Ginneken M., Gattacceca J., Perchiazzi N., Braucher R., Harvey R. P., *Proc. Natl. Acad. Sci. USA*, doi :10.1073/pnas.0806049105 (2008).
4. Engrand C., McKeegan K. D., Leshin L. A., Herzog G. F., Schnabel C., Nyquist L. E., Brownlee D. E., *Geochim. Cosmochim. Acta* **69**, 5365 (2005).
5. Yada T., Nakamura T., Noguchi T., Matsumoto N., Kusakabe M., Hiyagon H., Ushikubo T., Sugiura N., Kojima H., Takaoka N., *Geochim. Cosmochim. Acta* **69**, 5789 (2005).
6. Taylor S., Alexander C. M. O.' D., Delaney G., Ma P., Herzog G. F., Engrand C., *Geochim. Cosmochim. Acta* **69**, 2647 (2005).
7. Alexandre A., Sonzogni C. Basile I., Sylvestre F., Parron C., Meunier J. D., Colin F., *Geochim. Cosmochim. Acta* **70**, 2827 (2006).
8. Miller M. F., Franchi I. A., Sexton A. S., Pillinger C. T., *Rapid Commun. Mass Spectrom.* **13**, 1211 (1999).
9. Crespin J., Alexandre A., Sylvestre F., Sonzogni C., Paillès C., Garreta V., *Anal. Chem.* **80**, 2372 (2008).
10. Greenwood R. C., Schmitz B., Bridges J. C., Hutchinson R., Franchi I. A., *Earth Planet. Sci. Lett.* **262**, 204 (2007).
11. Clayton R. N., Mayeda T. K., Brownlee D. E., *Earth Planet. Sci. Lett.* **79**, 235 (1986).
12. Clayton R. N., Mayeda T. K., Olsen E. J., Goswami J. N., *Geochim. Cosmochim. Acta* **55**, 2317 (1991).
13. Clayton R. N., Mayeda T. K., *Geochim. Cosmochim. Acta* **63**, 2089 (1999).

14. Love S. G., Brownlee D. E., *Icarus* **89**, 26 (1991).

15. Thiemens M., Jackson T., Zipf E. C., Erdman P. W., Van Egmond C., *Science* **270**, 969 (1995).

16. Brown P. G., et al., *Science* **290**, 320 (2000).

17. Taylor S., Lever J. H., Harvey R. P., *Meteoritics & Planet. Sci.* **351**, 651 (2000).

18. Genge M. J., Engrand C., Gounelle M., Taylor S., *Meteoritics & Planet. Sci.* **43**, 497 (2008).

19. Choi B. G., McKeegan K. D., Krot A. N., Wasson J. T., *Nature* **392**, 577 (1998).

20. Franchi I. A., Baker L., Bridges J. C., Wright I. P., Pillinger C. T., *Phil. Trans. Royal Soc. Series A* **359**, 2019 (2000).

21. Suavet C., Gattacceca J., Rochette P., Perchiazzi N., Folco L., Duprat J., Harvey R. P., *J. Geophys. Res.* **114**, B04102, doi :10.1029/2008JB005831 (2009).

22. Dunlop D., *J. Geophys. Res.*, doi :10.1029/2001JB000486 (2002).

23. Matrajt G., Guan Y., Leshin L., Taylor S., Genge M., Joswiak D., Brownlee D., *Geochim. Cosmochim. Acta* **70**, 4007 (2006).

24. Flynn J., Durda D. D., Minnick M. A., Strait M., *Lunar Planet. Sci.* **LX** (2009).

25. Folco L., Rochette P., Perchiazzi N., D'Orazio M., Laurenzi M. A., Tiepolo M., *Geology* **36**, doi : 10.1130/G24528A.1 (2008).

26. Folco L., D'Orazio M., Tiepolo M., Tonarini S., Ottolini L., Perchiazzi N., Rochette P., Glass B. P., *Geochim. Cosmichim. Acta*, in press (2009).

Acknowledgements

This work was supported by the Italian Programma Nazionale delle Ricerche in Antartide, the French Institut Polaire Paul Emile Victor, the French Institut National des Sciences de l'Univers - Centre National d'Etudes Spatiales Planetology program, the European Union through the Marie Curie Actions - RTNs ORIGINS (Project ID : 35519),

and by the French Agence Nationale de la Recherche (Project ID : ANR-05-JCJC-0133). We would like to thank F. Sylvestre (CEREGE) for additional measurements on small masses of quartz standard. IAF and RCG were supported by STFC rolling grant.

Supporting Online Material

Materials and Methods

Thirty three silicate cosmic spherules (CSs) from the Transantarctic Mountains collection were selected for this study. Their masses range from 262 μg to 877 μg after the weathered rim was leached out using diluted HCl for most of the samples. Backscattered electron images of the samples were taken at CEREGE (Aix-en-Provence, France) with a scanning electron microscope (SEM, Hitachi S-3000N) using a 30 kV accelerating voltage. SEM images (Figure S1, S2, S3, S4, S5) allowed to distinguish between barred olivine (BO, 23 CSs), porphyritic olivine (PO, 3 CSs) and glassy (7 CSs) textures (Genge et al., 2008). This distribution by type of cosmic spherules is similar to that of large collections (e.g. Taylor et al., 2000), assuming that cryptocrystalline and BO textures are merged.

Hysteresis parameters (Table S1) were measured at CEREGE with a Princeton Measurements Corporation Vibrating Sample Magnetometer (VSM) with a peak field of 0.5 T (noise level of $\sim 10^{-9}$ Am^2). The remanent coercive field B_{cr} was determined by DC backfield demagnetization of the saturation remanent magnetization using the VSM.

Measurements of δ^{18}O and δ^{17}O were carried out on 28 spherules at the Stable Isotopes Laboratory of CEREGE. Molecular oxygen was extracted using the IR-laser fluorination technique (Alexandre et al., 2006 ; Crespin et al., 2008) and the three oxygen isotopic composition was measured with a dual inlet mass spectrometer DeltaPlus, Thermo-Finnigan. The gas (O_2) was passed through a -114°C slush to refreeze potential interfering gases before being sent to the mass spectrometer. In order to get sufficient 34/32 and 33/32 signals (2–3 V), the oxygen from <0.3 mg standards and all CSs samples was concentrated in the mass spectrometer in an auto-cooled 800 μl microvolume filled with silica gel and directly connected to the dual-inlet system. δ^{18}O and δ^{17}O values of the reference gas were fixed through the analysis of NBS28 (δ^{18}O = 9.60‰ , δ^{17}O = 4.99‰). The oxygen isotope results are expressed in ‰ vs. V-SMOW. Measured δ^{18}O and δ^{17}O values of the

samples were corrected on a daily basis using a 1.5 mg quartz laboratory standard "Boulangé" ($\delta^{18}O$ = 16.36‰ (Alexandre et al., 2006), $\delta^{17}O$ = 8.507‰, and $\Delta^{17}O$ = 0.006). During the analyzing period, replicate analyses of 1.5 mg NBS28 ($\delta^{18}O$ = 9.59±0.26‰, $\delta^{17}O$ = 4.98±0.16‰, $\Delta^{17}O$ = −0.004±0.055‰, n = 11), San Carlos olivine ($\delta^{18}O$ = 5.39±0.40‰, $\delta^{17}O$ = 2.78±0.20‰, $\Delta^{17}O$ = −0.026±0.032‰, n = 22) and UWG-2 (Valley et al., 1995) ($\delta^{18}O$ = 5.69±0.18‰, $\delta^{17}O$ = 2.96±0.11‰, $\Delta^{17}O$ = −0.004±0.055‰, n = 8) were made. Measurements made on microsamples (0.2–0.7 mg) of San Carlos olivine using the mass-spectrometer cooled microvolume (Fig. S6) show a systematic negative offset on the values of $\delta^{18}O$, $\delta^{17}O$ and $\Delta^{17}O$ (−0.27±0.14‰ for $\delta^{18}O$, −0.33 ±0.09‰ for $\delta^{17}O$, and −0.189±0.052‰ for $\Delta^{17}O$, n = 9). Such offsets were also observed for quartz standard "Boulangé" >0.25 mg samples (−0.1±0.1 for $\Delta^{17}O$, n = 31), and <0.25 mg samples (−0.16±0.05 for $\Delta^{17}O$, n = 19) when microvolume was used. This systematic offset related with the use of microvolume is of unknown origin but the magnitude does not have a major effect on the data. A direct correction based on the systematic offsets for San Carlos olivine was made for CS samples measured at CEREGE : +0.27 for $\delta^{18}O$, +0.33 for $\delta^{17}O$, and +0.189 for $\Delta^{17}O$. Five more BO and PO spherules were measured at the Open University (Milton Keynes, United Kingdom) using the IR-laser fluorination technique (Miller et al., 1999) : the three oxygen isotopic composition was measured using a Micromass (Wythenshawe, Manchester, UK) PRISM III dual inlet mass spectrometer. A systematic offset in $\delta^{18}O$ for small samples is also observed in this laboratory (Table 1 in Greenwood et al., 2007). This offset appears to be due to isotopic fractionation associated with transfer of the gases in the inlet system, and therefore independent of sample type. A correction for this offset was applied to the measured values based on the measurement of three samples of small masses of PSRI obsidian standard during the analyzing period : −0.49‰ for $\delta^{18}O$, −0.23‰ for $\delta^{17}O$ and −0.020‰ for $\Delta^{17}O$.

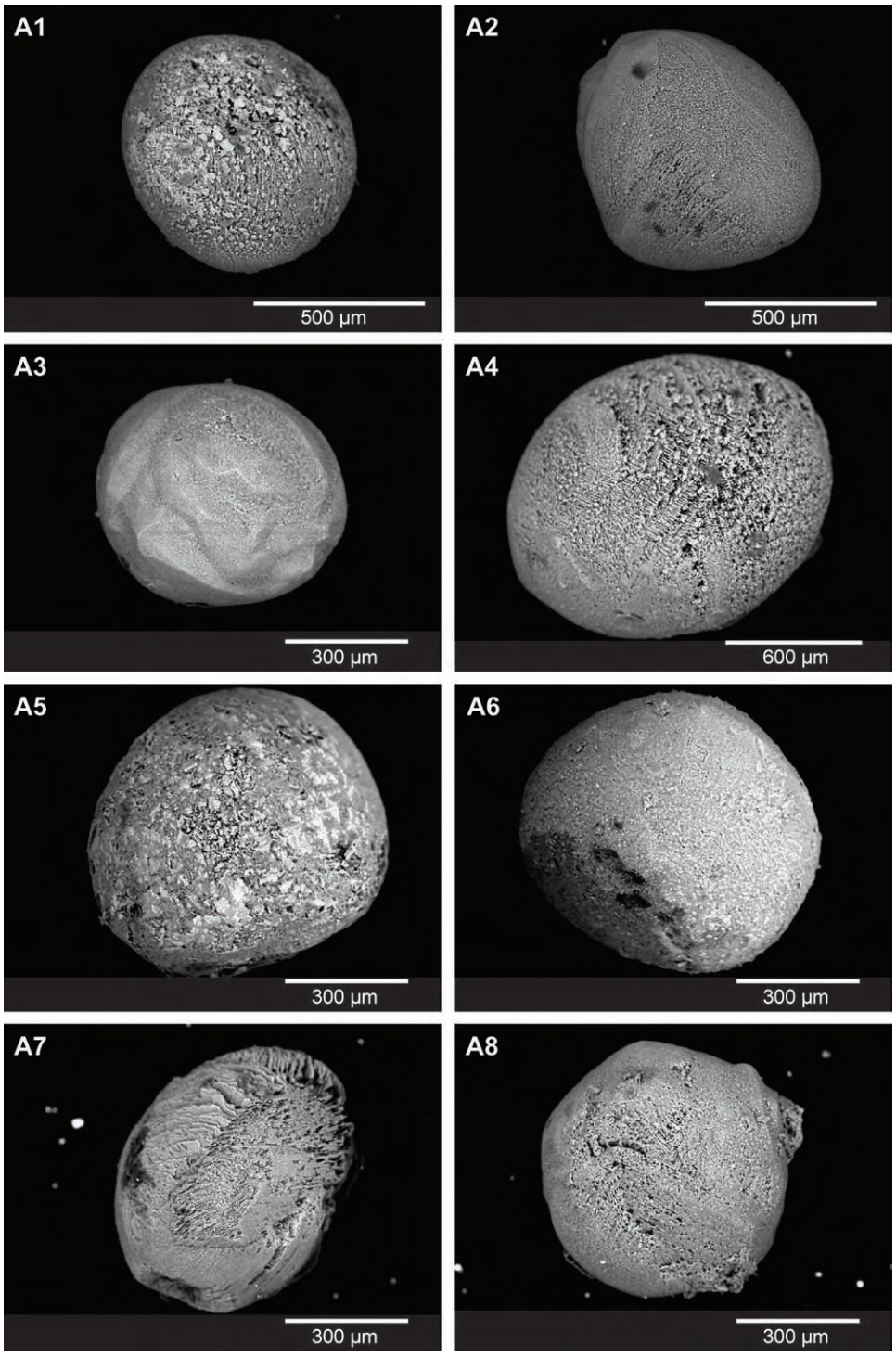

FIG. 8.4 – Backscattered electron images of cosmic spherules from Group 1.

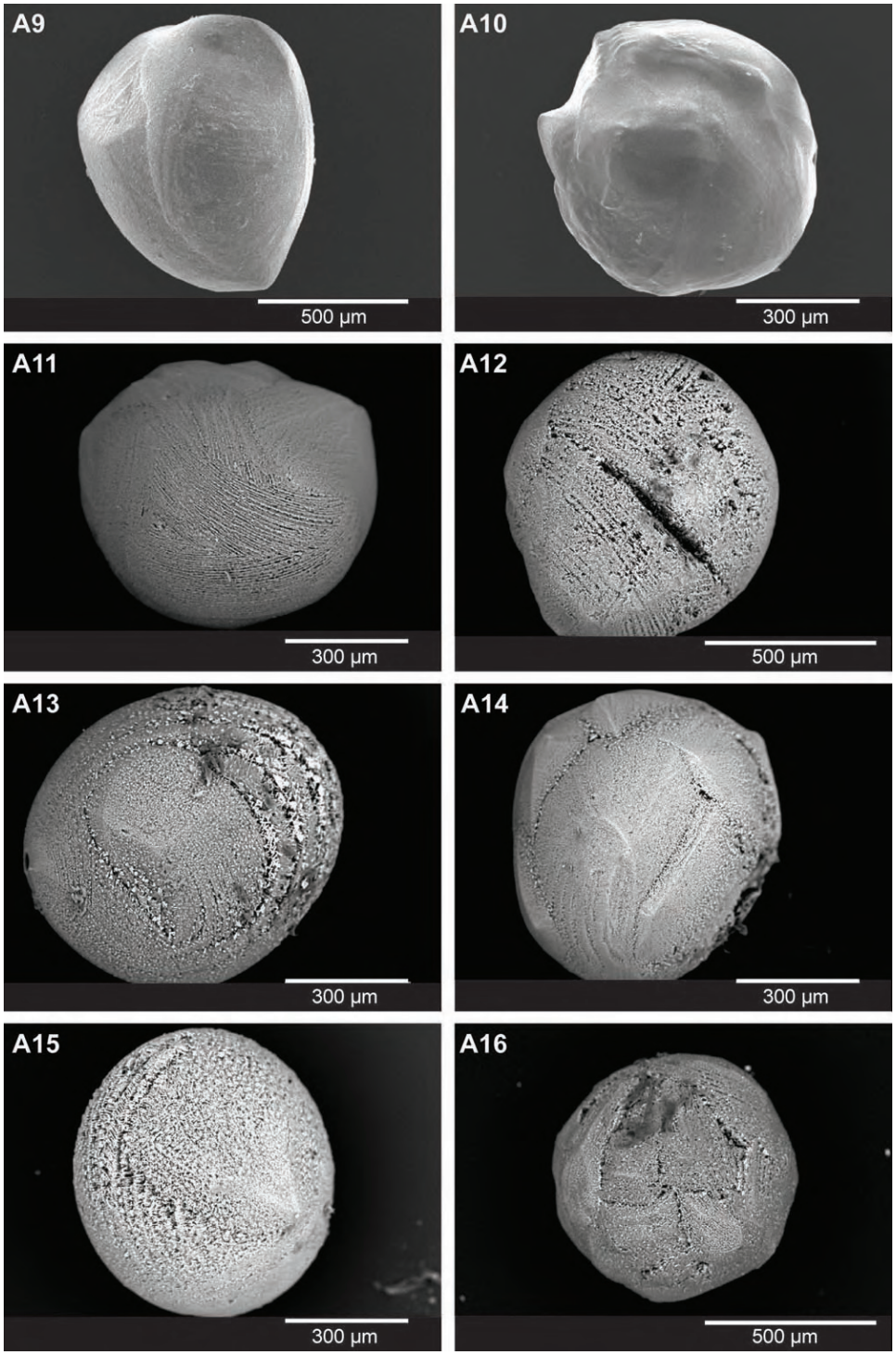

FIG. 8.5 – Backscattered electron images of cosmic spherules from Group 1 (continued).

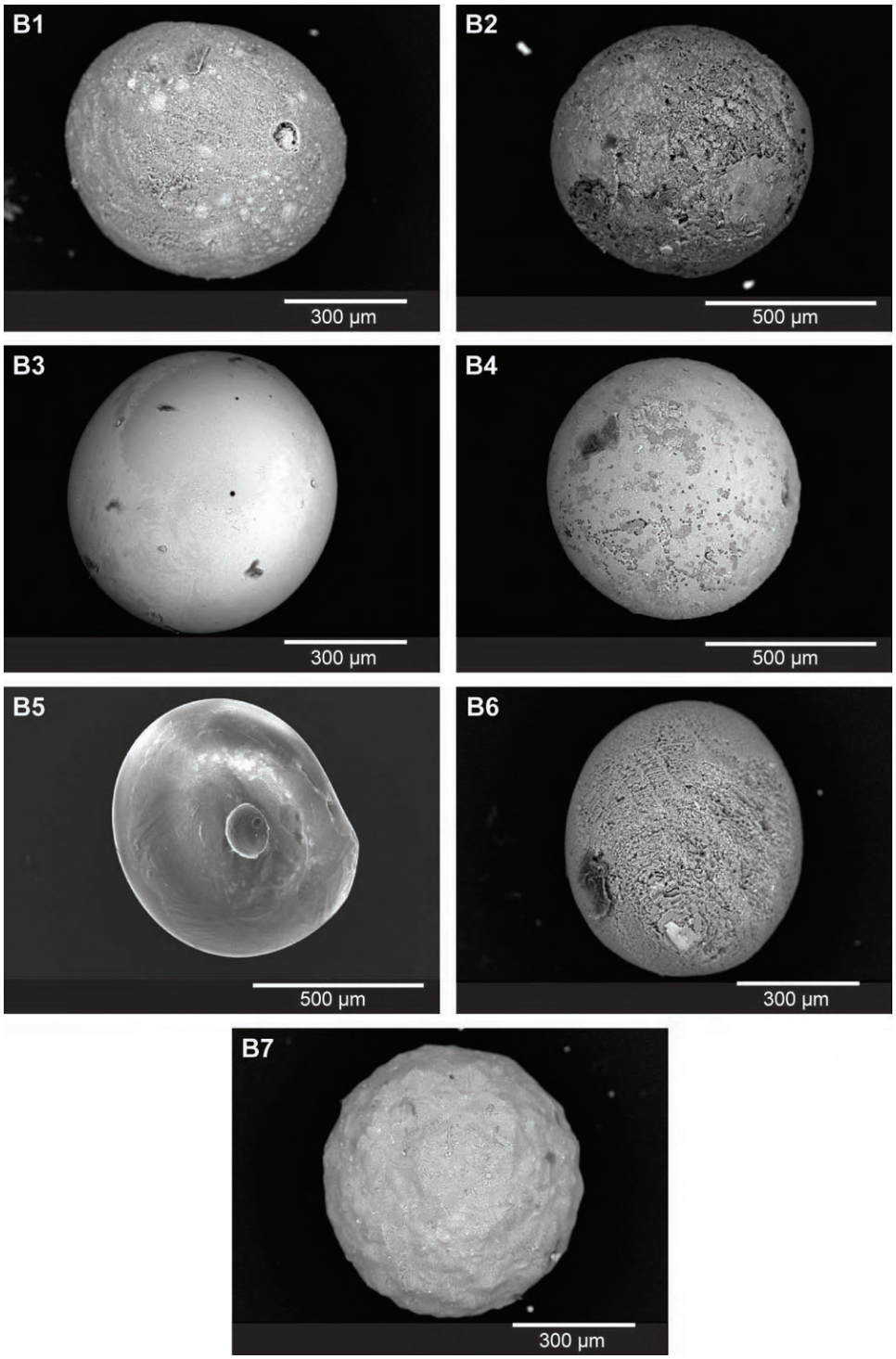

FIG. 8.6 – Backscattered electron images of cosmic spherules from Group 2.

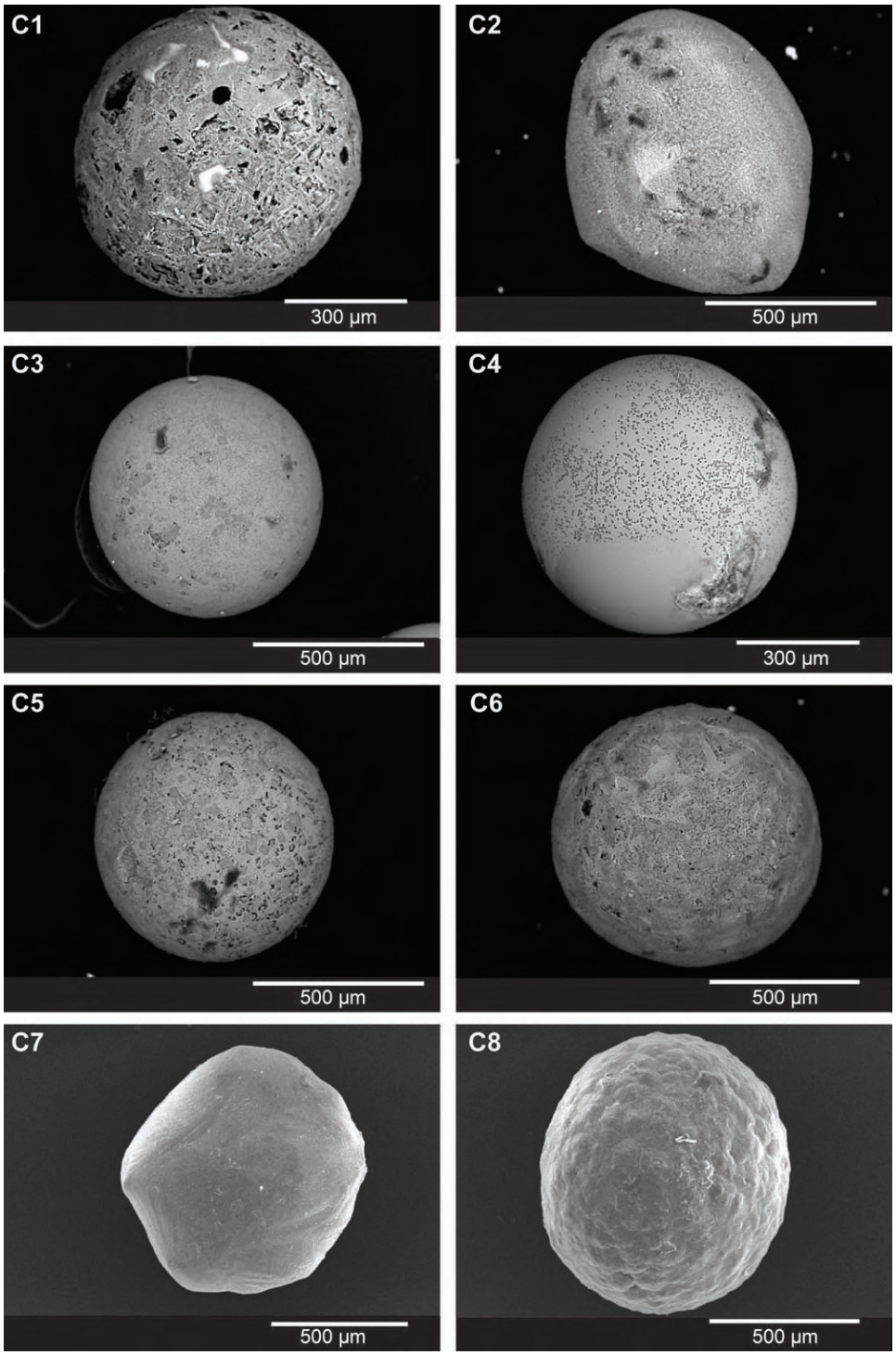

FIG. 8.7 – Backscattered electron images of cosmic spherules from Group 3.

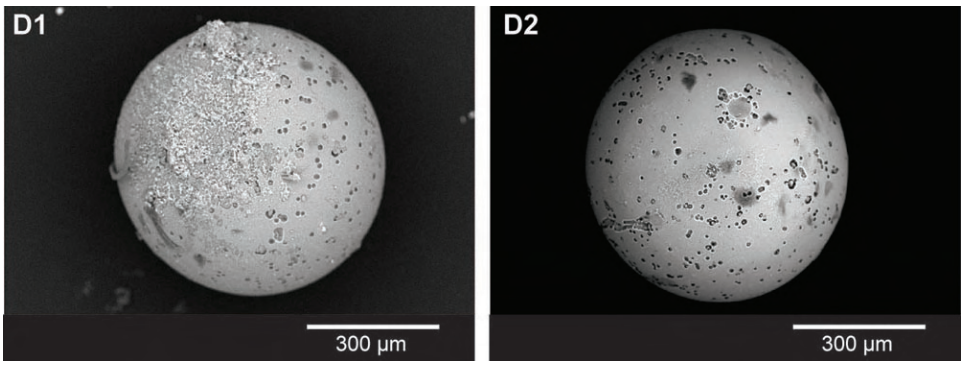

FIG. 8.8 – Backscattered electron images of cosmic spherules from Group 4.

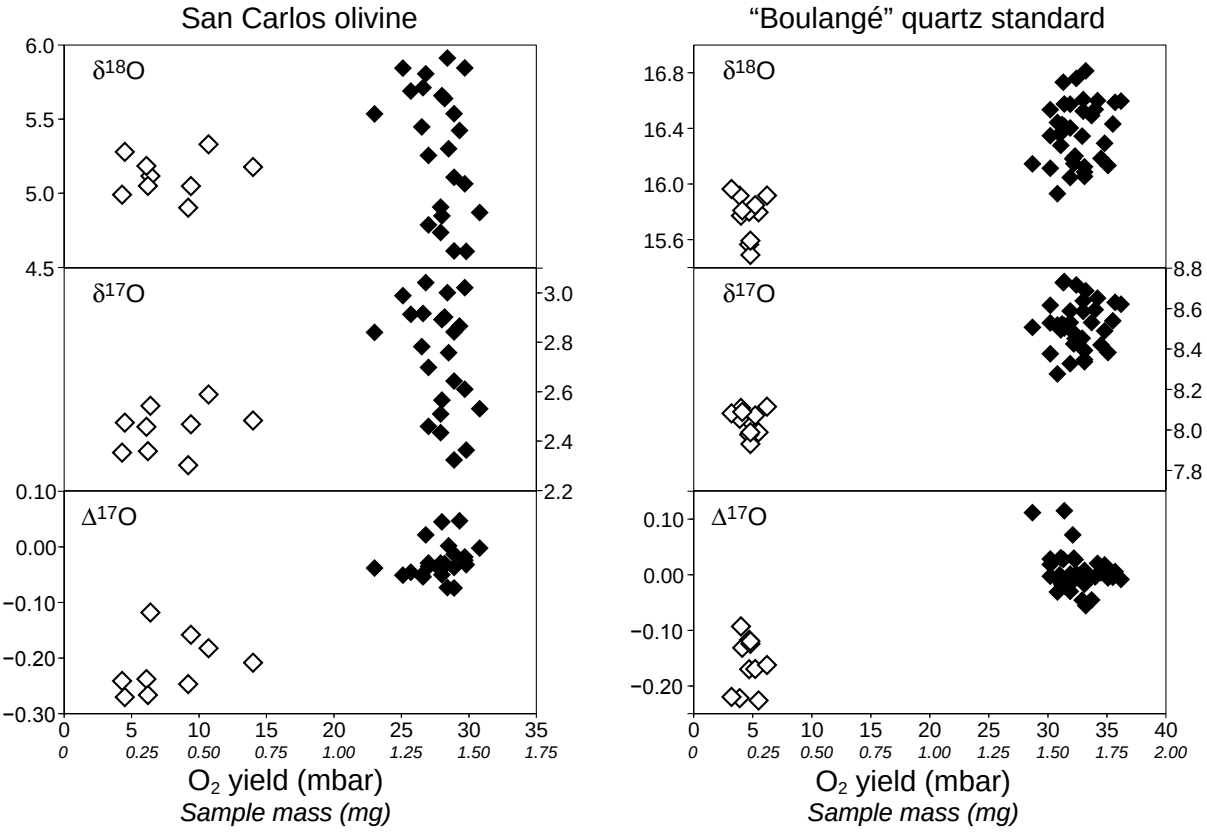

FIG. 8.9 – Standards.
$\delta^{18}O$, $\delta^{17}O$ and $\Delta^{17}O$ values (‰ vs. V-SMOW) obtained for replicate analyses of microsamples (empty diamonds) of San Carlos olivine (0.2–0.7 mg) and "Boulangé" quartz standards (<0.3 mg) compared with replicate analyses of 1.5 mg samples (solid diamonds). The approximate sample mass corresponding to the O_2 yield is indicated with the secondary labels.

TAB. 8.2 – Magnetic properties of cosmic spherules.

Name	Type	M_s (Am^2/kg)	M_{rs}/M_s	B_{cr}
A1	BO	11.40	0.08	19.46
A2	BO	8.85	0.16	24.83
A3	BO	9.46	0.13	26.49
A4	BO	13.15	0.10	19.01
A5	BO	9.67	0.09	17.04
A6	BO	10.91	0.11	21.72
A7	BO	3.24	0.28	56.91
A8	BO	10.37	0.18	28.31
A9	BO	5.95	0.32	38.8
A10	BO	5.20	0.33	29.58
A11	BO	5.95	0.21	24.98
A12	BO	7.35	0.17	23.83
A13	BO	10.55	0.11	16.26
A14	BO	8.62	0.19	26.13
A15	BO	11.99	0.13	18.81
A16	BO	10.69	0.12	21.37
B1	BO	7.64	0.34	64.08
B2	BO	11.15	0.27	56.03
B3	V	*NA*	*NA*	*NA*
B4	V	*NA*	*NA*	*NA*
B5	BO	0.62	0.56	70.83
B6	BO	6.87	0.49	40.58
B7	BO	4.43	0.34	59.42
C1	PO	10.16	0.41	71.65
C2	BO	8.25	0.39	66.74
C3	V	*NA*	*NA*	*NA*
C4	V	*NA*	*NA*	*NA*
C5	V	*NA*	*NA*	*NA*
C6	PO	5.96	0.40	68.54
C7	BO	3.00	0.56	86.3
C8	PO	2.87	0.54	70.72
D1	V	*NA*	*NA*	*NA*
D2	V	*NA*	*NA*	*NA*

BO : barred olivine. PO : porphyritic olivine. V : glass.

Additional References

Genge M. J., Engrand C., Gounelle M., Taylor S., *Meteoritics & Planet. Sci.* **43**, 497 (2008).

Taylor S., Lever J. H., Harvey R. P., *Meteoritics & Planet. Sci.* **351**, 651 (2000).

Alexandre A., Sonzogni C. Basile I., Sylvestre F., Parron C., Meunier J.D., Colin F., *Geochim. Cosmochim. Acta* **70**, 2827 (2006).

Crespin J., Alexandre A., Sylvestre F., Sonzogni C., Paills C., Garreta V., *Anal. Chem.* **80**, 2372 (2008).

Valley J. W., Kitchen N., Kohn M. J., Niendorf C. R. Spicuzza M. J., *Geochim. Cosmochim. Acta* **59**, 5223 (1995).

Miller M. F., Franchi I. A., Sexton A. S., Pillinger C. T., *Rapid Commun. Mass Spectrom.* **13**, 1211 (1999).

Quatrième partie

Conclusions et perspectives

Ce travail de thèse nous a permis de de mettre en évidence certaines des spécificités de la collection de micrométéorites TAM :

- Comme en attestent les distributions en taille et par type de sphérules cosmiques, cette collection est peu biaisée ; les particules ont subi peu de transports secondaires après leur chute sur Terre.
- La variabilité importante des degrés d'érosion confirme que les pièges des Monts Transantarctiques ont été exposés pendant des durées exceptionnellement longues.
- Ces longues durées d'exposition expliquent la présence au sein de la collection TAM d'un nombre exceptionnel d'échantillons de diamètre >400 μm.

Cette collection présente d'autres particularités qui justifient des études plus approfondies :

- Les micrométéorites de taille millimétrique ont fait l'objet de peu d'études dans les autres collections faute d'un nombre suffisant d'échantillons ; la collection TAM en comporte plusieurs dizaines qui sont en cours d'investigation (thèse M. Van Ginneken).
- Des agrégats sphérulitiques semblables à ceux trouvés récemment dans des carottes Antarctiques ont été découverts dans la collection TAM. Ces objets sont en cours d'investigation (thèse M. Van Ginneken).

L'étude de la collection TAM a permis de montrer que la pente de la distribution en taille des micrométéorites reste la même dans toute la gamme de taille 100–1600 μm, et donc qu'un processus unique contrôle la distribution sur toute cette gamme de taille. La collection TAM, avec ses micrométéorites géantes, constitue un outil de choix dans l'étude de la continuité entre météorites, "minimétéorites" et micrométéorites. La question de la

nature des micrométéoroïdes pour les micrométéorites pourrait être envisagée par des mesures de nucléides cosmogéniques sur un nombre statistiquement significatif d'échantillons. Quelle est la proportion de micrométéorites ayant des précurseurs de taille proche de la particule finale ? Quelle est la proportion de particules provenant de la fracturation et de l'ablation d'objets de plus grande taille lors de l'entrée atmosphérique ? Les mesures de nucléides cosmogéniques permettraient aussi d'étudier le temps de résidence sur Terre des micrométéorites.

Le fait que la collection TAM soit représentative du flux de matière extraterrestre vers la Terre et la disponibilité d'échantillons de gros diamètre en nombre important nous ont permis d'effectuer des mesures magnétiques inédites, ainsi que d'obtenir des résultats statistiquement significatifs. Nos mesures de susceptibilité magnétique à différentes températures et de désaimantation thermique ont permis de démontrer que le signal magnétique de ces objets est porté par la magnétite qui est formée lors de l'entrée atmosphérique des micrométéorites. Les analyses d'anisotropie de susceptibilité magnétique ont révélé une forte anisotropie (>15%) qui pourrait être en relation avec la texture de l'olivine en plans parallèles dans les sphérules de type olivine barrée. Les désaimantations en champ alternatif ont permis de conclure que l'aimantation des sphérules cosmiques est une aimantation rémanente thermique acquise dans le champ terrestre lors de l'entrée atmosphérique. Les quelques résultats obtenus sur des micrométéorites non-fondues semblent indiquer qu'elles peuvent conserver des aimantations pré-atmosphériques. Des mesures complémentaires pourraient permettre d'apporter des contraintes sur l'origine de ces aimantations, et de déterminer dans quelles régions et à quelle étape de l'histoire du Système Solaire elles ont été acquises.

En utilisant les résulats de la caractérisation magnétique des micrométéorites, nous avons pu démontrer que ces particules ont des valeurs d'aimantation suffisantes pour provoquer des anomalies de direction et d'intensité d'aimantation dans les sédiments dans lesquels elles se déposent, à l'échelle d'un échantillon standard pour études paléomagnétiques.

De même, les analyses des rapports isotopiques de l'oxygène par fluorination laser/ spectrométrie de masse – méthode destructrice pour les échantillons – ont pu être envisagée grâce au grand nombre de micrométéorites ayant une masse suffisante dans la collection TAM. Le principal résultat de cette étude a été d'apporter la preuve que les micrométéorites ne proviennent pas uniquement de corps parent de type chondrite carbonée, mais aussi de corps parents de type chondrite ordinaire. Ce résultat a des conséquences importantes pour la compréhension des transferts de matière dans le Système Solaire : il permet d'établir une continuité d'origine entre les météorites et les micrométéorites de gros diamètre, ainsi que de rattacher une partie des poussières interplanétaires accrétées par la Terre aux astéroïdes de type chondrite ordinaire. Certaines des sphérules cosmiques vitreuses mesurées indiquent un corps parent de type chondrite R, ou bien un corps parent encore inconnu ; des analyses isotopiques suppémentaires, précédées par une caractérisation géochimique plus poussée, permettront peut-être de mieux caractériser leur origine.

Liste des documents

Rochette, P., Folco, L., Suavet, C., van Ginneken, M., Gattacceca, J., Perchiazzi, N., Braucher, R., Harvey, R.P. (2008). Micrometeorites from the Transantarctic Mountains. *Proc. Natl. Acad. Sci. USA*, **105** :18206–18211, doi :10.1073/pnas.0806049105.

Suavet, C., Rochette, P., Kars, M, Gattacceca, J., Folco, L., Harvey, R. P. (2009). Statistical properties of the Transantarctic Mountains (TAM) micrometeorites collection. *Polar Science*, doi :10.1016/j.polar.2009.06.003.

Suavet C., Gattacceca J., Rochette P., Perchiazzi N., Folco L., Duprat J., Harvey R. P. (2009). Magnetic Properties of Micrometeorites. *J. Geophys. Res.*, doi :10.1029/2008JB005831.

Suavet, C., Rochette, P., Gattacceca, J., Folco, L. (2008). Micrometeorites : a possible bias on the sedimentary magnetic record. *Geochem. Geophys. Geosyst.*, **9**, Q11002, doi :10.1029/2008GC002160.

Marfaing, J., Rochette, P., Pellerey, J., Chaurand, P., Suavet, C., Folco, L. (2008). Study of a set of micrometeorites from Antarctica using magnetic and ESR methods coupled with micro-XRF. *J. Magn. Magn. Mater.*, **320** :1687-1695, doi :10.1016/j.jmmm.2008.01.037.

Suavet, C., Alexandre, A., Franchi, I. A., Gattacceca, J., Sonzogni, C., Greenwood, R. C., Folco, L., Rochette, P. (2009). A New Source of Interplanetary Dust. *Soumis à Science.*

Résumé

La collection de micrométéorites des Monts Transantarctiques comporte des micrométéorites accumulées pendant plusieurs centaines de milliers d'années, dont un nombre exceptionnel de particules de diamètre >400 μm, qui nous ont permis de démontrer que leur distribution en taille reste la même sur la gamme 100–1600 μm, ainsi que d'en effectuer une caractérisation magnétique et isotopique : la magnétite qu'elles contiennent en abondance est formée lors de l'entrée atmosphérique, elle enregistre une aimantation thermorémanente – lors du refroidissement dans le champ terrestre – qui peut être suffisante pour causer des anomalies dans l'enregistrement paléomagnétique des sédiments dans lesquels les micrométéorites se déposent ; les rapports isotopiques de l'oxygène indiquent, contrairement au dogme actuel, qu'une partie des micrométéorites est apparentée aux chondrites ordinaires ou à des corps parents encore inconnus, et non aux seules chondrites carbonées.

Mots-clés : micrométéorites, sphérules cosmiques, distribution en tailles, magnétisme des matériaux extraterrestres, aimantation rémanente détritique, isotopes de l'oxygène, corps parents des météorites.

Abstract

The Transantarctic Mountains micrometeorite collection comprises micrometeorites that accumulated for hundreds of thousands of years, among which particles larger than 400 μm in exceptional numbers, which allowed us to demonstrate that their size distribution remains the same on the 100–1600 μm size range, and to make a magnetic and isotopic characterization of these objects : the magnetite they contain in abundance is formed during atmospheric entry, it acquires a thermoremanent magnetization – by quenching in the Earth's magnetic field – that can be sufficient to induce anomalies in the palaeomagnetic record of sediments they deposit in ; the oxygen isotope ratios indicate that part of the micrometeorites are ordinary chondrite-related or originate from as yet unknown parent bodies, and not only from carbonaceous chondrites as stated by the current paradigm.

Keywords : micrometeorites, cosmic spherules, size distribution, magnetism of extraterrestrial materials, detrital remanent magnetization, oxygen isotopes, parent bodies of meteorites.